AD-A091 024 UNDERWATER SYSTEMS INC ROCKVILLE MD F/6 20/1
SOUND PROPAGATION SOUTH OF MARTHA'S VINEYARD.(U)
JUN 80 R J HECHT N00014-79-C-0466
UNCLASSIFIED NL

1 OF 2
AD A
091 024

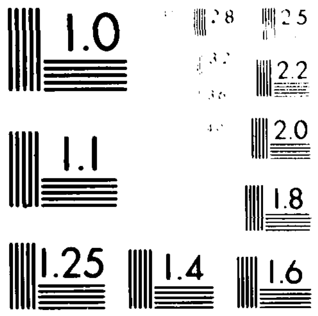

MICROCOPY RESOLUTION TEST CHART
NATIONAL BUREAU OF STANDARDS-1963-A

(12)

UNDERWATER SYSTEMS INC.

LEVEL II

AD A091024

DTIC
ELECTE
OCT 30 1980
S D
E

FILE COPY

DISTRIBUTION STATEMENT A
Approved for public release;
Distribution Unlimited

1776 EAST JEFFERSON STREET • ROCKVILLE, MD. 20852 • TELEPHONE: 301-770-[illegible]

80 10 22 009

SPECIAL NOTICES

CHANGE OF ADDRESS

ORGANIZATIONS RECEIVING REPORTS ON THE INITIAL DISTRIBUTION LIST SHOULD CONFIRM CORRECT ADDRESS. THIS LIST IS LOCATED AT THE END OF THE REPORT. ANY CHANGE OF ADDRESS OR DISTRIBUTION SHOULD BE CONVEYED TO THE OFFICE OF NAVAL RESEARCH, CODE 212, ARLINGTON, VIRGINIA 22217.

DISCLAIMER

REPRODUCTION

(12)

LEVEL II

SOUND PROPAGATION
SOUTH OF MARTHA'S VINEYARD

Prepared By:

Richard J. Hecht

Prepared For:

Office of Naval Research
Code 464
Arlington, Virginia 22217

Final Report For
Contract N00014-79-C-0466

June 1980

DISTRIBUTION STATEMENT A
Approved for public release;
Distribution Unlimited

UNDERWATER SYSTEMS, Inc.
1776 East Jefferson St. • Rockville, Md. 20852 • (301) 770-9190

UNCLASSIFIED

SECURITY CLASSIFICATION OF THIS PAGE (When Data Entered)

REPORT DOCUMENTATION PAGE

READ INSTRUCTIONS BEFORE COMPLETING FORM

1. REPORT NUMBER	2. GOVT ACCESSION NO. AD-A091 024	3. RECIPIENT'S CATALOG NUMBER
4. TITLE (and Subtitle) (6) Sound Propagation South of Martha's Vineyard.	(7)	5. TYPE OF REPORT & PERIOD COVERED FINAL REPORT
		6. PERFORMING ORG. REPORT NUMBER
7. AUTHOR(s) (10) Richard J. Hecht	(15)	8. CONTRACT OR GRANT NUMBER(s) N00014-79-C-0466, New
9. PERFORMING ORGANIZATION NAME AND ADDRESS Underwater Systems, Inc. 1776 East Jefferson Street Rockville, MD 20852		10. PROGRAM ELEMENT, PROJECT, TASK AREA & WORK UNIT NUMBERS
11. CONTROLLING OFFICE NAME AND ADDRESS Office of Naval Research, Code 464 Department of the Navy Arlington, VA 22217	(11) 30	12. REPORT DATE June [illegible] 1980
		13. NUMBER OF PAGES 109
14. MONITORING AGENCY NAME & ADDRESS (if different from Controlling Office) (12) 110		15. SECURITY CLASS. (of this report) UNCLASSIFIED
		15a. DECLASSIFICATION/DOWNGRADING SCHEDULE

16. DISTRIBUTION STATEMENT (of this Report)

UNLIMITED

17. DISTRIBUTION STATEMENT (of the abstract entered in Block 20, if different from Report)

18. SUPPLEMENTARY NOTES

19. KEY WORDS (Continue on reverse side if necessary and identify by block number)

Shallow Water Propagation
Seismic Propagation
Propagation Loss
Geophones
Geophone Implanter
Martha's Vineyard

20. ABSTRACT (Continue on reverse side if necessary and identify by block number)

An experiment was performed south of Martha's Vineyard, Massachusetts, on the Long Island platform using an embedded triaxial geophone and a colocated hydrophone as a receiver. The data shows low propagation loss even with a strong negative sound velocity gradient in the water. The signals from the embedded vertical geophone show 10 to 12 dB less apparent propagation loss than the signals from the hydrophone in the 30 to 200 Hz frequency band. At lower frequencies, signals from all four sensors were similar.

DD FORM 1473 1 JAN 73 EDITION OF 1 NOV 65 IS OBSOLETE

S/N 0102-014-6601

UNCLASSIFIED

SECURITY CLASSIFICATION OF THIS PAGE (When Data Entered)

356 [illegible]

ACKNOWLEDGEMENTS

The contributions of many individuals made this experiment a success. I would like to express my appreciation to CDR Julian E. Minard, ONR Code 463, for his suggestions; to Dr. Marvin S. Weinstein, Curtis I. Holmer and Charmaine P. Mrazek for participating in discussions of data interpretation; and to Robert P. Kocher, Richard L. Lawrence and Michael W. Vore for making the at-sea experiment a success.

ABSTRACT

An experiment was performed south of Martha's Vineyard, Massachusetts, on the Long Island platform using an embedded triaxial geophone and a colocated hydrophone as a receiver. The data shows low propagation loss even with a strong negative sound velocity gradient in the water. The signals from the embedded vertical geophone show 10 to 12 dB less apparent propagation loss than the signals from the hydrophone in the 30 to 200 Hz frequency band. At lower frequencies, signals from all four sensors were similar.

Table of Contents

List of Figures

List of Tables

1. INTRODUCTION

1.1 Previous Experiments

Previous experiments have shown that larger signal-to-noise ratios (SNR) may be observed for signals from geophones than from hydrophones. An experiment was conducted south of Martha's Vineyard, Massachusetts, to obtain information on the differences in received signal levels from a hydrophone and a triaxial geophone. The immediate purpose of the experiment was to determine whether or not a ship could be detected acoustically at a range of 30 km.

A sound field in the shallow water region of the ocean can be measured by using pressure sensors, particle velocity sensors or both. The acoustic levels sensed by the pressure and velocity sensors will depend on the location of the sensor in relation to the constructive interference pattern. A vertical geophone will sense maximum levels at a pressure node.[1]

Holmer analyzed the magnitude of the levels sensed on the vertical component as compared to the horizontal component of particle velocity.[2] He concluded that a horizontal geophone will sense maximum levels at a pressure anti-node. The horizontal velocity components will be greater than the vertical for bottom-to-water velocity ratios of 1.41 or less. In a bottom assumed to be a fluid, the magnitude of the horizontal velocity will always be greater than the vertical velocity for eigenray angles greater than 45° from normal. In a solid bottom that supports shear waves, the magnitude of the horizontal and vertical velocity components is expected to be about equal.

Urick observed acoustic propagation to sensors located in shallow water from sources in deep water.[3] Ray path diagrams showed no direct path between source and receiver. At Ft. Lauderdale, Florida, he observed higher SNR for horizontal geophones than for a colocated hydrophone for sources at a range of 3.3 and 6.4 kyd. Signals were observed off Assateague, Maryland, on sonobuoys to ranges of 160 miles even though no direct or reflected paths were present between source and receiver. In both of these experiments, the sound traveled a majority of its path in the water and a relatively short part of its path in the bottom to reach the receiver.

McLeroy conducted a shallow water experiment south of Panama City, Florida, in which he used both geophones and hydrophones as sensors.[4] The signal from the geophones generally showed higher levels at short ranges than that from the hydrophones. The signal level from the geophones at 141 Hz was higher than that from the hydrophone; whereas at 3.5 Hz, the signal levels from the several sensors were about equal.

1.2 Propagation Modes

The predominant modes of propagation in shallow water are water waves, the Airy phase, ground waves, head waves and surface and interface waves. Figure 1 shows the relationship between the first four of these wave types and the group velocity, phase velocity and the mode amplitude function for the first mode in a liquid medium. The surface and interface waves occur in elastic media.

The water wave propagates in a layered media such as shallow water with a minimum of interaction with the bottom. The intensity spreading loss is r^{-1} and attenuation is minimal. The path of the wave is almost

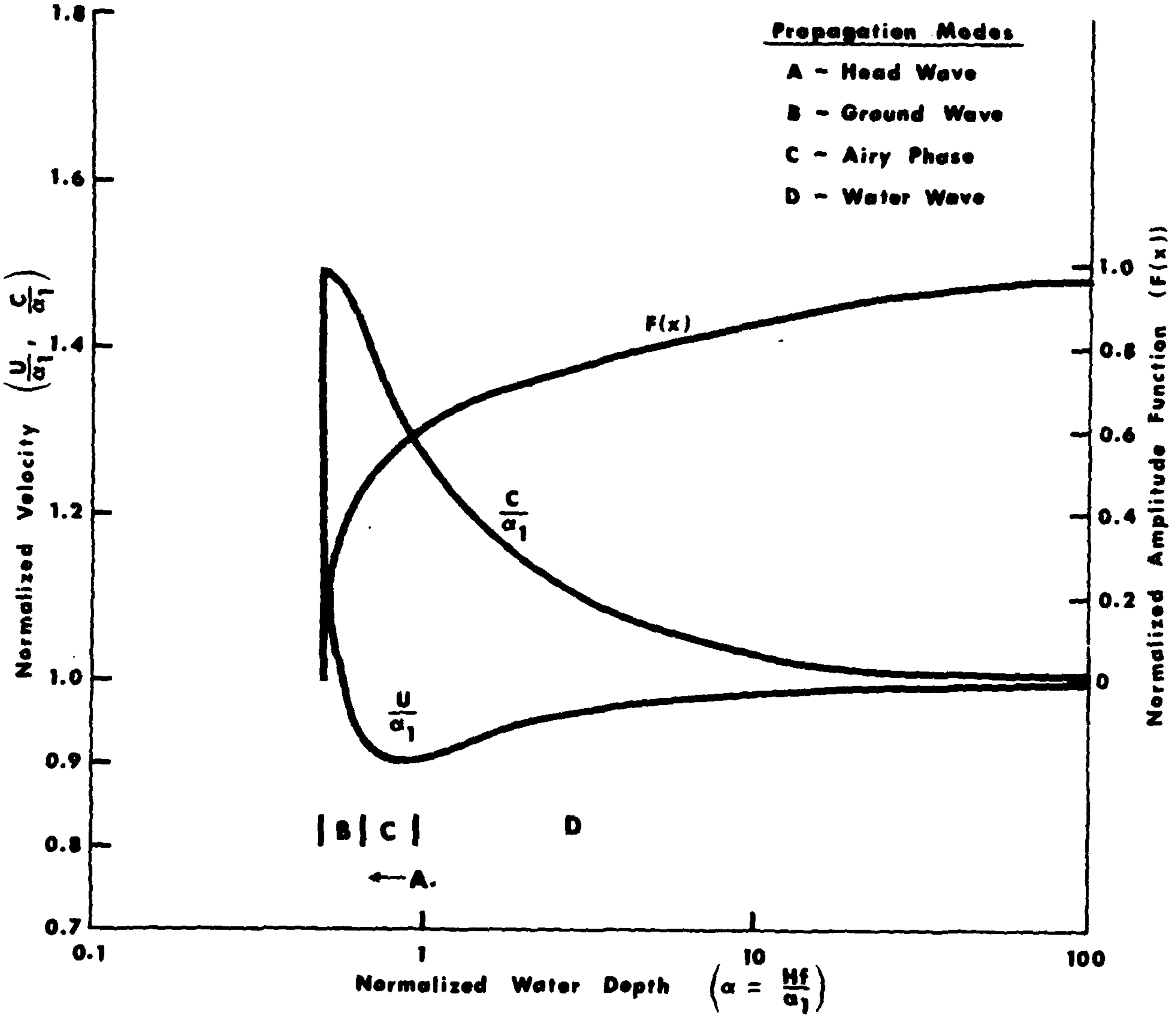

Figure 1. Diagrammatic Sketch Showing the Relationship of Four Propagation Modes with Respect to the Group Velocity, Phase Velocity and Amplitude Function.

Group velocity, U; phase velocity, C; amplitude function, F(x).

entirely in the water and hence attenuation due to absorption by the bottom is small.[5] For energy incident upon a viscoelastic bottom at angles greater than the critical angle determined by the compressional velocities, the energy will be partitioned between reflected compressional energy and refracted shear energy. The observed attenuation at the lower frequencies is mainly due to the energy partition.

The Airy phase occurs at the group velocity minimum. The intensity spreading loss for this wave is $r^{-5/6}$ and the wave is characterized by a high-amplitude signal over its characteristically narrow frequency range.

The ground wave is comprised of the narrow range of frequencies between mode cut off and the Airy phase. The intensity spreading loss is r^{-1}, but the received amplitude is a strong function of frequency being controlled by amplitude function F(x) as shown in Figure 1. The attenuation of the ground wave is controlled mainly by the attenuation in the bottom.

The head waves are also known as "refraction arrivals." The intensity spreading loss is r^{-2} except in special cases where constructive interference takes place in which case it is r^{-1}.[6] Since the trajectory of these waves is totally in the bottom, the attenuation decrements for the several bottom layers are fully applicable to this propagation mode. Therefore, the refraction arrivals tend to disappear quickly with increasing range for sediments having high attenuation. Theoretically, head waves are not restricted to any frequency domain as are ground waves, the Airy phase, etc. However, at long ranges they are always low frequency due to the bottom attenuation which increases with increasing frequency.

The surface and interface waves are only present when the medium has rigidity. For bottom sediments in shallow water, the rigidity characteristics of the viscoelastic model are generally accepted. One of the attributes of this model is that it permits guided propagation with shear wave velocities much lower than the sound velocity in the overlying water medium. True Rayleigh waves are seldom if ever observed from sound sources in shallow water. Horton showed that the particle velocity for a Rayleigh wave assumes a lissajous figure from the attenuation in a viscoelastic solid.[7] A generalized Rayleigh wave, now usually called a "Stonely wave," is often observed during shallow water propagation experiments. This wave shows high amplitude, a narrow dispersive frequency interval and the frequency interval being controlled by the characteristics of the bottom media. For a Stonely wave, the axis of particle motion of the ellipse is vertical for small amounts of shear wave attenuation in the bottom sediment and assumes more of a lissajous shape tilting forward as the attenuation increases. Thus, for highly dissipative sediments, the vertical component of the Stonely wave may be quite small. The dissipation or attenuation of the Stonely wave is proportional to the attenuation decrement for shear waves. The spreading loss for interface waves is $r^{-1/2}$, which is very low, so that their propagation range is largely controlled by the dissipation characteristics of the media. Another characteristic of an interface wave is that it decays exponentially with increasing distance from the interface. As far as can be determined, there are no reported observations of Stonely waves or Love waves along the deeper sediment interfaces or the sediment-basement interface originating from experiments conducted in shallow water.

Propagation through the bottom or at the interfaces is largely controlled by the attenuation decrement per cycle in the media. Thus, it can be concluded that in a high-speed media with long wavelengths, propagation loss in the sediment or basement will be minimal. Under these conditions, the expectation is that sound propagated through the bottom may show a better SNR than sound propagated through the water.

The propagation modes described above may or may not be identifiable in a received signal. The medium may attenuate certain paths so that they are inconsequential when compared to other paths, some propagation modes may not be present due to medium characteristics, and individual modes may be difficult to isolate in a record.

Previous observations of better SNR from geophones as compared to hydrophones were observed over a fine-grained bottom. An experiment was designed to test the relative performance of geophones and hydrophones in an environment having a coarse-grained bottom, preferably a well-sorted sand.

2. DESCRIPTION OF THE EXPERIMENT

2.1 Experiment Site

The large sand-covered shelf south of New England consists mostly of sand of Pleistocene or recent age. Schlee found that most of this underwater plain was covered with sand having a modal grain size between .0625 and 1 mm.[8] More than half of the area has more than a 75% sand content.

In defining the experiment area, the only other experimental constraint was that the water depth be at least 45 m. The site selected is shown in Figure 2. Point L is the receiver location with the L-R radial being over relatively constant depth water, whereas run L-P would be upslope propagation. The areas east and south of Point L have a 2 to 3 m layer of mud (30% silt and clay, 70% sand) overlaying better-sorted sand.[9]

The acoustic bottom structure in the area is shown in Table 1. The structure given by Barakos was determined by geometric dispersion based on normal mode theory, whereas the structure given by Ewing et al. was determined by standard seismic refraction techniques.[10,11] Layers 2 and 3 from Barakos probably represent the single sediment layer of Ewing et al. For long-range propagation, no significant amount of sound energy penetrates to the crystalline basement; therefore, the basement is undetectable by dispersion measurements.

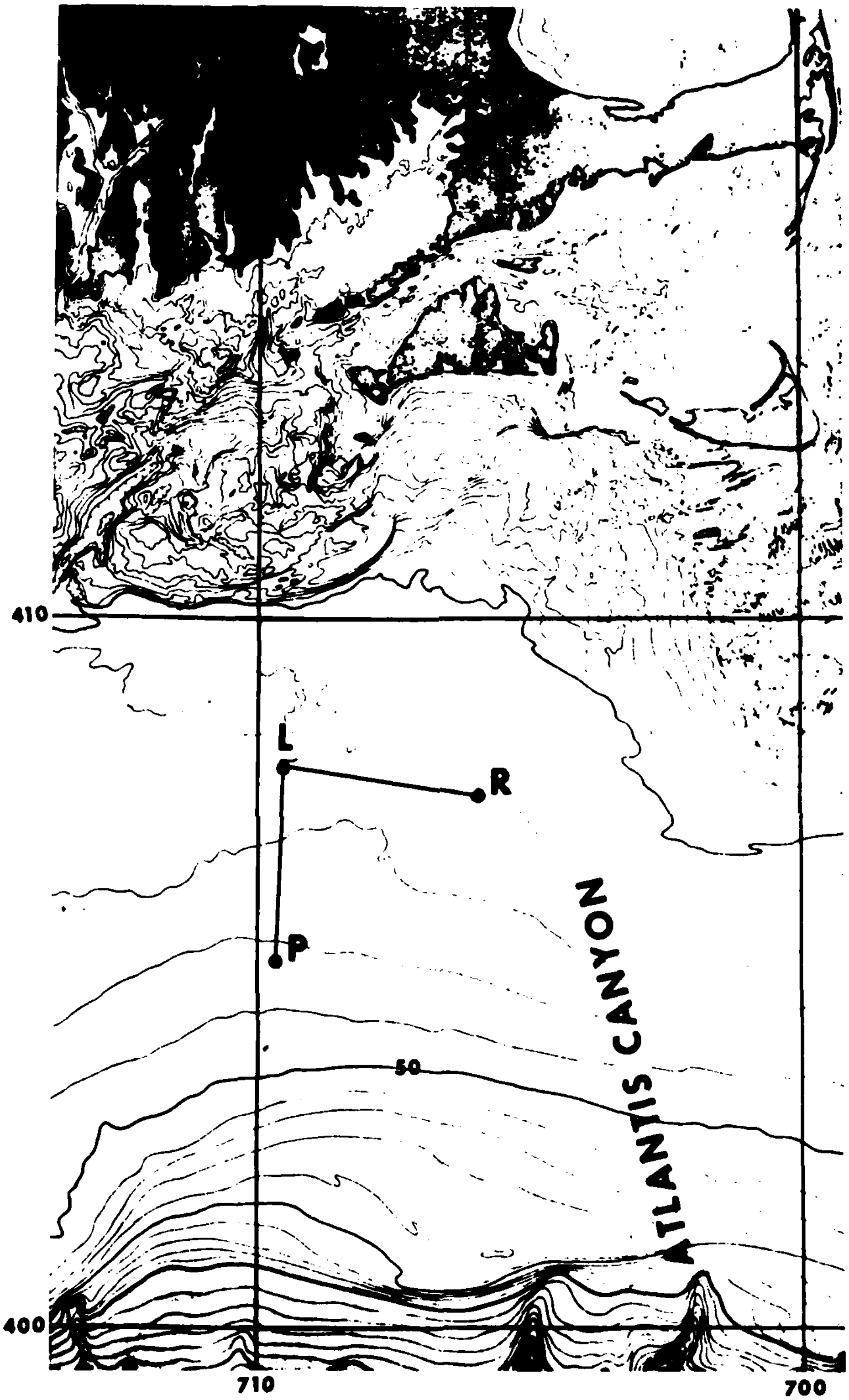

Figure 2. Location of Experiment Site.

Pt. L is the receiver location.

Table 1. Velocities and Thicknesses of Layers in the Areas of the Experiment.

	from Barakos[10]		from Ewing et al.[11]	
Layer No.	Layer Thickness m	Sound Speed m/sec	Layer Thickness m	Sound Speed m/sec
1	55	Water	55	Water
2	170	1555	655	1800
3		1830		5595

2.2 Experiment Description

The experiment was conducted south of Gay Head, Martha's Vineyard on 1 September 1979 in 55 m of water. The receiver consisted of a SENSOR-SM6D triaxial geophone implanted in the bottom and a mechanically isolated hydrophone, an OSTRONICS H-90, supported about 0.4 m off the bottom. Cables brought the signal from the sensor preamplifiers to the recording electronics located in an anchored boat as shown in Figure 3. Details concerning the geophone implantment tool are given in Appendix A.

The experiment consisted of making four runs centered on the receiving boat, dropping a MK 61 SUS charge set to detonate at 18.3 m. The shot signal from the boat was radioed to the receiving ship for recording. The first two runs were east-west runs over a relatively flat bottom from the receiving location to Point R and beyond to a 21 nm range with the return constituting the second run. The third and fourth runs were from the receiving location to Point P and return. On the outgoing runs, the SUS charges were dropped every 0.33 mile to a range of 8 nm and every mile thereafter. On the return runs, the SUS were dropped every 0.5 mile. The shooting boat operated its echo sounder during all four runs and took XBT's at the three designated points. The bathymetry and thermal structure of the water are shown in Figures 4 and 5.

A block diagram of the recording and playback system is shown in Figure 6. The system was calibrated using the insert calibration technique; i.e. a signal is introduced in series with the geophone coil and the hydrophone crystal. The recording and playback system response is shown in Figure 7.

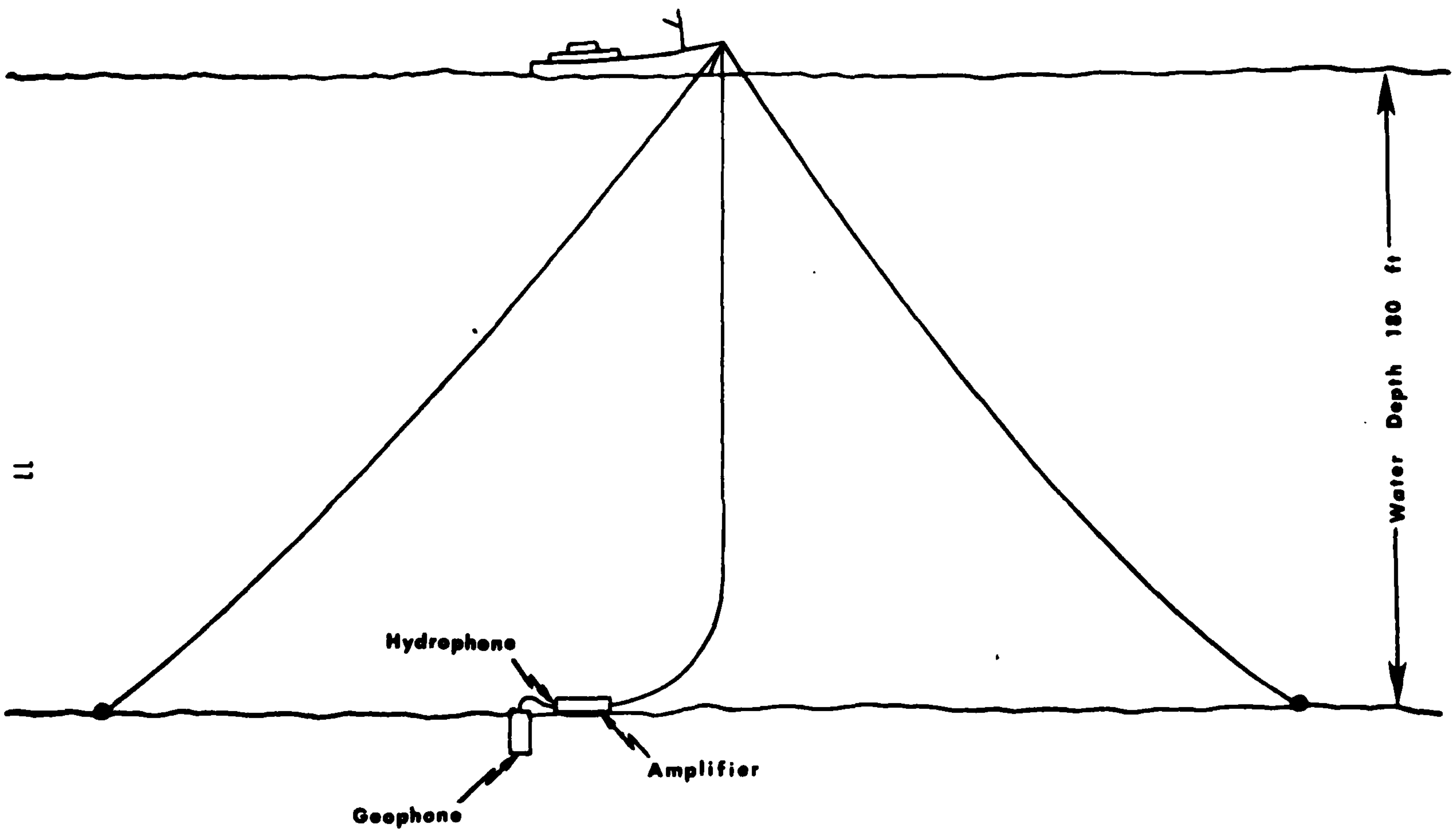

Figure 3. Signal Receiving Arrangement at Pt. L.

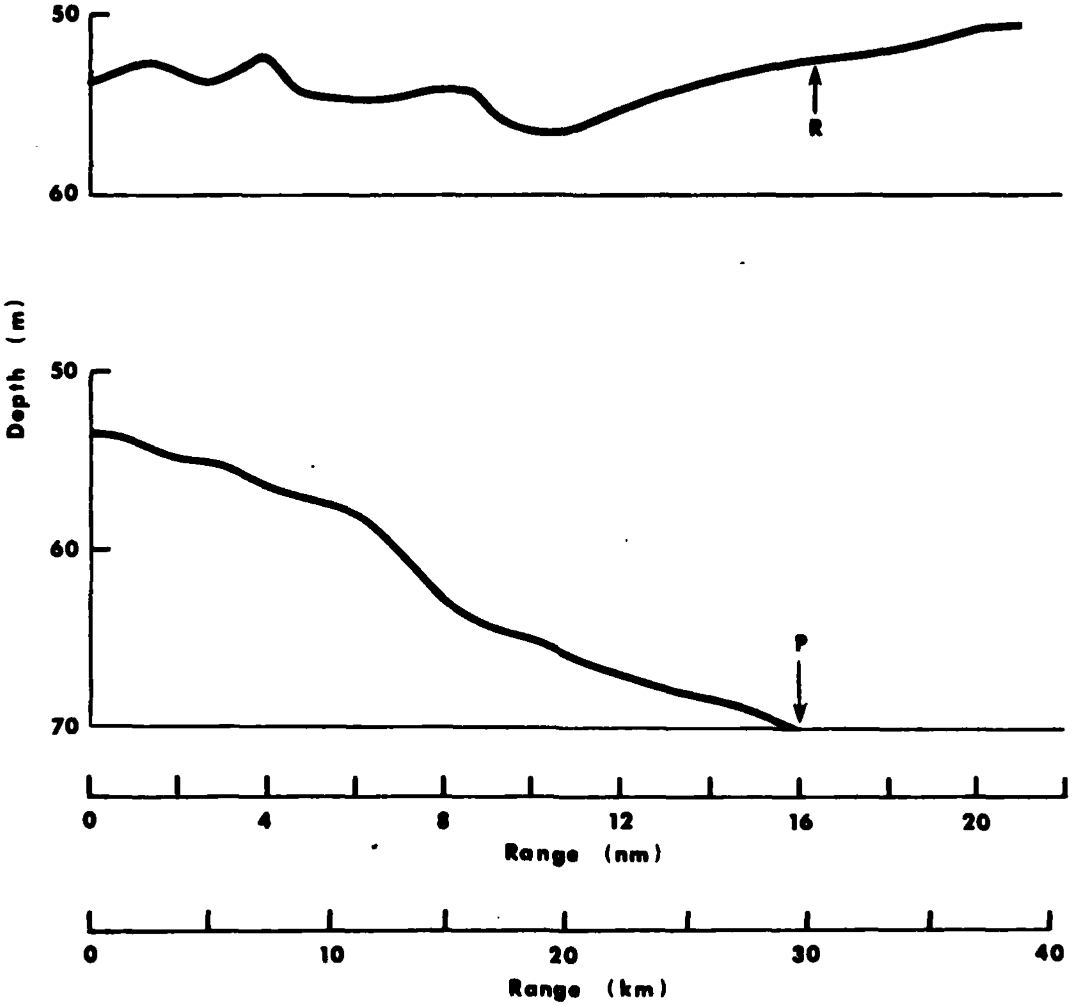

Figure 4. Water Depth Along Propagation Tracks.

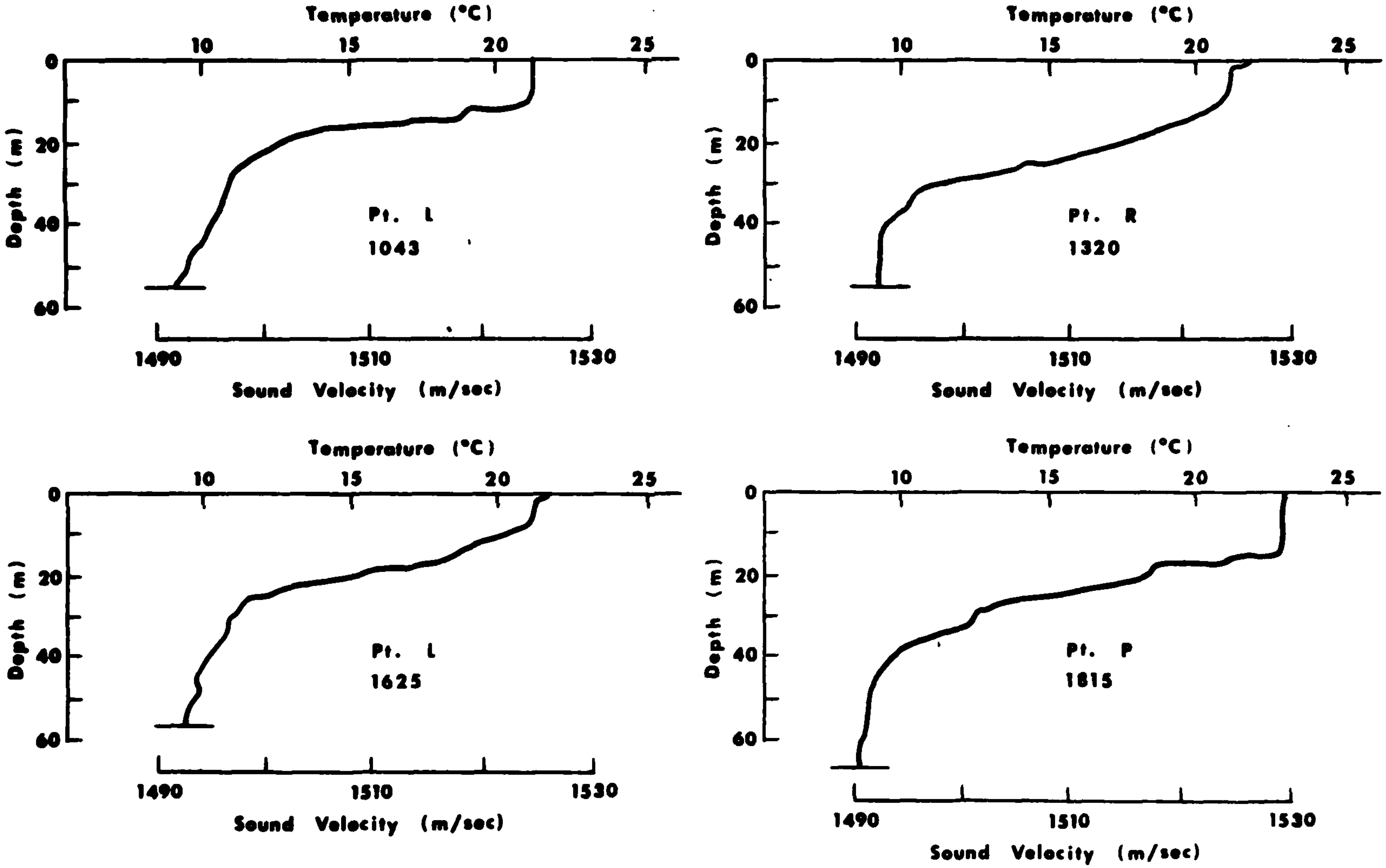

Figure 5. Thermal Structure of the Ocean During the Experiment.

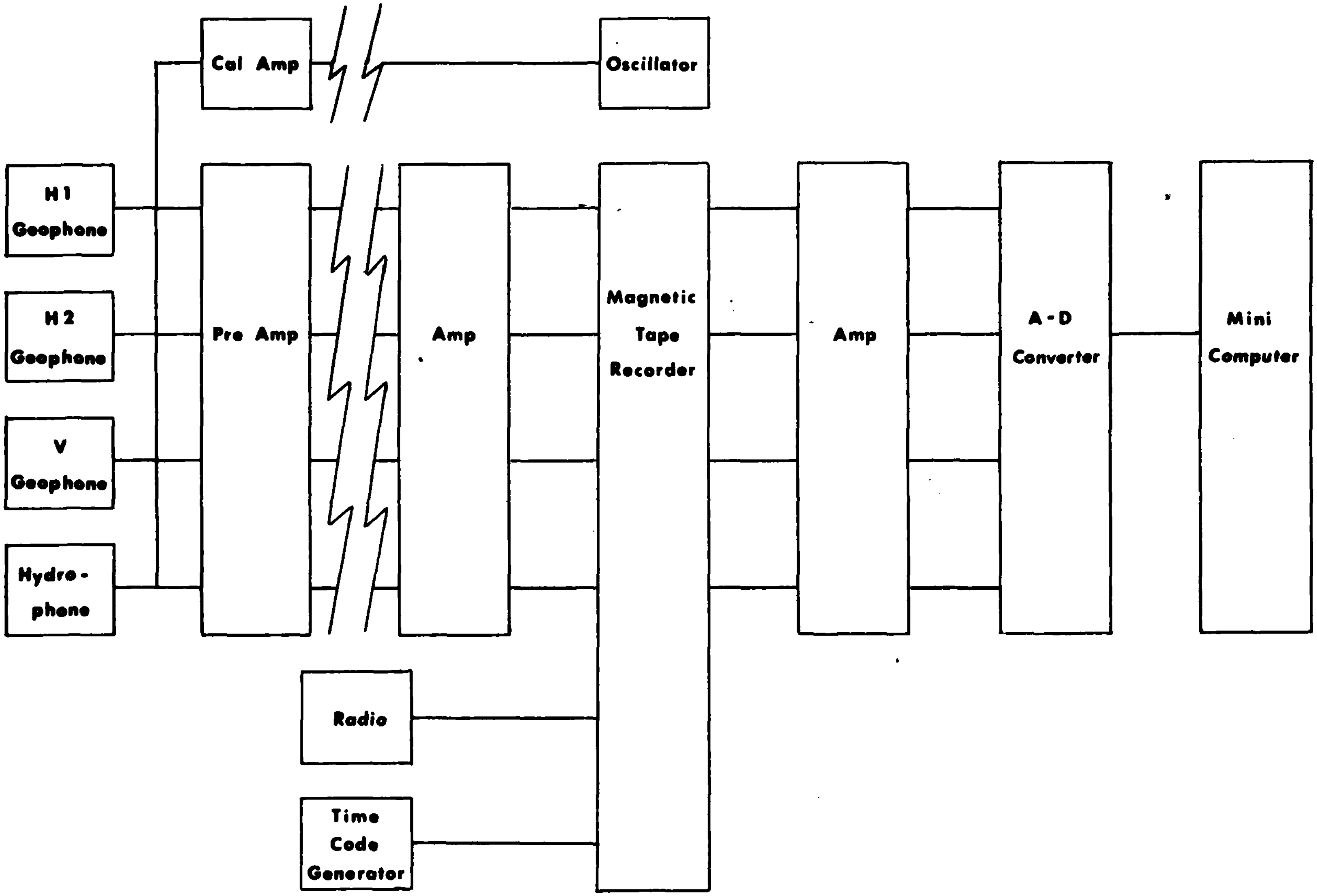

Figure 6. Receiving and Recording System Block Diagram.

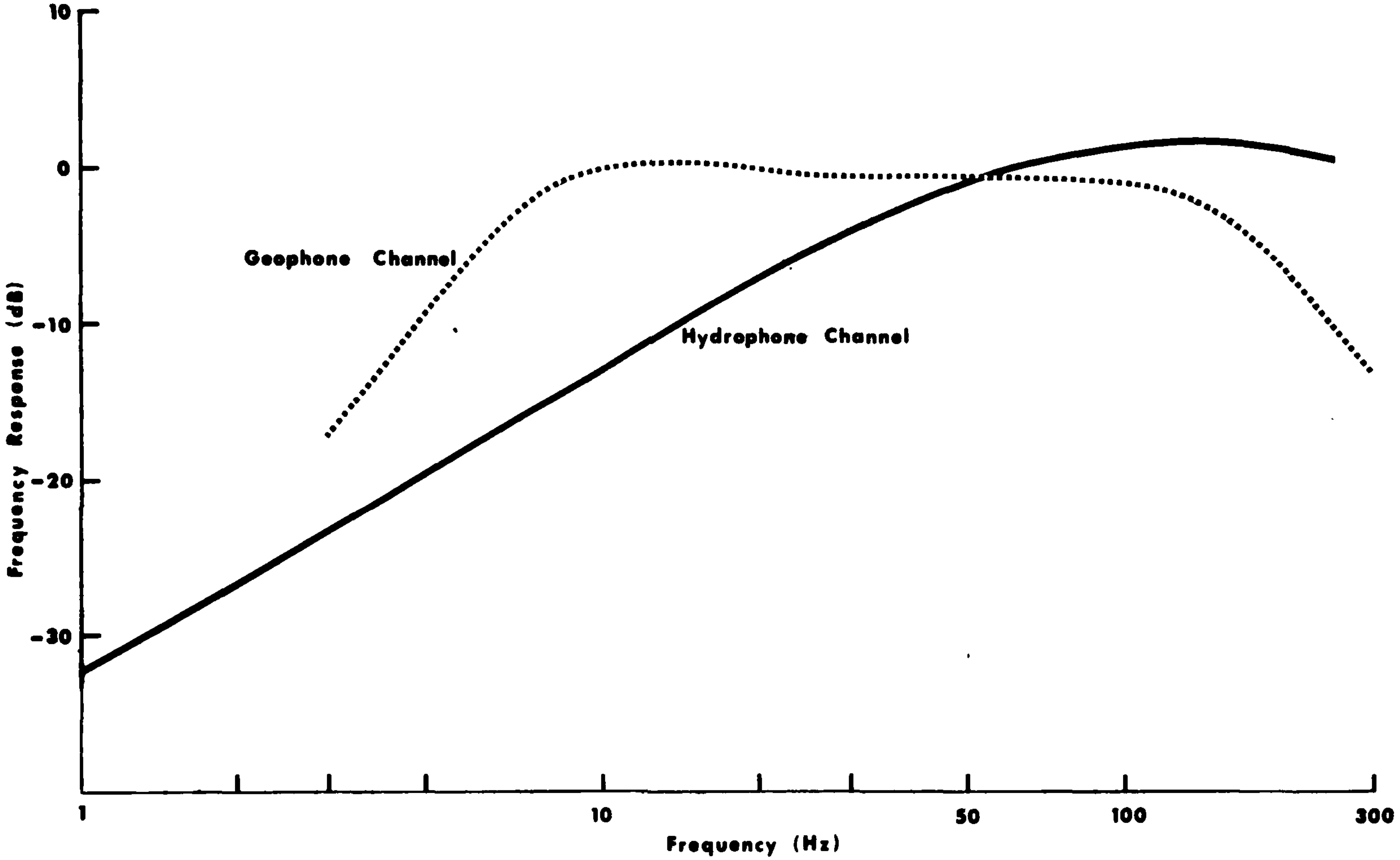

Figure 7. Frequency Response of Geophone and Hydrophone Channels.

During data acquisition, gain settings were maintained to prevent electronic overload on the highest amplitude arrivals. These arrivals undergo the least attenuation and are most useful for ship detection.

During the experiment, some failures occurred. The shot hydrophone and electronics did not function as anticipated and the radio channel was lost which caused the inability to measure travel times to a high degree of accuracy. The number 2 horizontal geophone was no longer recorded after two-thirds of Run 2 because of a cable opening. Run 4 was not recorded due to a magnetic tape threading error.

3. SIGNAL PROCESSING

The data was converted to acoustic intensity levels (erg/sec-cm^2) for the background noise and to energy flux density levels for the SUS signals (erg-sec/cm^2).[12,13,14] With these common references, the received signals from the geophones and hydrophone can be directly compared. Propagation loss was determined using standard 1/3-octave band source levels for a SUS detonated at 18.3 m.[15] Further details concerning the signal processing are contained in Appendix B.

4. BACKGROUND NOISE

Background noise levels were measured before each received SUS signal. At close range, the observed noise levels are system noise. At ranges beyond 15 nm, the monotonic decrease in levels with range indicates that the noise levels may be controlled by the source ship. The background noise spectrum shown in Figure 8 was acquired when the source ship was 19 nm from the receiver. The high-level, low-frequency noise decreases at a rate of 10 dB/octave from 8 to 40 Hz. This noise is believed to be related to the retrieval line attached to the implanter. Noise levels observed when the source ship was at maximum range are comparable to those observed in the Philippine Sea and Mariana Basin.[16]

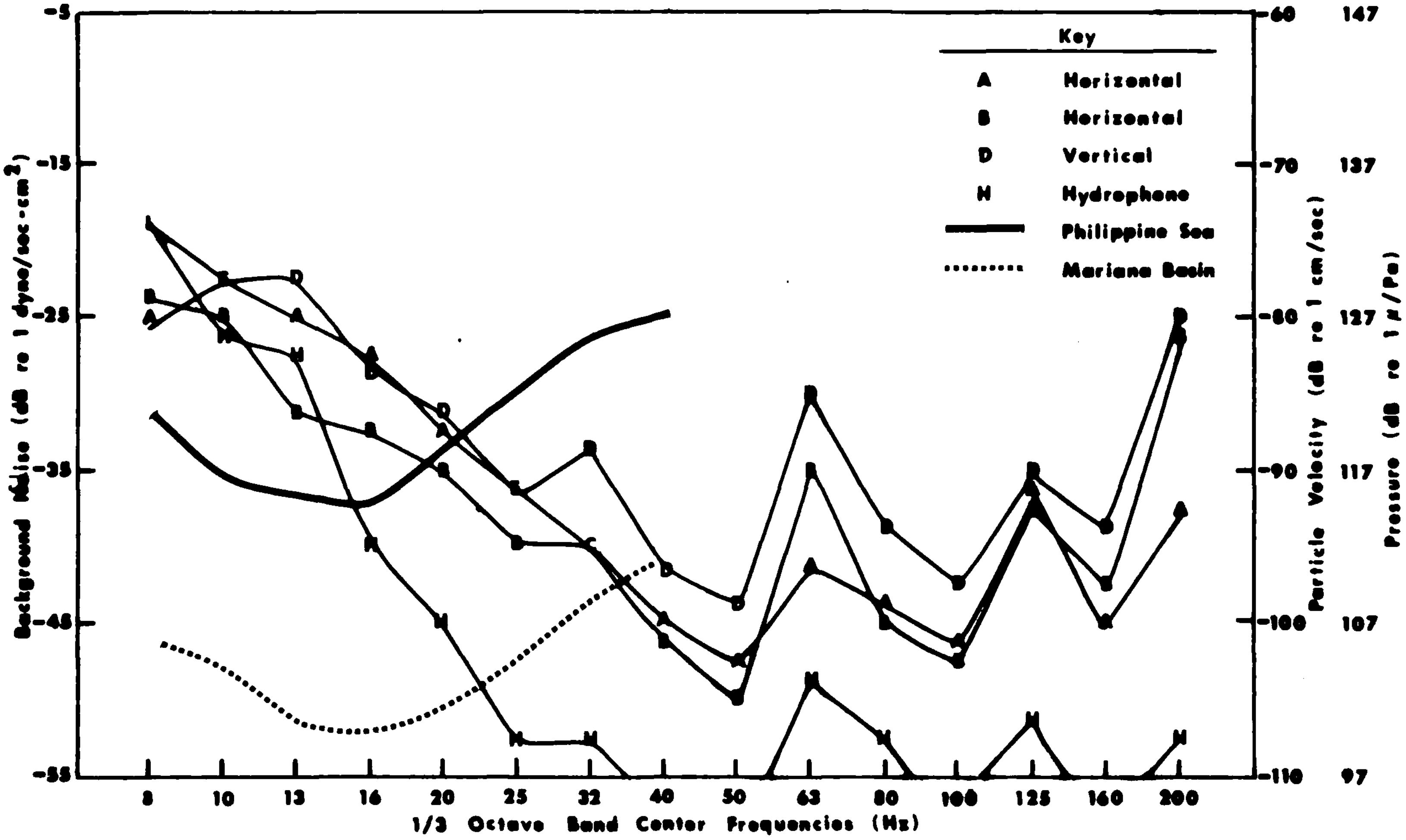

Figure 8. Spectrum Levels of the Background Noise Observed with the Source Ship at a Range of 19 nm.

5. SOUND PROPAGATION

5.1 Background

The propagation of sound in this experiment will be discussed in terms of acoustic arrivals, sound intensity, particle velocity and sound pressure levels. The discussion of the transmission of acoustic energy will be for the medium as a whole instead of attempting to separate certain parts of a signal in terms of seismic or waterborne propagation paths. To relate the observations to previous work, descriptive terminology will be used from both the seismic and ocean acoustic community. Propagation data will be presented and discussed from three different aspects: time series, dispersion and propagation loss.

5.2 Time Series Data

Figures 9, 10 and 11 present pressure and particle velocity vs time for three signals to demonstrate changes in received signal structure as a function of range. Figure 9 shows the received signal from a range of 0.5 nm with a ground wave preceding the arrival of the water wave by 0.07 sec. A large amplitude sinusoidal wave trails the water wave arrival by 1.015 sec. This arrival is most likely a Stonely wave. It differs from most Stonely wave arrivals in that the vertical component is small when compared to the horizontal components. The velocity ratio of these arrivals to the water wave is 1.132 for the ground wave arrival on the hydrophone, 1.108 for the ground wave arrival on the vertical geophones

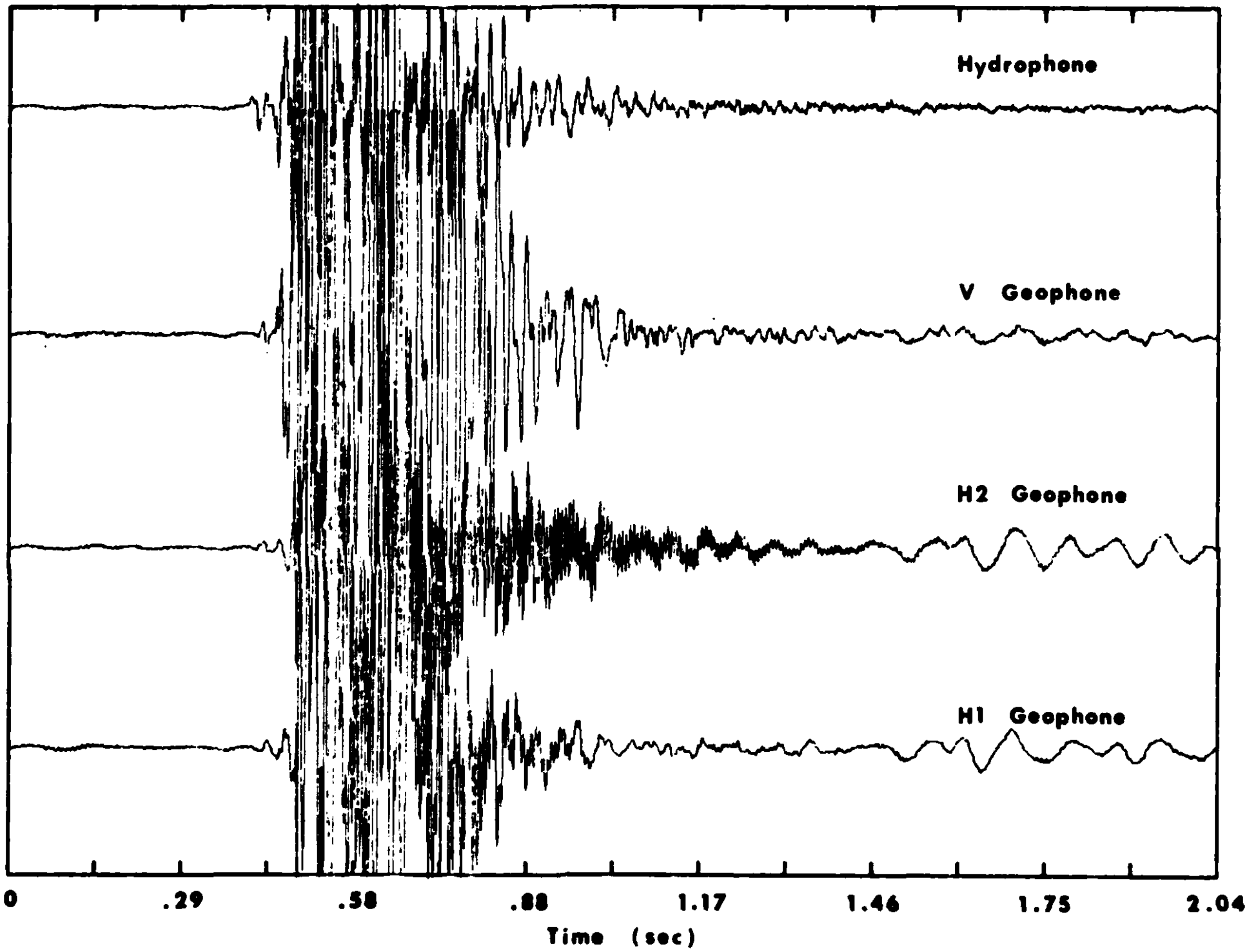

Figure 9. Relative Amplitude of the Received Signal for the Four Sensors at a Range of 0.5 nm.

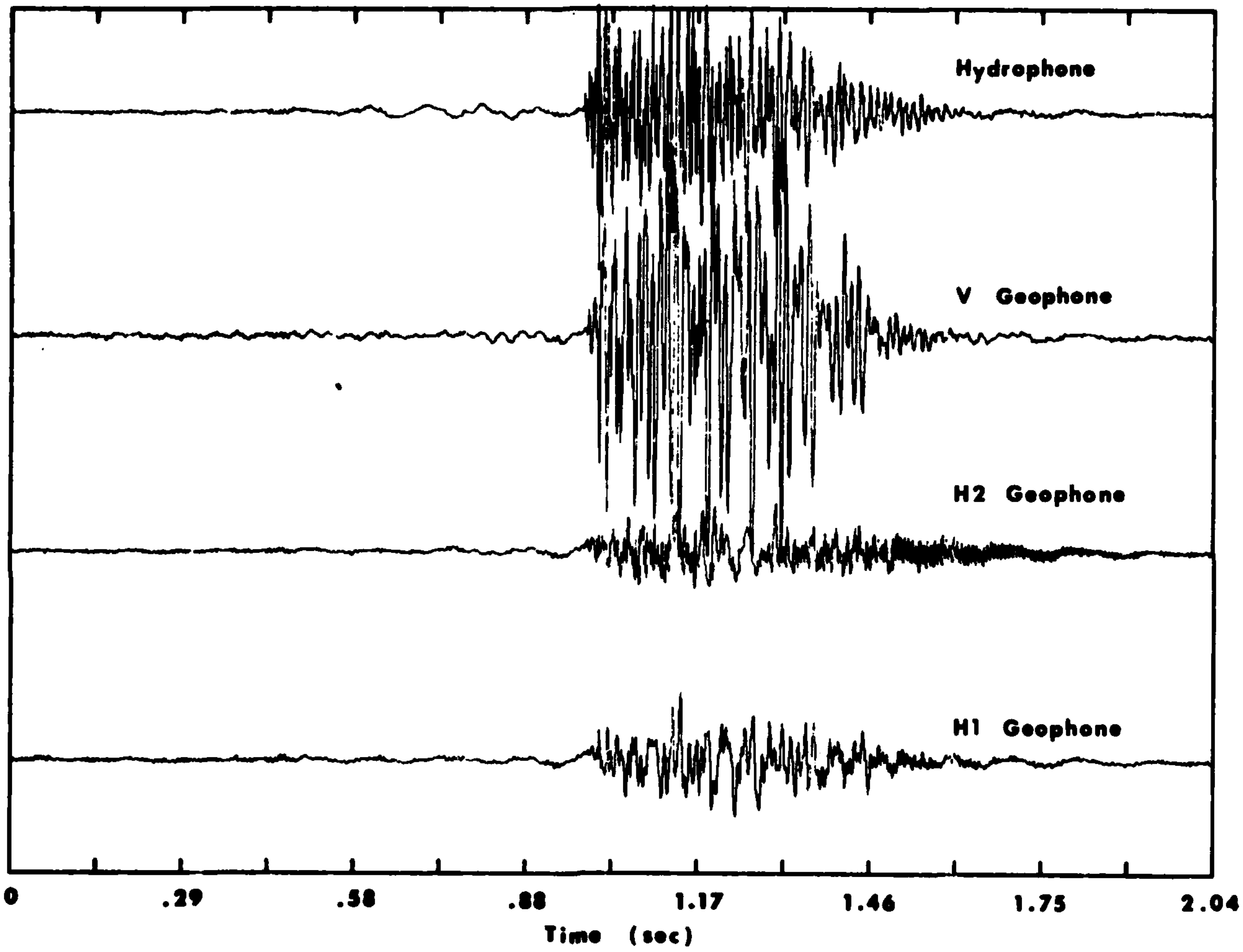

Figure 10. Relative Amplitude of the Received Signal for the Four Sensors at a Range of 3 nm.

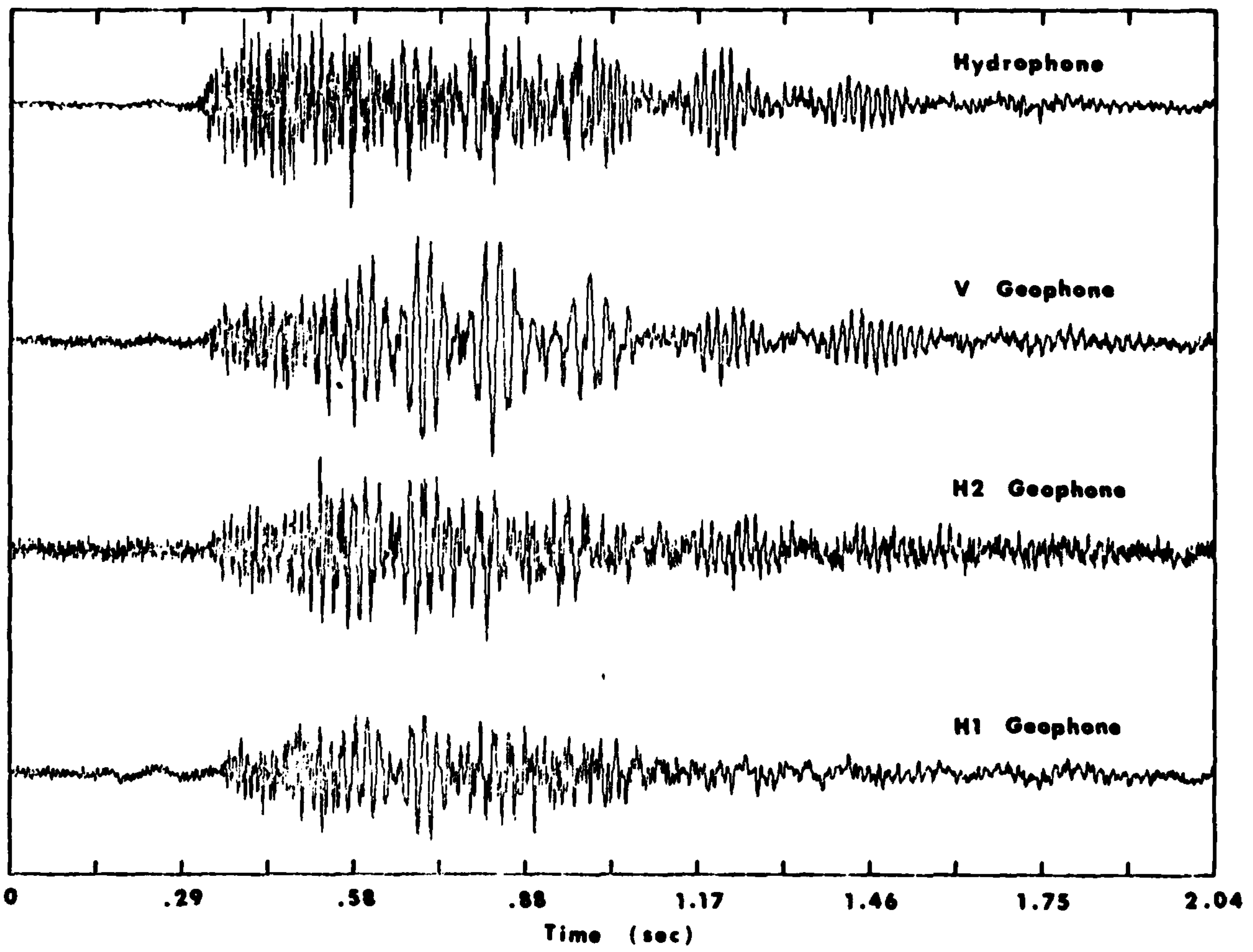

Figure 11. Relative Amplitude of the Received Signal for the Four Sensors at a Range of 19 nm.

and 0.38 for the Stonely wave arrival on the horizontal geophone. The shear wave velocity, computed from the Stonely wave velocity, was found to be 680 m/sec.[17]

The phase relationships of the last cycle of the ground wave for the four sensors are:

Hydrophone	0°
Geophones:	
Vertical	180°
Horizontal-2	90°
Horizontal-1	0°

The high-frequency wave that is prominent on Horizontal-2 is believed to be an artifact; the same signal at lower amplitude is also present on Horizontal-1.

The received signal structure at a range of 3 nm is shown in Figure 10. The structure of the arrivals has changed significantly. The Stonely wave is no longer visible, the well-defined low-frequency ground wave from the vertical sensor is greatly reduced in amplitude and the frequency has increased to 35 Hz. The relative amplitudes of both horizontal sensors with respect to the vertical sensor have decreased significantly. The next signal at a range of 3.33 nm does not show any ground waves and none are evident at the longer ranges.

The received signal structure at a range of 19 nm is shown in Figure 11. For the vertical geophone arrival, the frequency of the first arrival decreases to about 35 Hz in the Airy phase. This is followed by the beginning of another high-frequency arrival that also decreases in frequency. The approximate 10 Hz wave in front of the Horizontal-1 arrival is considered to be noise from the recovery line. The arrival structure of three representative received signals shows the changes in signal from Run 1. The most notable deviation from the expected structure is the lack of low-frequency ground waves at these ranges.

5.3 Dispersion

The experiment environment is comprised of a water layer over one or more sedimetary layers resting on a crystalline basement. Dispersion in this environment is the result of layer thickness, density and velocity profiles within this waveguide.[18] The normal structure of the bottom in the shallow water environment is increasing sound velocity and density with depth. In this type of environment, the sound is channeled between the surface and some depth; 99% of the energy in the bottom is trapped above the depth of penetration.[19] Thus, frequency dispersion shows the effect of the medium on propagation and can be used to obtain information about the bottom to the depth of penetration.

The observed frequency dispersion for the 3-mile shot is shown in Figure 12. The most notable observation is the preceding ground wave at 35 Hz on the vertical sensor. The wave is present to a lesser extent on the other three sensors. Two modes are clearly visible on the dispersion curve for the signal received from 19 nm range in Figure 13. No ground waves are obvious. For the 19 nm shot, a normalized dispersion curve was measured from the half-periods and periods of the time series from the vertical seismograph, as shown in Figure 14. The observed dispersion curves of Barakos are shown for comparison. The sound velocity profiles in the water were similar for all three sets of data; the overall gradient

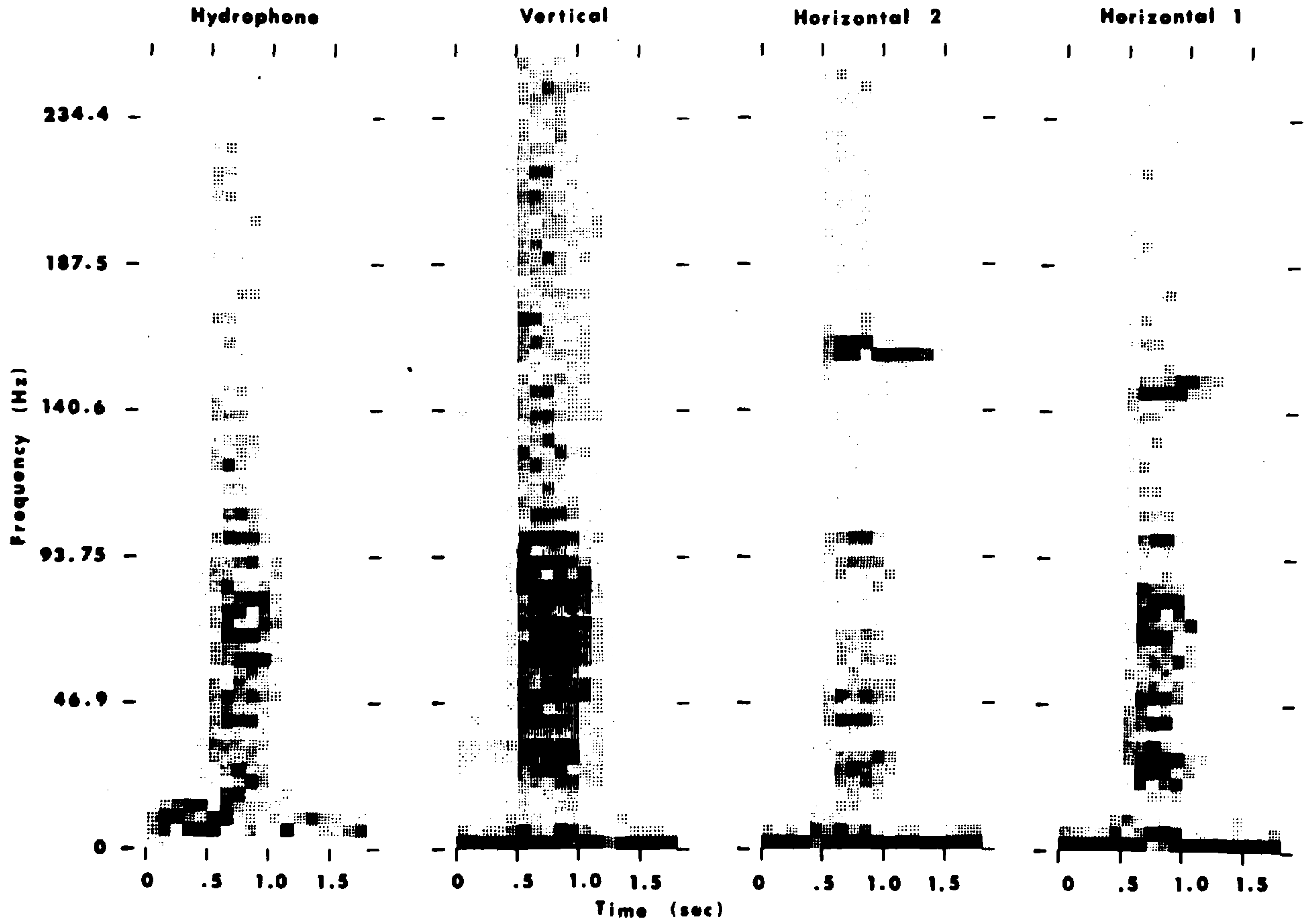

Figure 12. Geometric Dispersion from a Shot at a Range of 3 nm.

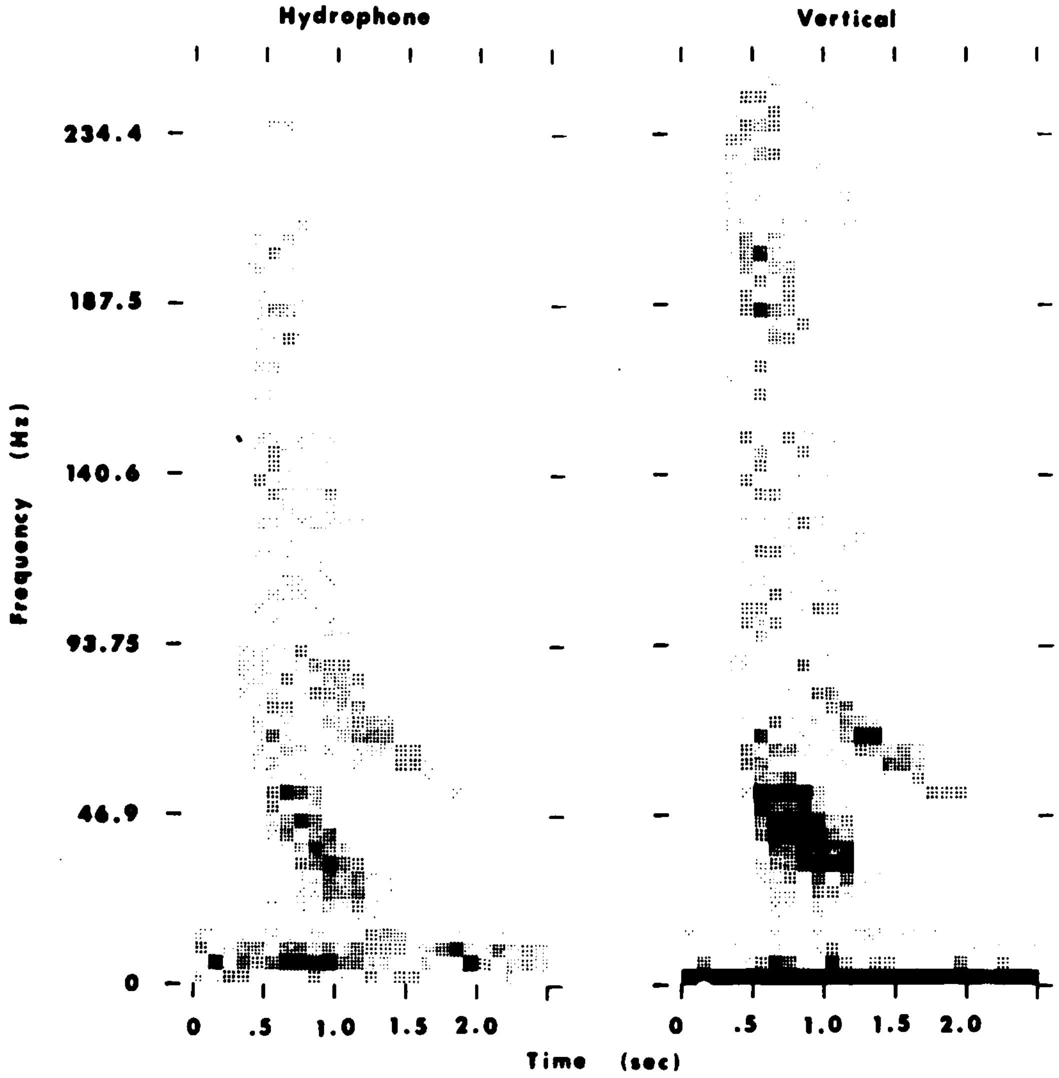

Figure 13a. Geometric Dispersion from a Shot at a Range of 19 nm.

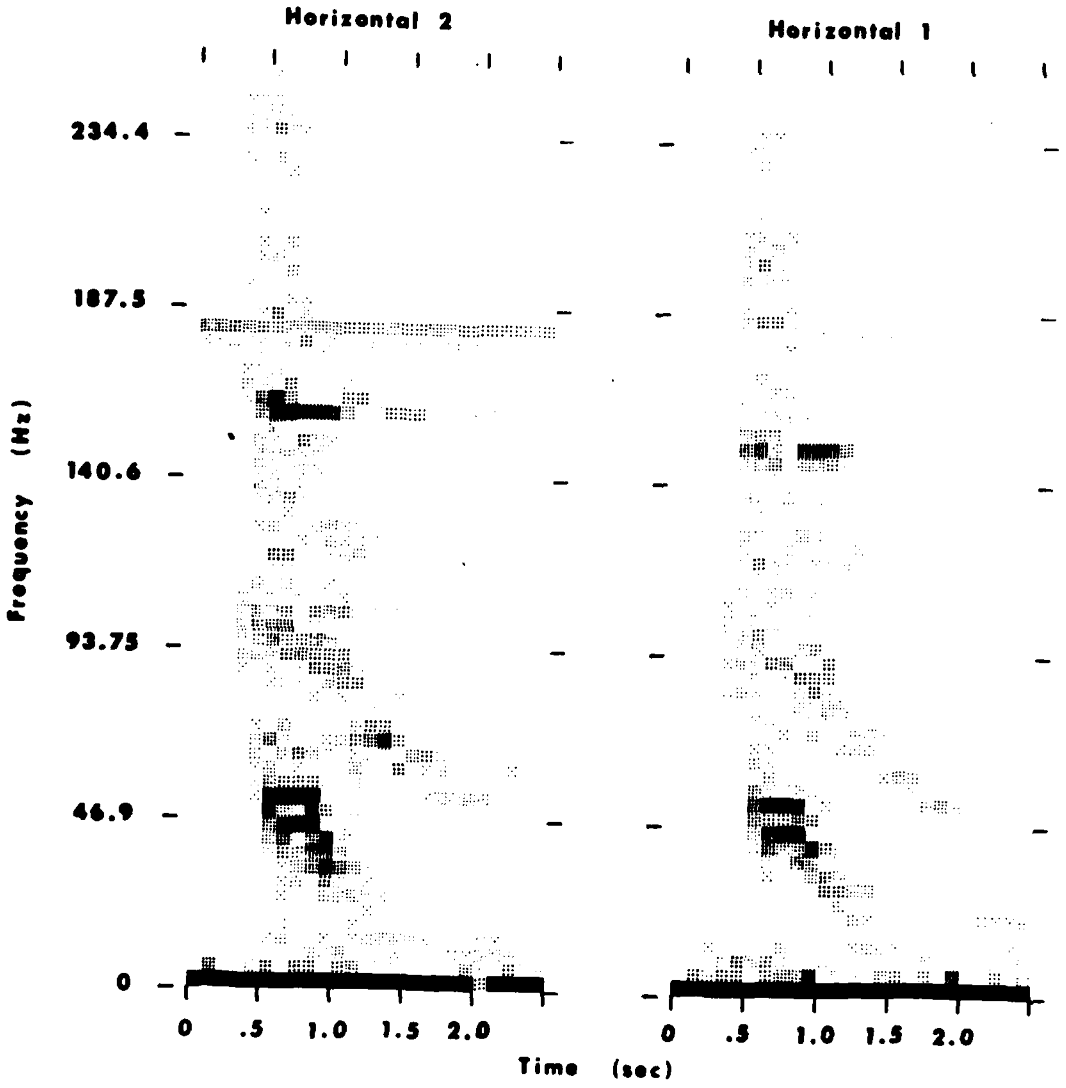

Figure 13b. Geometric Dispersion from a Shot at a Range of 19 nm.

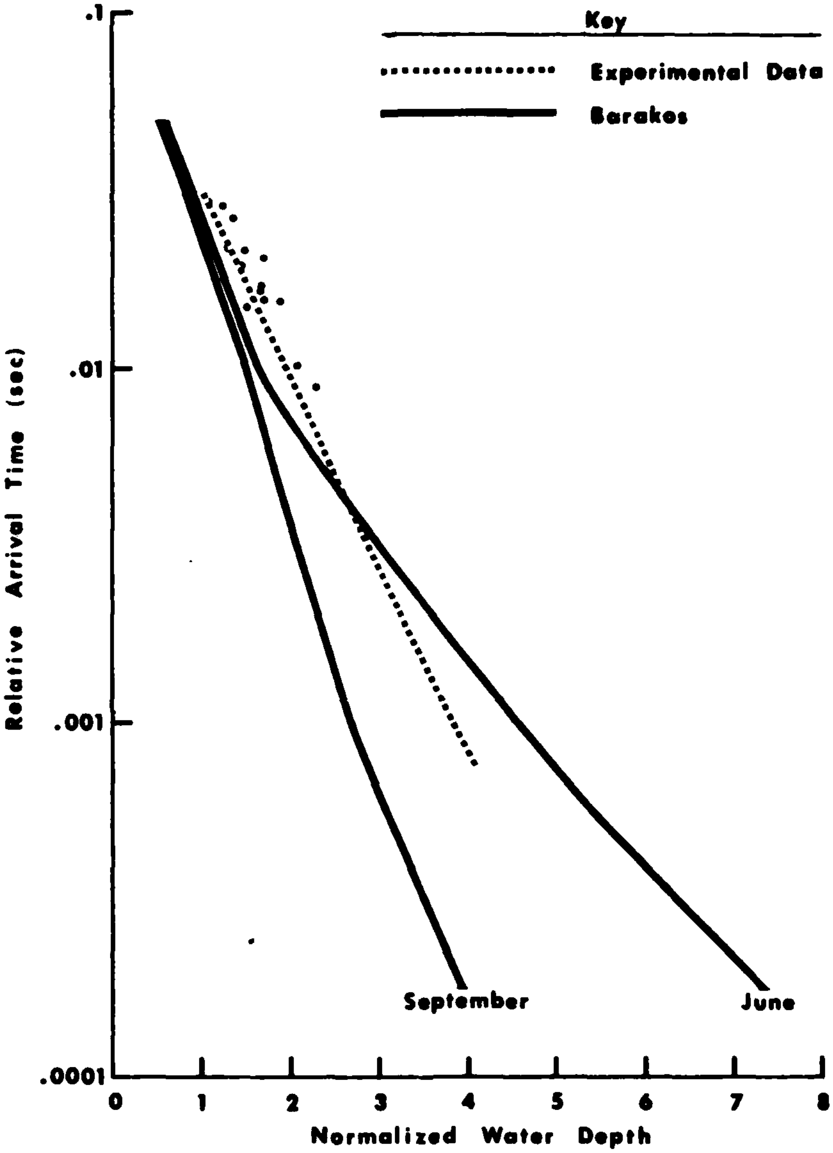

Figure 14. Normalized Geometric Dispersion Curve from a Shot at 19 nm in Relation to Curves from Barakos.

was strongly negative. The June profile and the profile from this experiment are the most similar, and so are the dispersion curves. Barakos concluded from his measurements made during isovelocity conditions that the velocity of the bottom is effectively 5100 ft/sec with a layer thickness of 550 ft.[10]

5.4 Propagation Loss

Observed signal propagation during the experiment showed several distinct features. In the frequency range of 8 to 16 Hz, the propagation loss on the hydrophone was less or about equal to that on the geophones. For the frequency range of 30 to 200 Hz, the vertical geophone had lower propagation loss than the hydrophone or the horizontal geophones. A complete set of plots of propagation loss vs range are presented in Appendix B.

Propagation loss determined from hydrophone measurements refers to the difference in energy flux density at a 1 m reference range from the source and the apparent flux density based on a pressure measurement and the assumption of plane wave conditions at the receiver (strictly speaking, the assumption of the ρc impedance condition is sufficient). It is a measure of the difference between the observed pressure level and the pressure level for a plane wave in free field whose flux density is equal to that of the source actually employed. This is a standard well-understood procedure in underwater acoustics. The propagation loss curve as a function of range can be interpreted as the apparent reduction in energy flow from source to receiver. When multiple paths or modes are present, the phase relationships effect the measured pressure so that a measurement at any one point does not yield the true energy flow. Smoothed propagation loss curves based on incoherent summation of the energy propagated along each multipath or mode closely approximates the true reduction of energy flow, particularly at long range where the propagation paths are all near horizontal. (Note: This can only be done mathematically or by an appropriate sum of signals from a hydrophone array.)

When measurements are made with a geophone, the vector components of a particular velocity component are measured. To compute an analogous "propagation loss" for each of these components, the measured particle velocity is also associated with a plane wave and ρc impedance conditions. However, in this case, the plane wave is assumed to be propagating in the direction of the particle velocity component. For the vertical component this corresponds to a vertically propagating wave in contrast to the horizontally propagating wave in the case of a pressure measurement at long range. Thus the "propagation loss" curve derived from the vertical component of velocity has a very complex relationship to the outward flow of energy and should not be interpreted in terms of the reduction of energy flow with range.

Yet, comparisons between the "propagation loss" curve for pressure and particle velocity measurements are useful because they relate the relative change in level of the two measured quantities. Any other interpretation of the propagation loss curves based on the geophone measurements should be approached cautiously.

A typical low-frequency propagation loss for the hydrophone and triaxial geophones is shown in Figure 15. The individual values are reasonably well clustered except at 8 Hz. The most notable result represented by this measurement is the low propagation loss. By using all the propagation loss curves in the frequency range of 8 to 20 Hz, an empirical spreading loss term in dB of 10 Log R + 20 is obtained with R in meters. The constant 20 represents spherical spreading to a range of 100 m. On cursory examination, the short range to which spherical spreading apparently takes place opens the measurements to question. Measurements of calibration signals during the test and the computation of the expected signal level from the gains and losses of the individual components making up the system compare within 2 dB at 50 Hz. Part of the observed difference is undoubtedly due to the loss in the 500 ft signal cables which were not measured as a component. Since the measured propagation loss values are low enough to be questionable and the system calibration shows a properly working system, potential causes of the low propagation loss will be examined.

The sensor implantment technique is similar to that used by McLeroy.[4] The hydrophone is located about 0.4 m above the bottom and the geophones are in the top 0.4 m of the bottom. The main difference is that the geophones for McLeroy's experiment were implanted by driving and in this experiment they were remotely implanted. Since the low propagation loss occurs on the hydrophone as well as on the geophones, the implantment technique used appears to have little affect on the observed low propagation loss values.

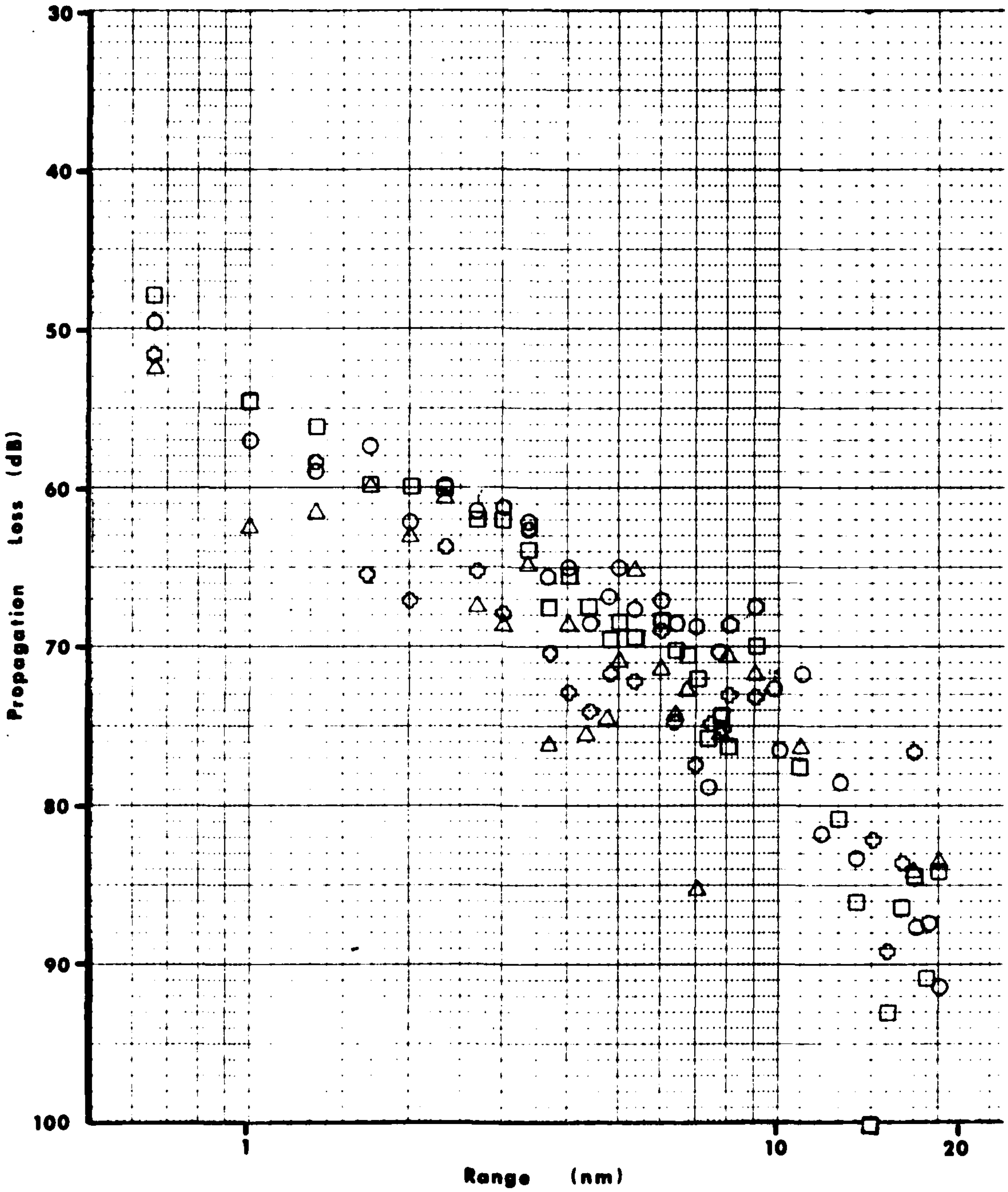

Figure 15. Measured Propagation Loss for Run 1 at a Frequency of 12.6 Hz.

○ = Hydrophone. Triaxial Geophones: △ = Vertical, □ = Horizontal-2,
⬡ = Horizontal-1.

Pekeris states that the normal modes are not orthogonal in his development of the normal mode theory for shallow water sound propagation for media of differing densities.[19] Tolstoy and Clay are careful to define orthogonality for the water medium and discuss the bottom as being unimportant because the greatest part of the sound energy is within the water column with only an insignificant part in the bottom.[20] Clay and Medwin give the conditions for orthogonality with the assumption that both the velocity and density profiles are continuous well-behaved functions.[18] This latter requirement can be difficult to attain at the water-sediment boundary for a hard bottom. For an elastic bottom, the maximum porosity is less than 50% and depending on the sorting the porosity can be as low as 25%. Nominal values of porosity in undisturbed sand sediments determined by ground water hydrologists by pumping tests and recharge cycles is 30% to 35%. If we assume a density of 2.7 for the sand particles, then the composite density for the sediment layer of the bottom is 1.8. This creates a discontinuity in the density-depth profile at the water-bottom boundary.

The top part of the bottom is often thought of as a loaded fluid. With this concept, a more gradual change in the density profile would be anticipated. In shallow water, less than 30 m in depth, wave motion continually works the bottom sediment, creating a layer that may be associated with the loaded-fluid theory. At greater depths on the shelf, the currents tend to sweep the bottom clean of any disturbed layer resulting in undisturbed sediment very close to the water-bottom interface. For the Martha's Vineyard experiment in a water depth of 55 m, the sediment at the water-bottom interface is believed to be undisturbed. Therefore, the density profile for the experimental data will be non-continuous at the bottom resulting in the modes being non-orthogonal. Junger and Feit show that the modes developed in a submerged plate are non-orthogonal and coupled, thereby interchanging energy in proportion to a coupling coefficient.[21] A treatment of the coupling coefficients for shallow water parameters have not been found in the literature. One would expect that the sharper the discontinuity in the density profile, the greater the coupling. Thus, interpretation of measurements made close to the water-sediment interface using modes assumed to be orthogonal can be in error unless a correction for mode coupling is made.

Figure 16 shows that if the angles at the source for the two ray families are compared, the subtended solid angle for the refracted-bottom reflected (RBR) family is twice as large as for the surface-bottom reflected (SBR) family. From this larger included angle at the source for the RBR family, one would expect a greater amount of energy to be present in the RBR family than in the SBR family. The higher level of the main mode (the dark areas in Figure 13) attributed to the RBR family is consistent with this analysis of energy radiated from the source.

From a straightforward geometric ray tracing analysis, an understanding of the low propagation loss can be attained. Figure 16 shows the critical ray paths for the linearly segmented sound speed profile computed from the XBT data at the receiving site. Using 1555 m/sec for the sound speed in the bottom, the critical incident angle at the water-bottom interface is 73.8° for compressional waves corresponding to 75° at the source. The critical angle ray reflects from both the

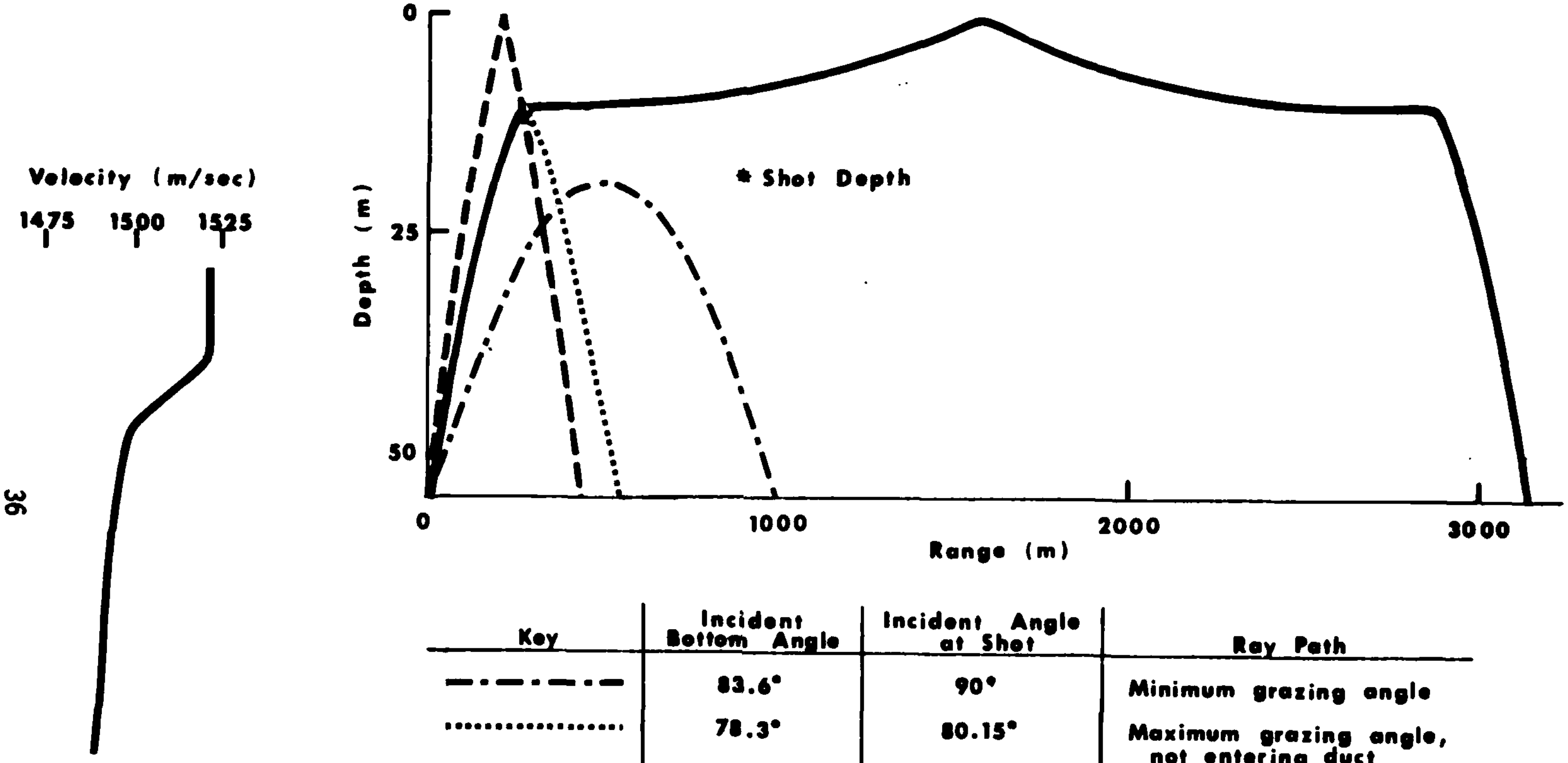

Key	Incident Bottom Angle	Incident Angle at Shot	Ray Path
— · — · —	83.6°	90°	Minimum grazing angle
··················	78.3°	80.15°	Maximum grazing angle, not entering duct
———	78.3°	80.15°	Minimum grazing angle, entering duct
— — — —	73.8°	75°	Maximum grazing angle, θ_c

Figure 16. Critical Ray Paths for the Computed Sound Velocity Profile at the Receiving Site.

surface and the bottom (SBR) and has a loop length of 440 m. The SBR ray with the largest incident angle at the bottom has a loop length of 3125 m. This long loop length is caused by the well-developed surface duct. Because of the negative gradient profile, a family of RBR ray paths exist that are bounded by the two ray paths, one of which vertexes at the bottom of the surface duct and the other at the 18.3 m SUS depth. The SBR and RBR ray families are represented in the dispersion curves of Figure 13 by the two modes, the higher frequency mode being caused by the SBR family.

If we apply energy conservation principles and assume that all rays which strike the bottom at grazing angles less than critical are reflected back into the water media without loss, the spreading loss measured on the hydrophone is readily predictable. Neglecting the high angle rays which do not contribute at long range, spherical spreading should be observed to a range of $R_0 = H/2 \tan \theta$, when H is the water depth and θ is the angle to the horizontal subtended at the source for the critical angle ray. For $H = 55$ m and $\theta = 15^\circ$, we obtain $R_0 \approx 100$ m. At longer range cylindrical spreading is approached, yielding observed spreading loss of $10 \operatorname{Log} R + 20$. In actuality some losses do exist for the reflection of rays which strike the bottom at grazing angles less than critical, resulting in an additional term, $\alpha_0 R$, which when added to the spreading loss yields the propagation loss.

The interpretation of the measured propagation loss for attenuation follows Tolstoy.[22] We assume a complex wave number of the form $(K + i\alpha)$ where α is the attenuation coefficient. The computed attenuation per meter for the signal from the hydrophone is shown in Figure 17 for

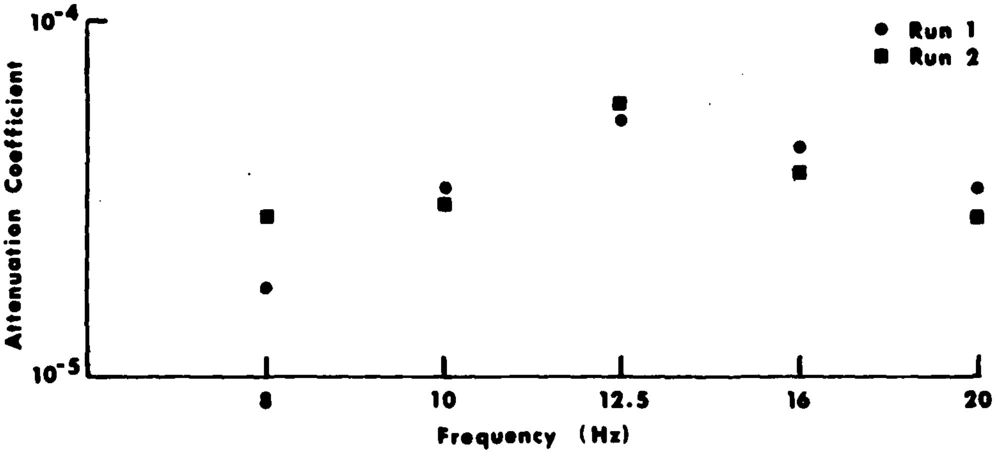

Figure 17. Attenuation Coefficients for Runs 1 and 2.

frequencies of 8 to 20 Hz. The observed attenuation is approximately an order of magnitude lower than that observed by Tolstoy. The lower attenuation can be attributed to the bottom being a better reflector when the bottom damping is high. The high bottom damping is confirmed by the flattened ellipsoid of the Stonely wave.

A comparison of the efficiency of the vertical geophone with the hydrophone as a sensor of acoustic energy was made as a function of frequency. The comparison was made by subtracting the propagation loss observed on the hydrophone from that observed on the vertical geophone. The result for the frequency range of 8 to 200 Hz is shown in Figures 18 and 19. The figures illustrate the spread in values observed for all ranges as well as the average value.

The phenomenon of a vertical geophone sensing larger amplitudes than the hydrophone is not unexpected, but has not been observed previously to the author's knowledge. Ewing et al. predicted that a vertical geophone would be better than a hydrophone at a pressure node. The RBR and SBR families are each made up of many modes and it is possible that one or more of the nodes have a pressure node at the bottom.

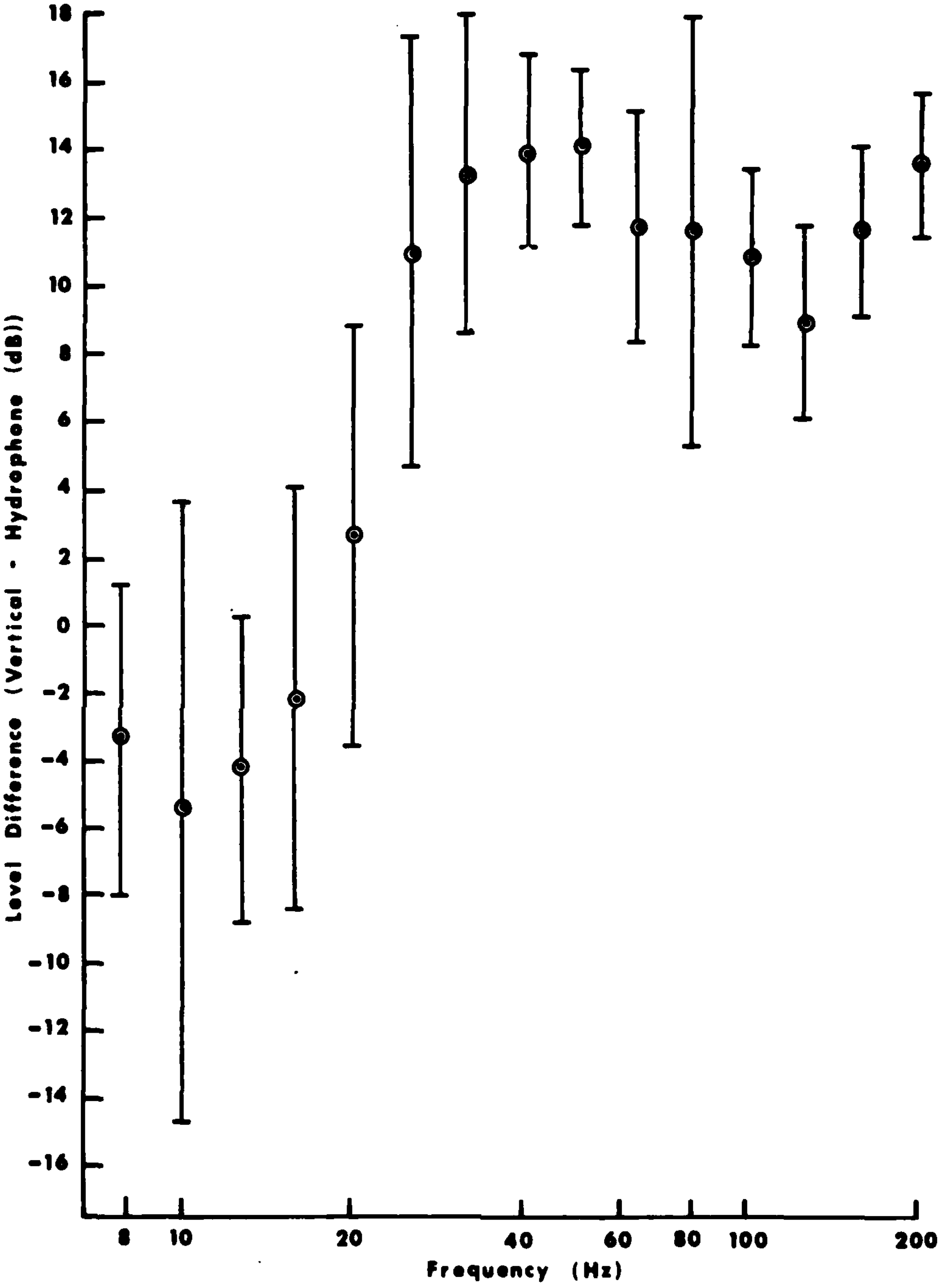

Figure 18. The Difference in Measured Propagation Loss Between the Vertical Geophone and the Hydrophone as a Function of Frequency, Run 1.

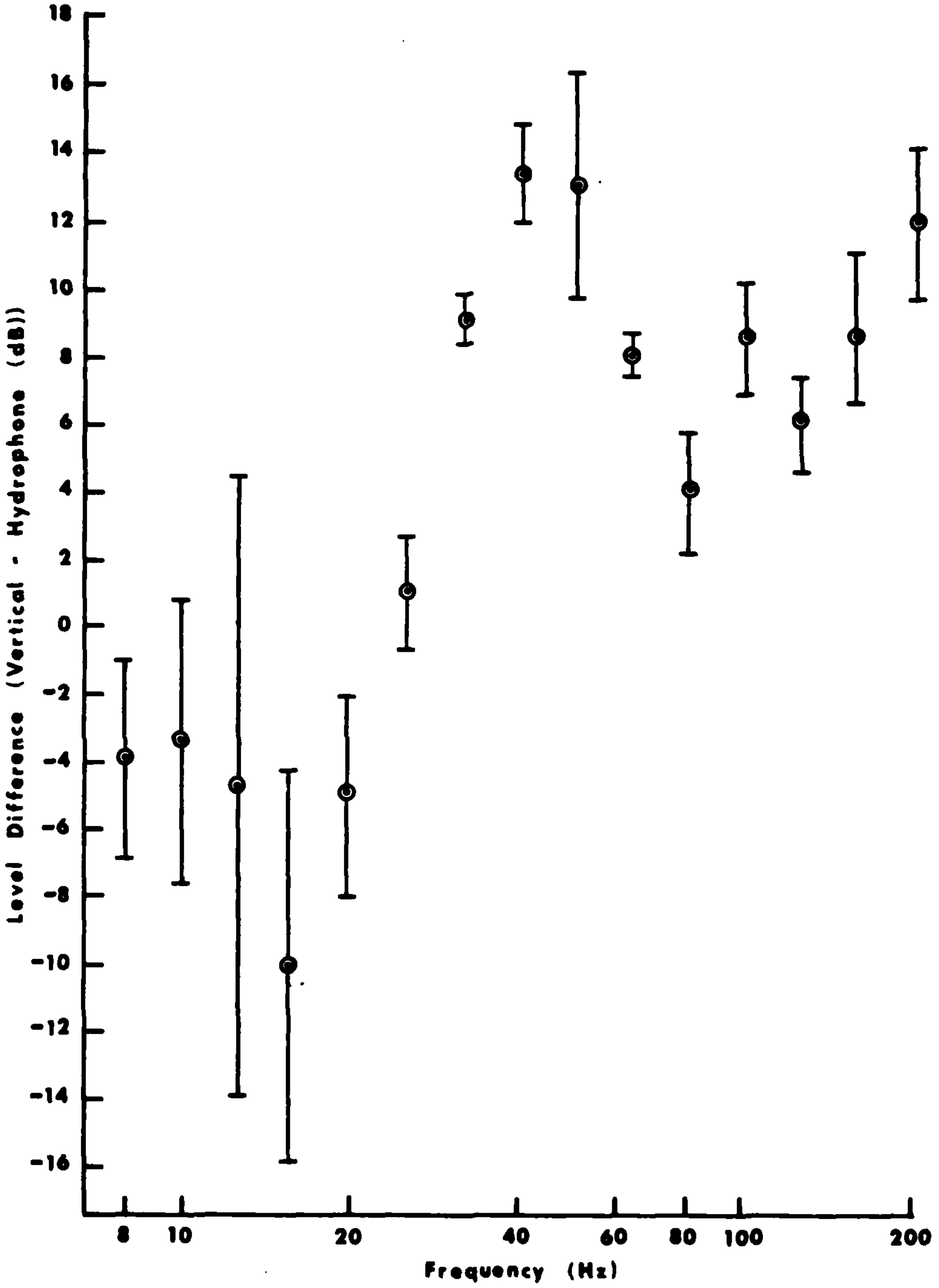

Figure 19 The Difference in Measured Propagation Loss Between the Vertical Geophone and the Hydrophone as a Function of Frequency, Run 2.

6. CONCLUSIONS AND RECOMMENDATIONS

The experimental data indicates that sound propagation in the area south of Martha's Vineyard is very good. Even with a strong negative sound speed profile in the water, the sound speed in the bottom is fast enough so that propagation in the water column is efficient enough to permit detection of a 160 dB/1μPa target at a range of 30 km.

The vertical geophone appears to be a superior sensor when compared to a hydrophone at frequencies above 30 Hz.

For bottom conditions similar to those in the experiment area, propagation paths predominantly through the bottom will offer little if any improvement in decreasing propagation loss.

A complete theoretical explanation of the data has not been attained. It is recommended that further studies be conducted to define the sound field in the immediate region of the water-bottom interface.

References

1. Ewing, W. M., W. S. Jardetzky and F. Press, Elastic Waves in Layered Media, McGraw-Hill, New York, 1957.

2. Holmer, C. I., "Relation of Particle Velocity and Pressure in a Two Layer Shallow Water Area, Appendix B," from R. J. Hecht, "Investigation of the Potentialities of Using Seismic Sensors for the Detection of Ships and Other Naval Platforms," DDC-AD-A0-63218, September 24, 1978.

3. Urick, R. J., "Underwater Sound Transmission Through the Ocean Floor," Physics of Sound in Marine Sediments, ed. by Lloyd Hampton, Plenum Press, New York, 1974, p. 161.

4. McLeroy, E. G., "The NCSC Shallow Water Seismic Propagation Study," Proceedings of the Workshop on Seismic Propagation in Shallow Water, sponsored by the Office of Naval Research, July 7, 1978.

5. Kornhauser, E. T. and W. P. Raney, "Attenuation in Shallow-Water Propagation Due to an Absorbing Bottom," J. Acoust. Soc. Am., Vol. 27, No. 4, July 1955, p. 689.

6. Officer, C. B., "The Refraction Arrival in Water Covered Areas," Geophys., Vol. 18, 1953, p. 805.

7. Horton, C. W., "On the Propagation of Rayleigh Waves on the Surface of a Viscoelastic Solid," Geophys., Vol. 18, 1953, p. 70.

8. Schlee, J., "Sand and Gravel on the Continental Shelf Off the Northeastern U.S.," USGS Curricula 602, 1968.

9. Aaron, J. M., Personal communication with the author, March 1980.

10. Barakos, P. A., "Experimental Determination of Compressional Velocity for the Bottom Layer by the Dispersion Method," J. Acoust. Soc. Am., Vol. 34, No. 12, December 1962, p. 1919.

11. Ewing, M., Worzel, J. L., Steenland, N. C. and F. Press, "Geophysical Investigations in the Emerged and Submerged Atlantic Coastal Plain," Bull. Geol. Soc. Am., Vol. 61, September 1950, p. 877.

12. Horton, J. W., Fundamentals of Sonar, U.S. Naval Institute, Annapolis, Maryland, 1959.

13. Bendat, J. S. and A. G. Piersol, Random Data: Analysis and Measurement Procedures, Wiley-Interscience, New York, 1971.

14. Heuter, T. F. and R. H. Bolt, Sonics, John Wiley and Sons, New York, 1955.

15. Underwater Systems, Inc., "SUS Source Level Handbook," draft report, December 1, 1979.

16. Asada, T. and H. Shimamura, "Observations of Earthquakes and Explosions at the Bottom of the Western Pacific: Structure of Oceanic Lithosphere Revealed by Longshot Experiment," The Geophysics of the Pacific Ocean Basin and its Margin, ed. by G. H. Sutton, M. H. Magnhnani and R. Moberly, Geophysical Monograph 19, American Geophysical Union, Washington, D.C., 1976, p. 135.

17. Strick, E. and A. S. Ginzberg, "Stonely Wave Velocities for a Fluid-Solid Interface," Bull. Seis. Soc. Am., Vol. 46, 1956, p. 281.

18. Clay, C. S. and H. Medwin, Acoustical Oceanography: Principles and Applications, Wiley-Interscience, New York, 1977.

19. Pekeris, C. L., "Theory of Propagation of Explosive Sound in Shallow Water," Propagation of Sound in the Ocean, Memoir 27, Geological Society of America, New York, 1948.

20. Tolstoy, I. and C. S. Clay, Ocean Acoustics: Theory and Experiment in Underwater Sound, McGraw-Hill, New York, 1966.

21. Junger, M. C. and O. Feit, Sound, Structures and Their Interaction, MIT Press, Cambridge, Massachusetts, 1972.

22. Tolstoy, I., "Shallow Water Test of Theory of Layered Wave Guides," J. Acoust. Soc. Am., Vol. 30, No. 4, April 1958, p. 348.

APPENDIX A

A GEOPHONE IMPLANTER FOR SHALLOW WATER

The need to couple a velocity geophone to the earth has been recognized from the time of the earliest seismograph designs. Concern about the coupling of the many Ocean Bottom Seismograph (OBS) designs was demonstrated in the comparison measurements sponsored by the Office of Naval Research (ONR). Sutton et al. recognized the coupling problem and formulated an approximate relationship to assess the effect of the OBS resting on the bottom.[A1]

In the experiment performed south of Martha's Vineyard, the interest was to have the triaxial geophone coupled to the bottom as firmly as possible and to have the least weight possible on the bottom in the vicinity of the sensor. The objective was to implant the geophone in the top 18 in of the bottom sediment as firmly as possible and to have a hydrophone located within 1 ft of the bottom directly above the geophone. To accomplish the implantment of the geophone and the positioning of the hydrophone, a geophone implanter was designed.

The properties of the implanter that were considered to be essential were:

1. A triaxial geophone would be inserted perpendicular to the bottom.
2. The geophone would always be totally implanted in the bottom.
3. The implanted geophone would be approximately the same density as the bottom.

4. There would be minimal excess weight to modify the response of the sediment to displacement.

5. The operation must be remotely operable, preferably self-actuated and self-finishing.

The first concept was to free-fall the triaxial geophone contained in a sediment corer tube and thus embed it in the bottom. Several laboratory experiments showed that penetrations in hard sand of 6 to 9 in could be expected for a 1-5/8 in diameter cylinder with a 45° cone for a head. From these experiments it was concluded that the free-fall implantment technique would not reliably achieve the desired results in a hard sand bottom.

The method finally adopted was to place sufficient weight on the geophone container such that oscillating rotation of the geophone ±10° would cause the implantment to be reliable in hard sand bottoms. Several laboratory tests were performed to determine the number of oscillations required to obtain implantment of a 12 in long geophone probe vs head weight. The experimental results shown in Figure A-1 indicated that a head weight of 100 lb was sufficient to install the sensor.

Experimental results showed that a 45° cone was an acceptable angle for the penetrating point. The critical parameter was the roughness of the cone. The cone needed to have a roughness sufficient to engage the sand grains so that the oscillating motion would move the grains and open the packing. Through experimentation, a cone with 3/16-in deep V-grooves located every 20° proved very effective.

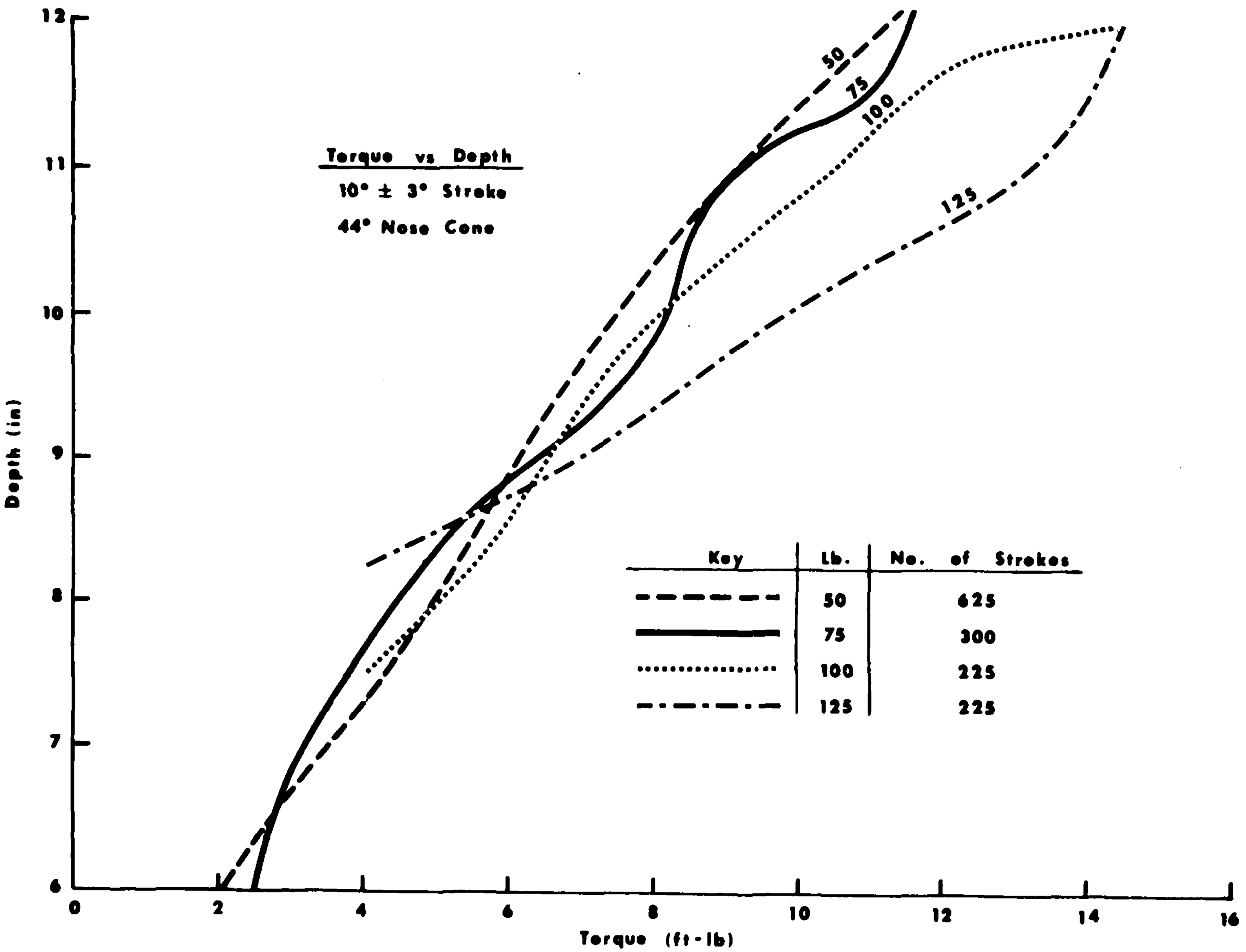

Figure A-1. Amount of Oscillation Torque Required vs Cylinder Penetration with Weight as a Parameter.

The geophone probe has an outside diameter of 2-1/4 in and is 14 in long including the penetration cone. The probe is constructed of 0.125 in wall aluminum tubing with a wood head cone. The density of the probe is approximately 2, a reasonably good match for a sand bottom.

Several sources of power were initially considered for driving the implanter. Compressed air was determined to be the most effective from a size, weight and cost standpoint. The energy in a single scuba diver tank was only marginally sufficient to carry out the implantment and recovery operations in 55 m of water, so a second tank was added for reliability. The use of compressed air is considered a viable power source to depths of 200 m. At greater depths, electric power is probably more desirable but more costly.

Since the implanter was self-contained, a logical sequence of functions needed to be implemented. The steps in this sequence are:

1. When the implanter comes to rest on the bottom, the operators at the surface need to know if the implanter is reasonably level; ±5° is excellent, ±15° is a no-go situation. An attitude sensor within the preamplifier case emits three tones: <5°, 5° to 15°, >15°. The operators have 2 min to evaluate the attitude of the implanter before the implanting operation begins. If the attitude is unsatisfactory, the implanter can be raised off the bottom to reset the sequence and a new location found. The tolerable attitudes are determined by the horizontal geophones. The SENSOR Model 6B geophone can tolerate a 20° tilt.

2. Next, the geophone housing and weights are released and the oscillation of the geophone housing begins. When the geophone housing penetrates 1/4-in below the implanter, oscillation ceases.
3. When oscillation has ceased, the weights are raised off the geophone and are caught by a mechanical trigger. The preamplifier case is released, and two air bags are filled to raise the implanter to the surface where it can be recovered. The geophone and the preamplifier case are the only components left on the bottom.

The basic concept of the implanter is shown in Figure A-2. A prototype was constructed using a 1.35 m square plywood base. The remainder of the machine was constructed of steel and aluminum. Standard air cylinders, air timers and air valves were used. From the first experiments in the Potomac River, the need to terminate every exhaust port with a relief valve to keep out the mud was learned. The weights consisted of 5-1/2 in thick steel round plates, each weighing 35 lb. In this way the weight is adjustable.

The implanter was first used in the Martha's Vineyard experiment. On the first launch, difficulty was experienced in lowering the signal cables and the implanter simultaneously from the anchored boat. The two sets of lines became unsynchronized and the implanter overturned, tearing off the preamplifier case.

Since there was no time for redesign of the preamplifier case hold-down, the implanter was refitted and its logic changed so that it would remain over the implanted geophone after implantment. With these

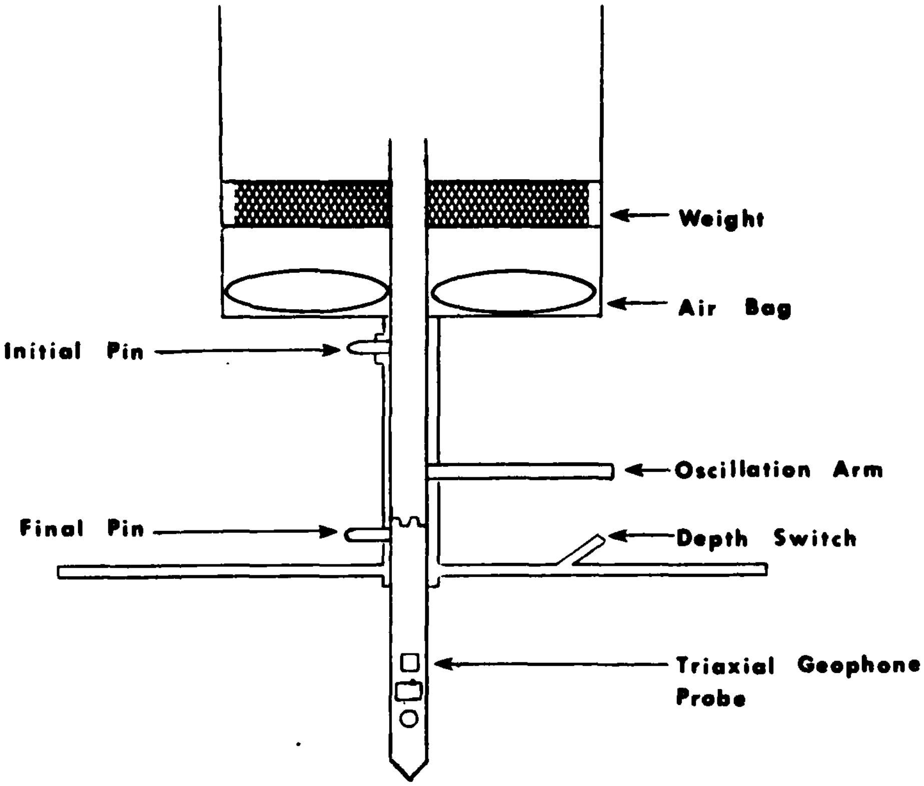

Figure A-2. Cross-Sectional View of Implantment Tool During Implantment Process.

modifications, the second try was a success. A cross-sectional view of the relationship of the implanted geophone to the implanter is shown in Figure A-3. The hydrophone remained attached to the implanter 0.4 m above the bottom.

Since the implanter remained over the geophone, the vertical resonance of the implanter was calculated after Sutton et al. and was found to be approximately 9 kHz.[A1] It was concluded that it had little, if any, affect on the data gathered by the sensors. However, a line remained attached to the implanter for its recovery after the exercise. The currents caused this line to tug on the implanter, thereby generating a large amount of low-frequency noise.

In conclusion, a successful method for inserting a geophone into the bottom without divers has been developed. Calculations show that the present air-driven implanter can be used to depths of 200 m. With slight modifications, the implanter can be used to implant geophones for use with present internal recording OBS's.

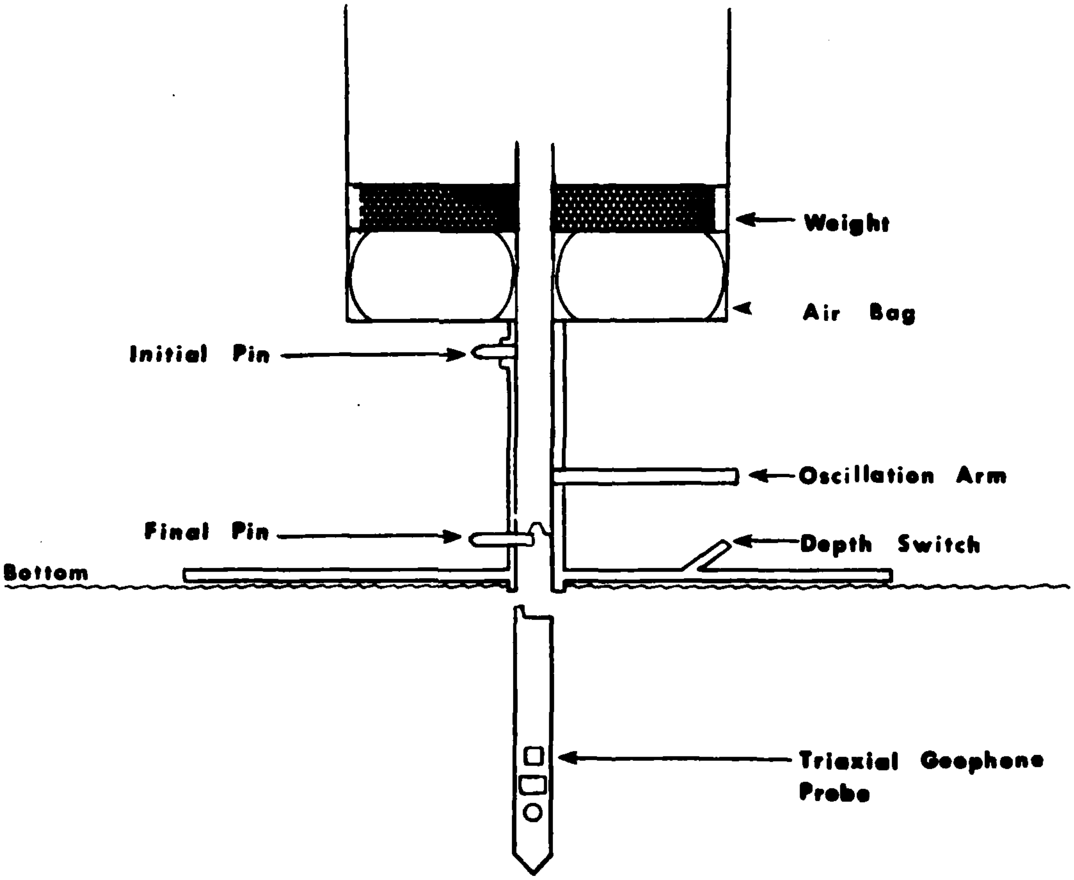

Figure A-3. Cross-Sectional View of Implantment Tool After Implantment.

Reference

Appendix A

A1. Sutton, G. H., W. G. McDonald, D. D. Prentis and S. N. Thanos, "Ocean Bottom Seismic Observations," Proceedings of the IEEE, Vol. 53, No. 12, December 12, 1965, p. 1909.

APPENDIX B

PROPAGATION LOSS MEASURED SOUTH OF MARTHA'S VINEYARD

The objective of this appendix is to present the propagation loss data obtained during the shallow water experiment. The receiver consisted of a triaxial geophone that was implanted in the top 0.3 m of the bottom and an omnidirectional hydrophone positioned 0.4 m off the bottom. The receiver location was 40°47.14'N, 70°57.74'W. Runs 1 and 2 were east-west runs over a sandy bottom of constant depth and Run 3 was an upslope propagation run perpendicular to the bottom contours. The sound velocity profile was strongly negative with a well-developed surface duct that varied in thickness between 10 and 18 m. Further details on the environment can be found in Reference B1.

The acoustic source was a SUS MK 61 set to detonate at 18.3 m. The received signals were processed in 1/3-octave bandwidths for energy flux density. The difference between the received energy and the source level energy is the propagation loss. The MK 61 source levels are given in Table B-1.

The insert calibration technique was used to determine the frequency response of the electronics portion of the system. The sinusoidal calibration signals were processed through the same system as the signal. The FFT outputs were converted in level for the bandpass characteristics of the FFT.

TABLE B-1. Acoustic Source Level of 1.8 LB TNT Detonated at 18.3 m in 1/3-Octave Bands.[B1]

Frequency Hz	Source Level dB*
8	59.5
10	59.5
12.5	59
16	58.5
20	57
25	57
31.5	56
50	53
63	53.5
80	53.3
100	51
125	51
160	49.5
200	48

Note: The 8 Hz level is interpolated from the 10 Hz level.

*Source levels are in dB re 1 erg-sec/cm^2 at a range of 1 m.

The overall frequency response of the system is the combined response of the transducers and the electronics normalized to 0 dB at 50 Hz. The same frequency response was used for the three geophone channels. Differences in overall gain for the three geophone channels and the hydrophone channel are reflected in the 50 Hz calibration constant (C_{50X}).

SENSOR SM-6 Model B geophones were used in the triaxial unit. They have a coil resistance of 375 ohms and a resonant frequency of 8 Hz. The calibration constant for the geophone is 0.29 V/cm/sec or -10.85 dBV/cm/sec for no electrical damping for frequencies well above resonance. For the experiment, the geophone was terminated by 4.2 K which lowered the calibration constant to 0.27 V/cm/sec or -11.4 dBV/cm/sec.

A 2.0 V peak-to-peak 50 Hz signal, -3 dBV, was applied to the calibration input. The calibration circuit reduces the level inserted in series with each sensor by individual decoupling networks, each having a 40 dB loss. The signal inserted in series with the sensor was -43 dBV and was measured to be the same at the input to the preamplifiers. The electrical calibration signal was equivalent to -31.6 dB re 1 cm/sec. The calibration sinusoids were measured with the FFT and amplitude corrections were made for the FFT amplitude response using a modification of the methodology of Burgess.[B3]

We define a calibration constant (C_i) in dB as the number of dB that must be added to the processor output to obtain plane wave acoustic energy or power, where the i's represent the different channels:

$$C_i = A_i - B_i - D_i$$

where

A_i is the FFT output in dBV.

B_i is the adjustable gain setting.

D_i is the equivalent velocity of the calibration signal.

The hydrophone, an OSTRONICS H-90, was calibrated at the Brighton Dam facility of NAVSWC after the field experiment. The sensitivity of the hydrophone was determined to be -194 dBV for an applied pressure of 1μPa. The -43 dBV calibration signal is equivalent to an acoustic plane wave pressure of 151 dB//1μPa or 51 dB//1 dyne/cm^2, which is equal to D_i for the hydrophone channel. The calibration constant together with the values of several of its components are shown in Table B-2.

The received data was processed using a FFT algorithm following which bins or portions of bins were assembled to form equivalent 1/3-octave band filters. The computation performed for background noise intensity for the hydrophone was:

$$I_H = 10 \log \left(\frac{1}{T\rho c} \int_0^T e^2 dt \right) - G - FR + C_{50}$$

where

T	is the sample length.
ρ	is the medium density.
C	is the medium velocity.
e	is the signal voltage in the band of interest.
G	is the amplifier gain.
FR	is the frequency response.
C_{50}	is the calibration constant for 50 Hz.

TABLE B-2. Calibration Constants for the Four Data Channels With Individual Components.

Sensor	A_i	B_i	Equivalent dBV for 0 Gain	C_i Calibration Constant for Acoustic Level	i
H_1	17.7	14	3.7	-35.3	1
H_2	17.6	14	3.9	-35.3	2
V	9.1	6	3.1	-34.7	3
Hydr.	-5.9	6	-11.9	62.9	4

Similarly, intensity from the geophone signals was computed as:

$$I_V = 10 \log\left(\frac{\rho c}{T} \int_0^T e_s^2 dt\right) - T_1 T_H - G - FR + C_{50}$$

where the variables apply to the particular sensor. The impedance term ρc converted to dB used for the hydrophone in the water was -52 dB and for the geophone in the bottom was 54.6 dB. The density of sand in which the geophone was embedded was estimated to be 1.8 g/cm^3 and the velocity was estimated to be the same as that in the water. The energy flux density of the shot signals received on the hydrophone was computed as:

$$E_H = 10 \log\left(\frac{1}{\rho c} \int_0^{T_1} e_s^2 dt\right) - T_1 I_H - G - FR + C_{50}$$

Similarly, the energy flux density of the received shot signal on the geophones was computed as:

$$E_V = 10 \log \left(\rho c \int_0^{T_1} e_s^2 dt\right) - T_1 I_V - G - FR + C_{50}$$

The implementation of the energy processing followed the methodology outlined in Reference B4.

The data processing was based on plane wave assumptions with the pressure and the particle velocity in phase. Any deviations of the data from these assumptions can cause a proportional error in the energy determination.

The propagation loss measurements are given in Figures B-1 through B-45. The losses for the four sensors at a specific frequency are shown on each curve.

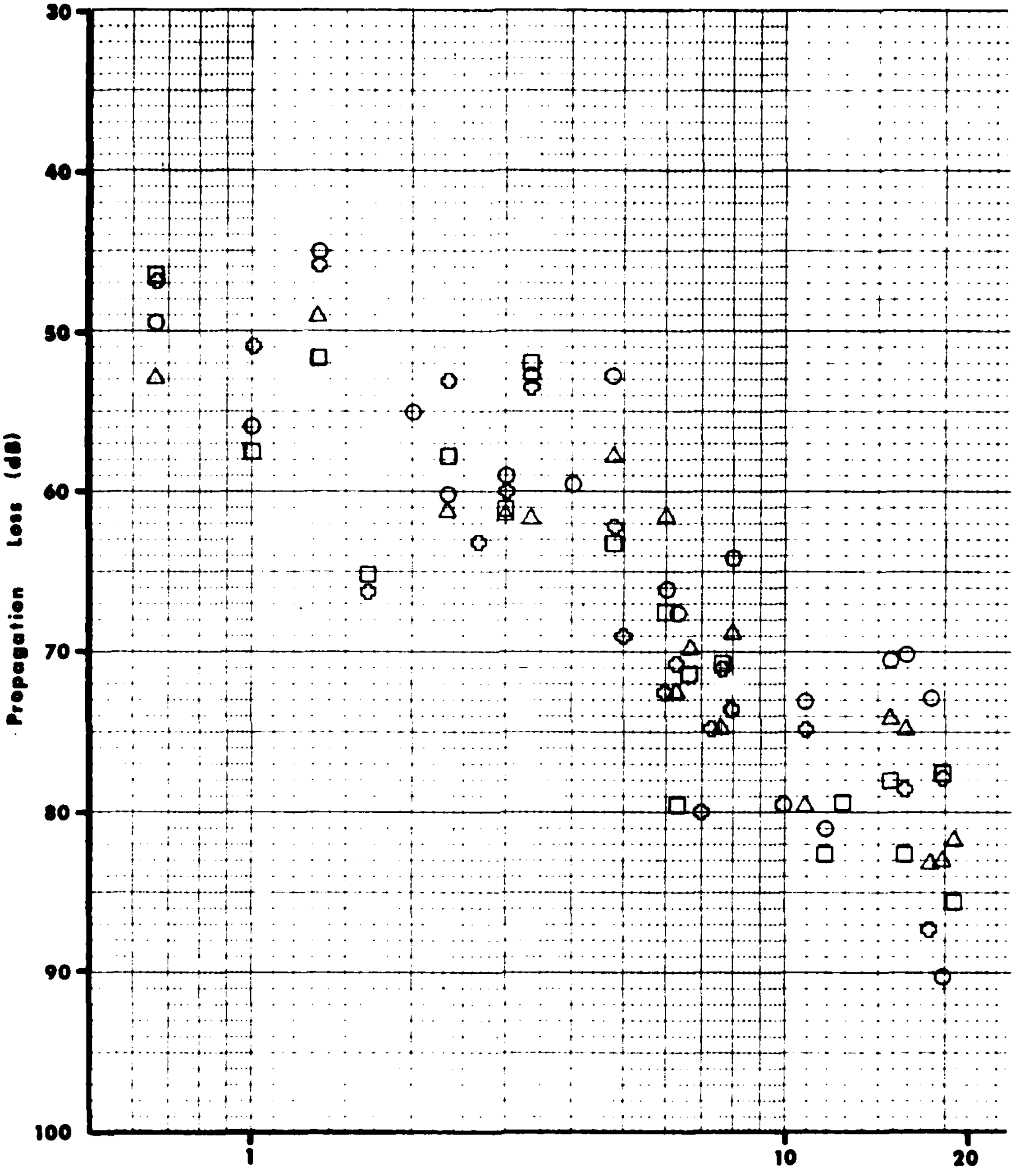

Figure B-1. Measured Propagation Loss for Run 1 at a Frequency of 8 Hz.

○ = **Hydrophone.** Triaxial Geophones: △ = Vertical, □ = Horizontal-2,
○ = **Horizontal-1.**

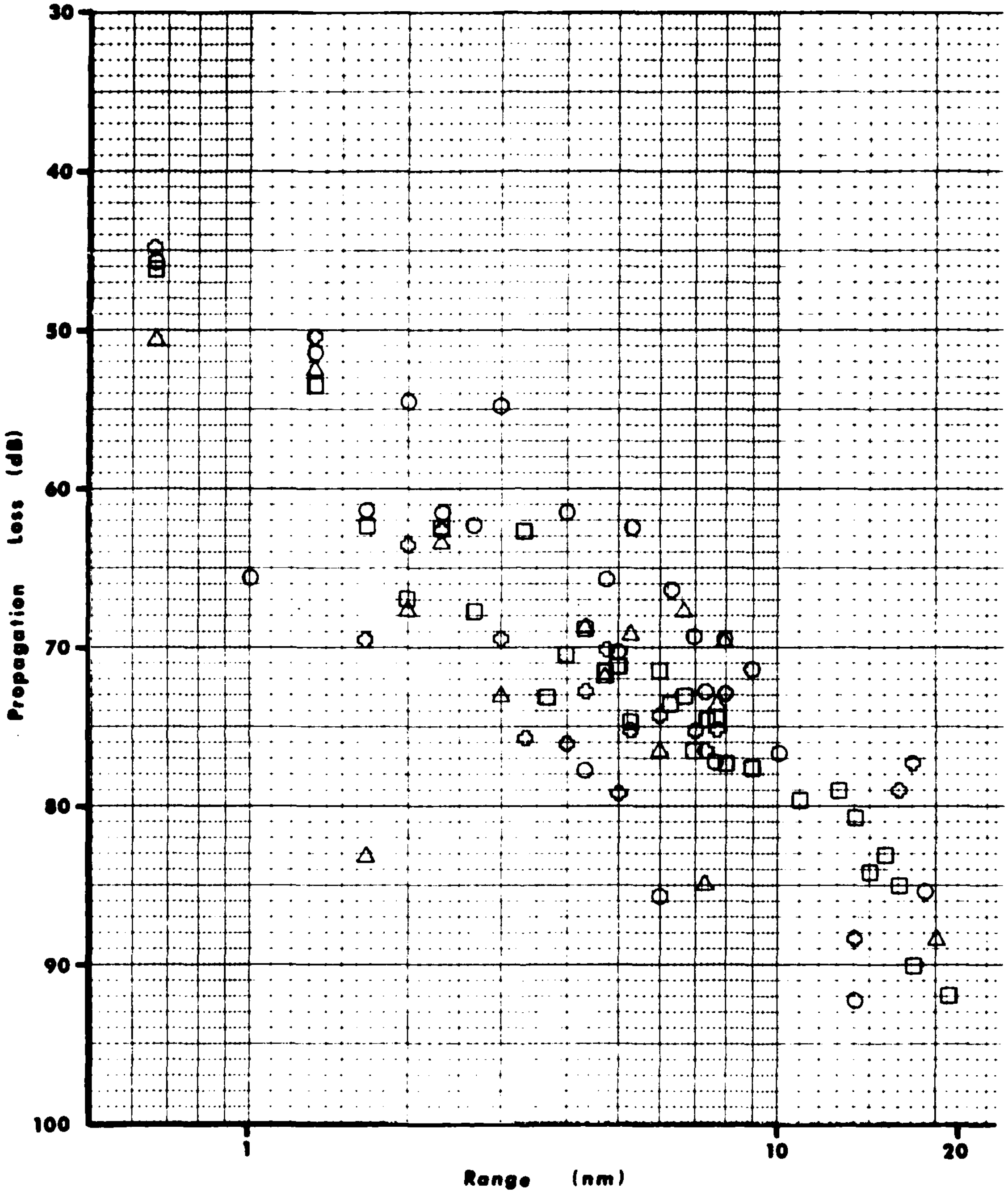

Figure B-2. Measured Propagation Loss for Run 1 at a Frequency of 10 Hz.

○ = Hydrophone. Triaxial Geophones: △ = Vertical, □ = Horizontal-2, ⬡ = Horizontal-1.

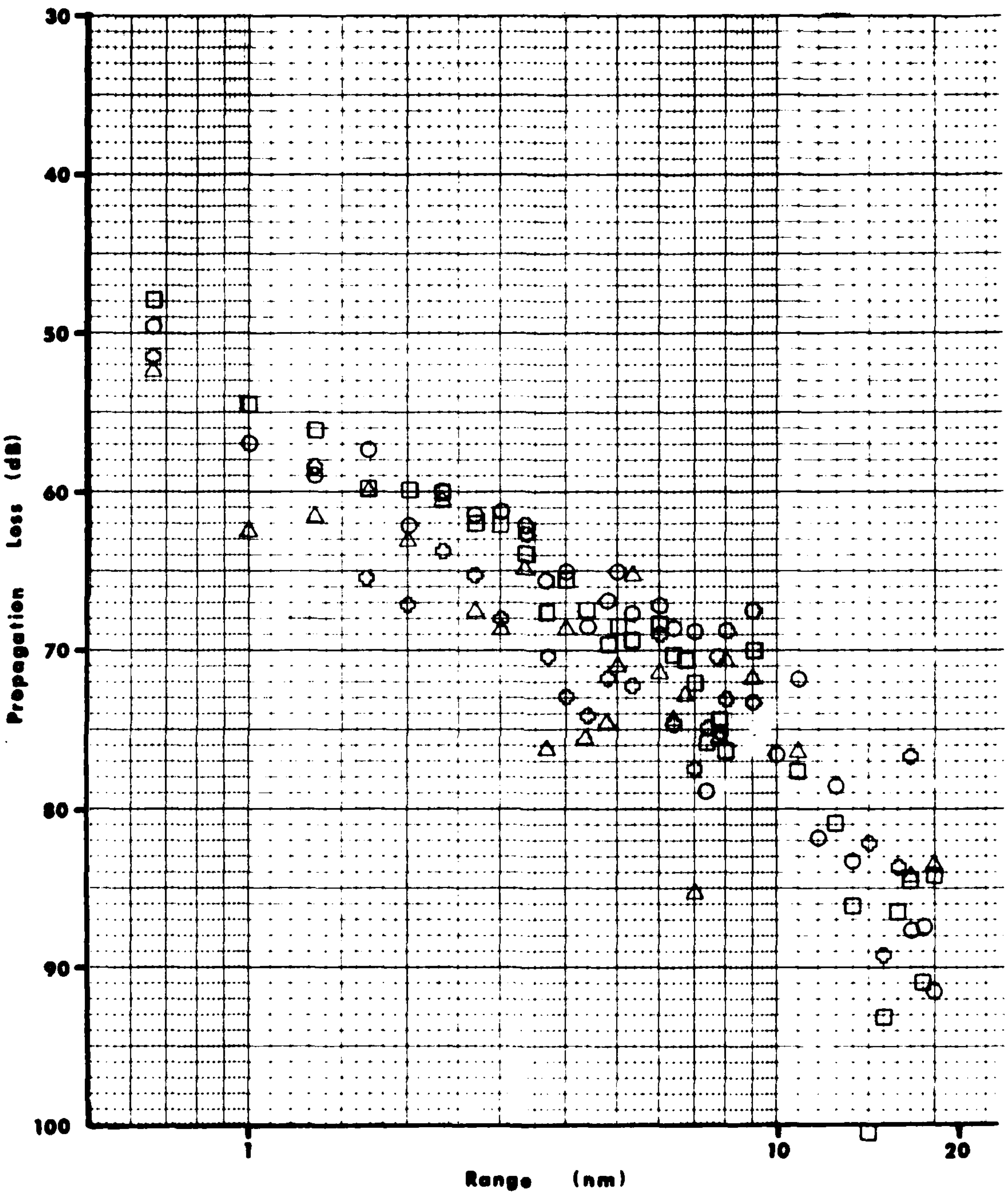

Figure B-3. Measured Propagation Loss for Run 1 at a Frequency of 12.5 Hz.

○ = Hydrophone. Triaxial Geophones: △ = Vertical, □ = Horizontal-2, ⬡ = Horizontal-1.

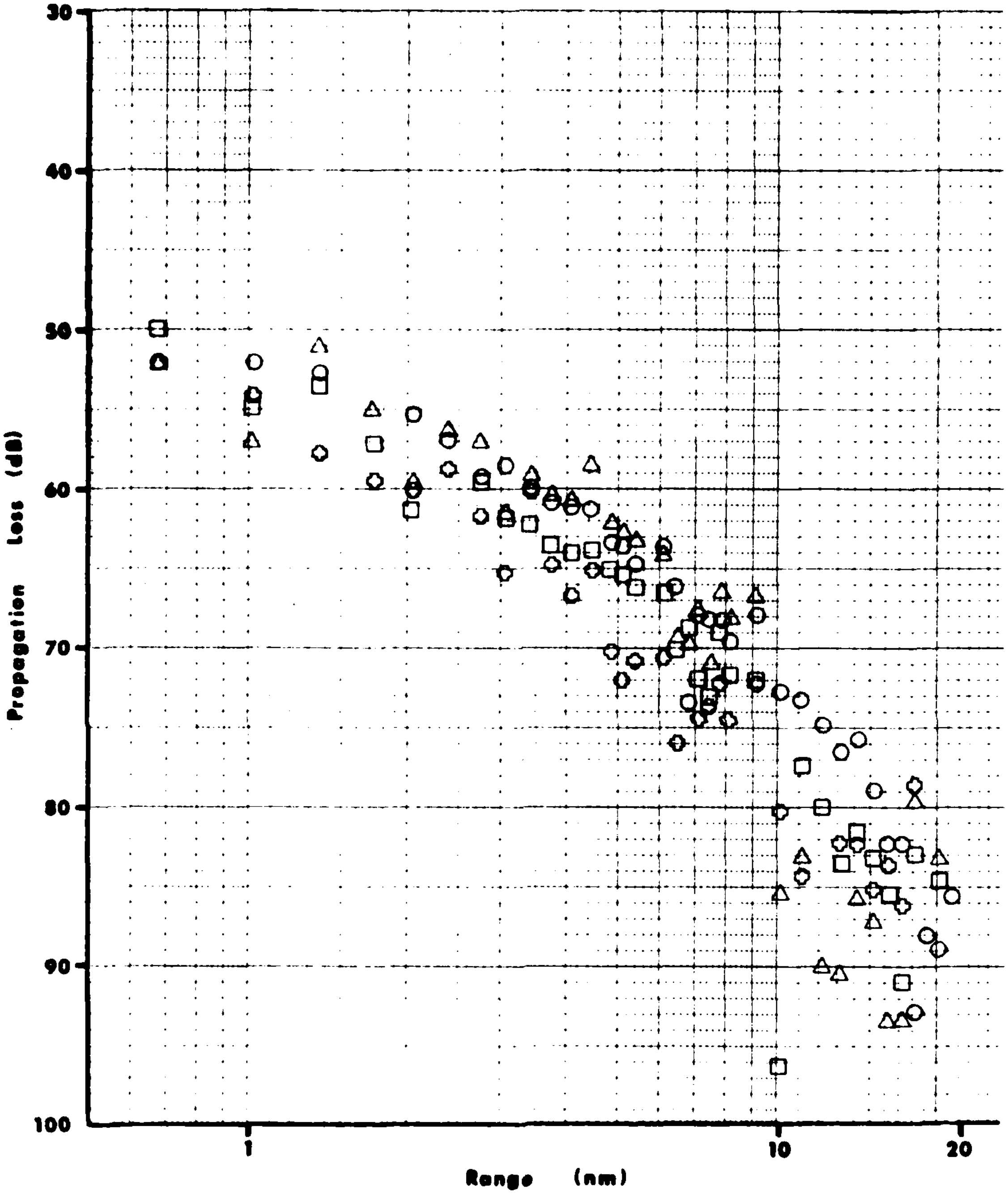

Figure B-4. Measured Propagation Loss for Run 1 at a Frequency of 16 Hz.

○ = Hydrophone. Triaxial Geophones: △ = Vertical, ☐ = Horizontal-2, ⬡ = Horizontal-1.

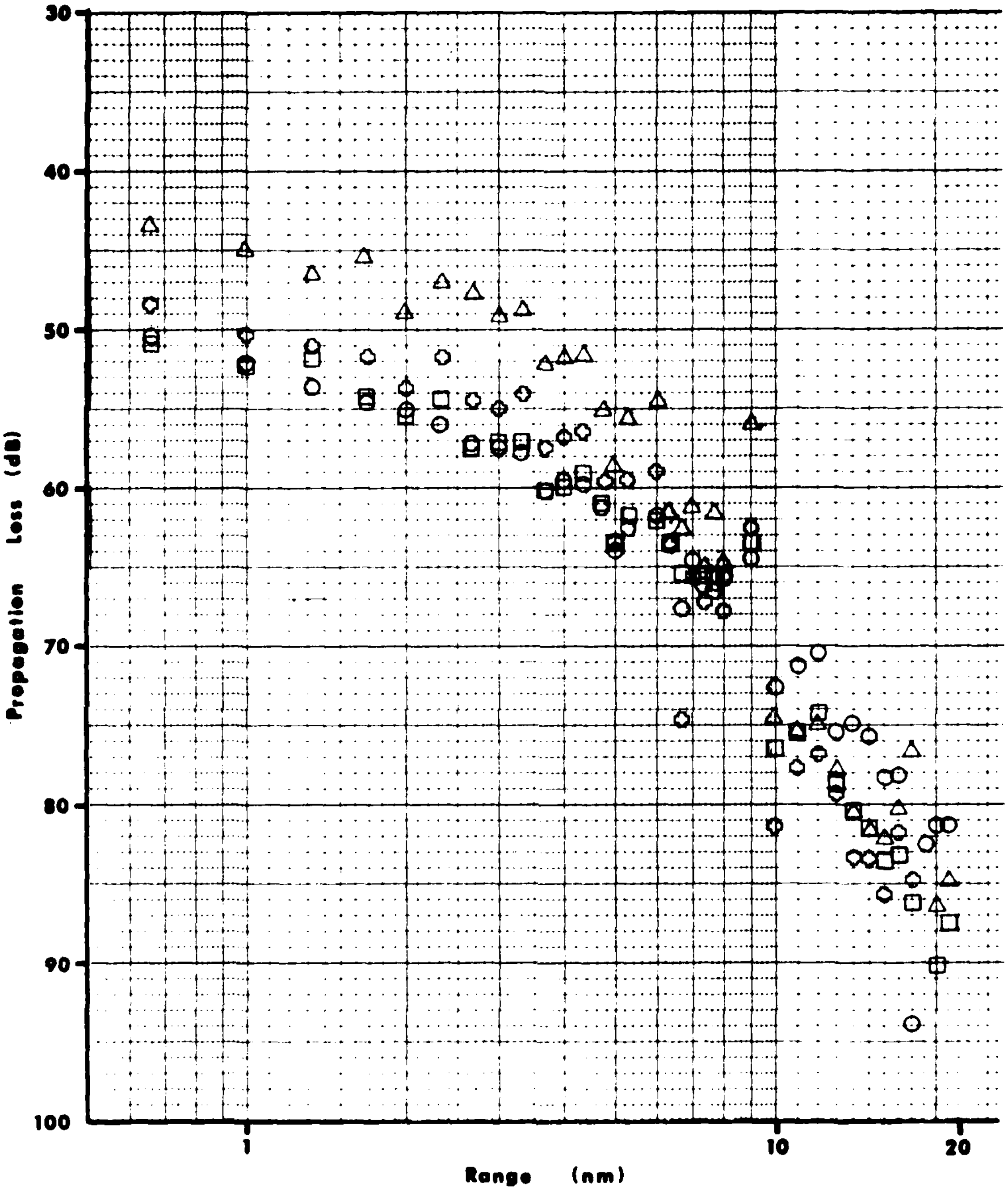

Figure B-5. Measured Propagation Loss for Run 1 at a Frequency of 20 Hz.

○ = Hydrophone. Triaxial Geophones: △ = Vertical, □ = Horizontal-2, ⬡ = Horizontal-1.

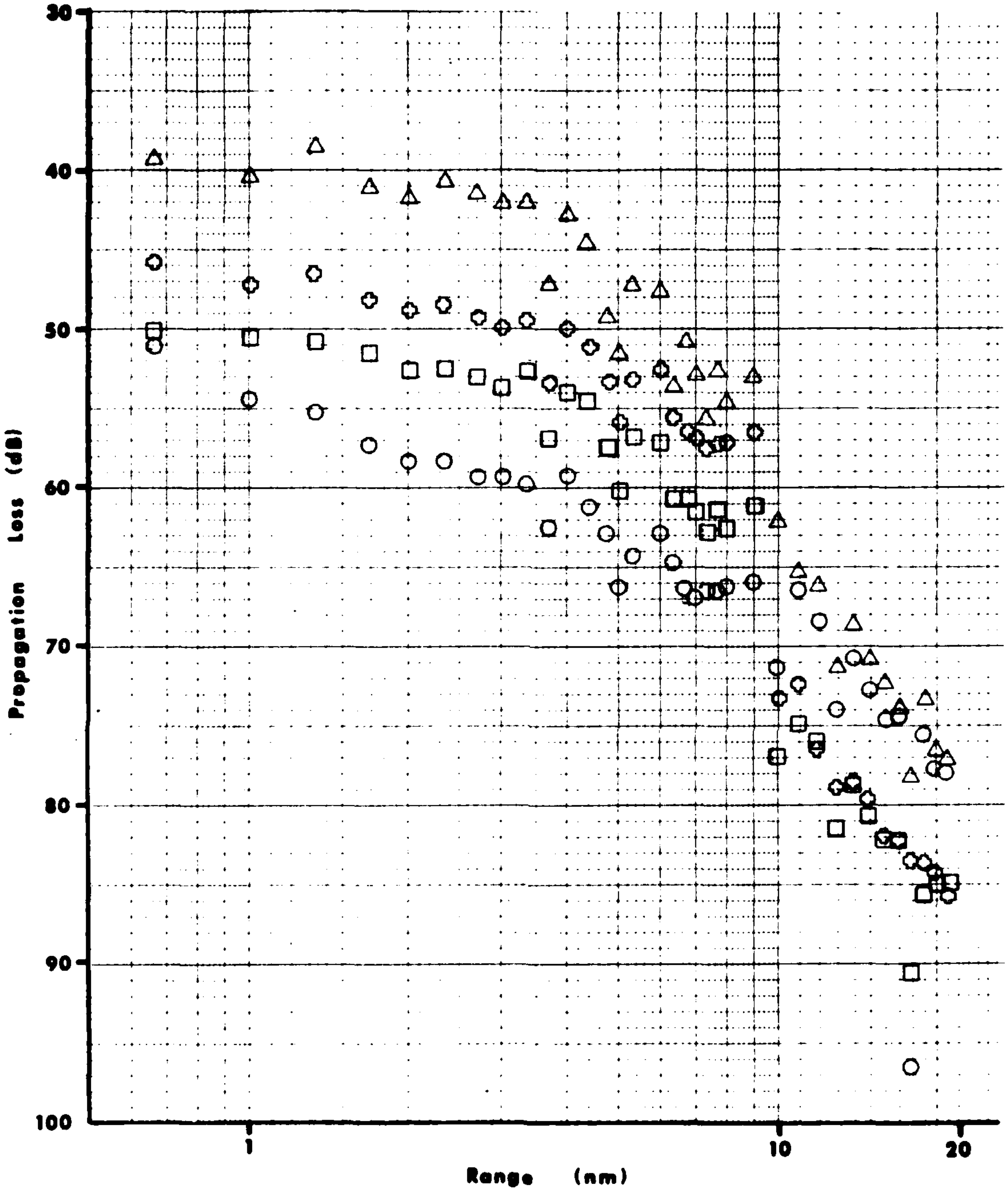

Figure B-6. Measured Propagation Loss for Run 1 at a Frequency of 25 Hz.
○ = Hydrophone. Triaxial Geophones: △ = Vertical, □ = Horizontal-2,
○ = Horizontal-1.

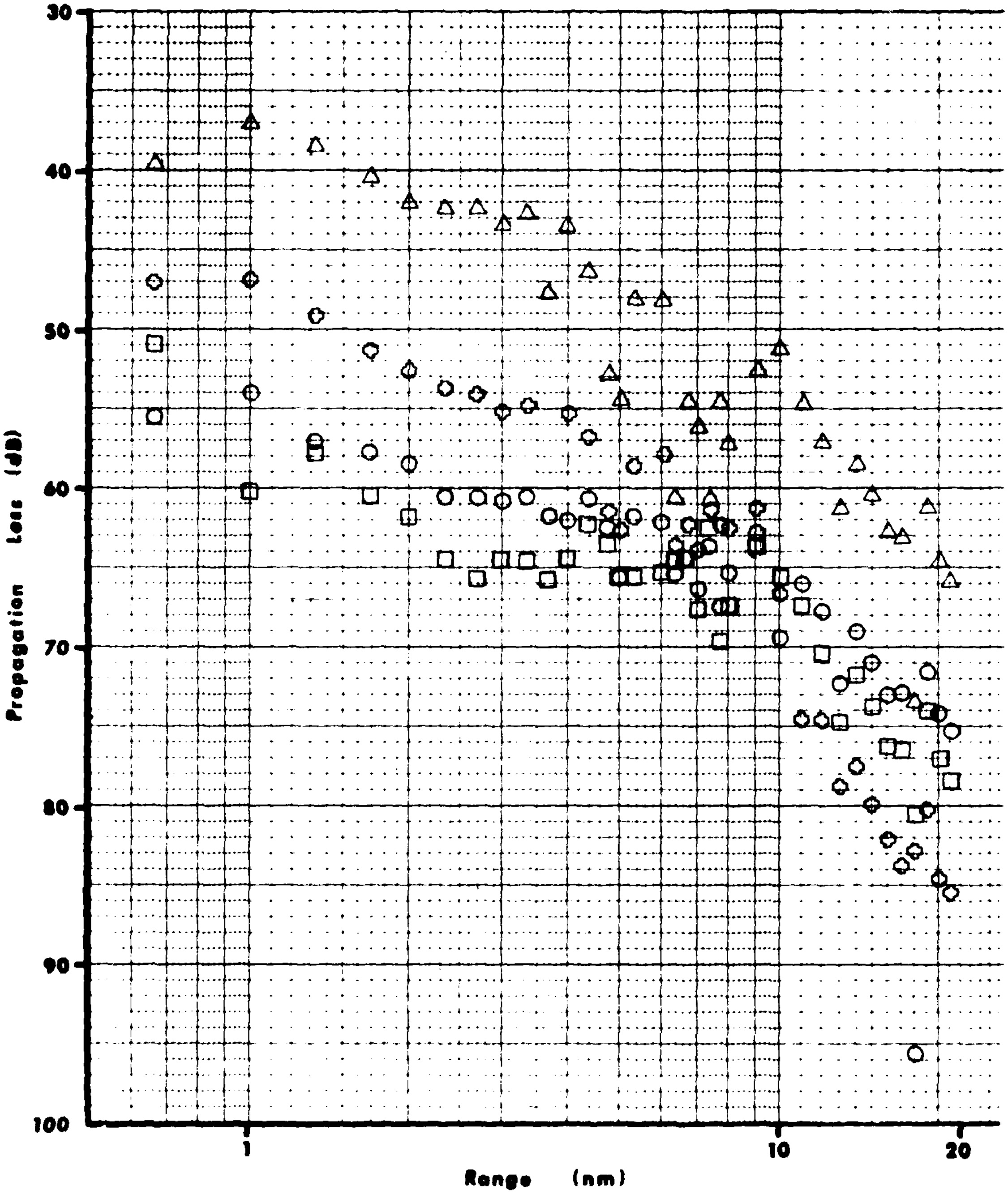

Figure B-7. Measured Propagation Loss for Run 1 at a Frequency of 31.5 Hz.

○ = Hydrophone. Triaxial Geophones: △ = Vertical, □ = Horizontal-2, ⬡ = Horizontal-1.

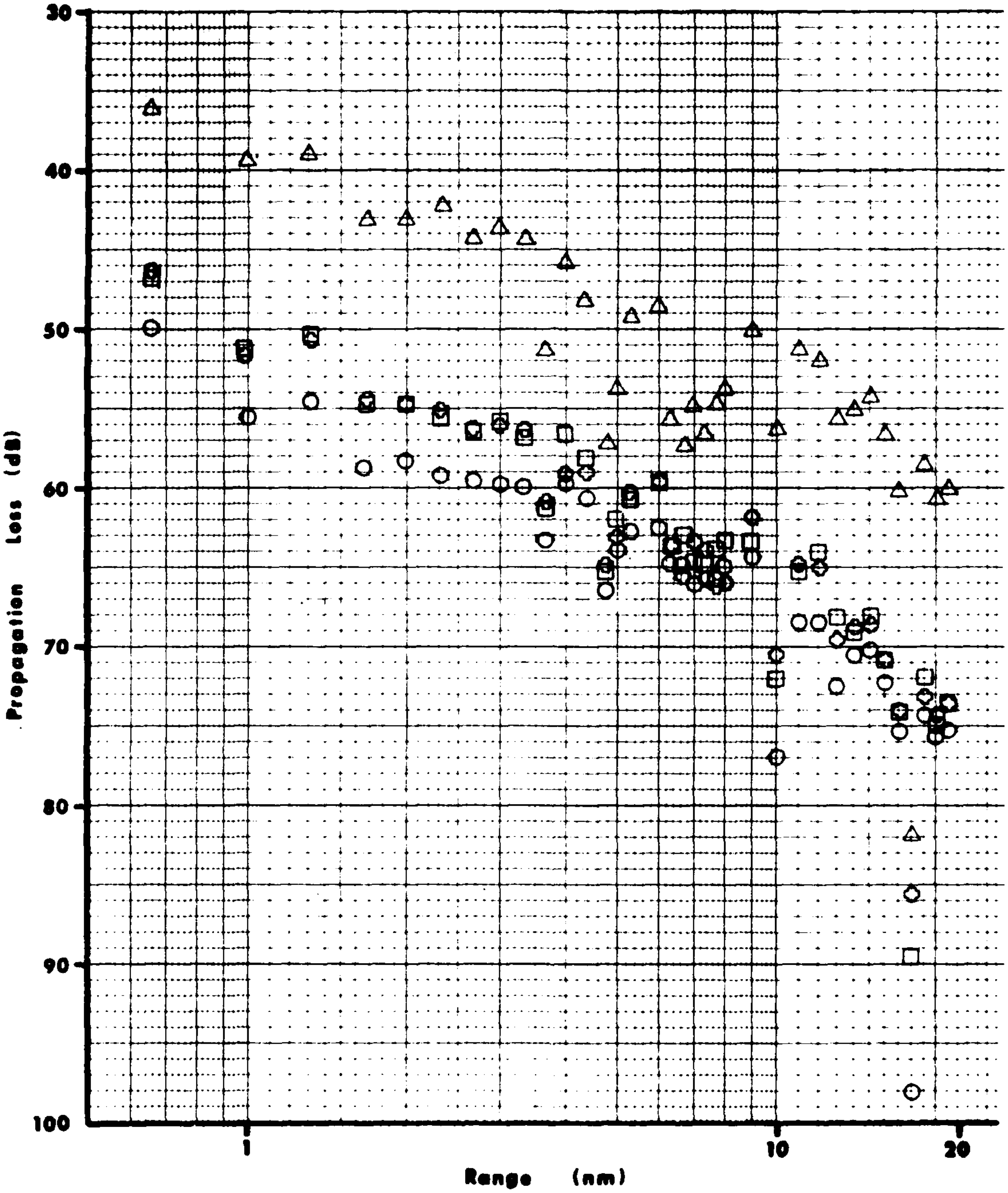

Figure B-8. Measured Propagation Loss for Run 1 at a Frequency of 40 Hz.

○ = Hydrophone. Triaxial Geophones: △ = Vertical, □ = Horizontal-2, ○ = Horizontal-1.

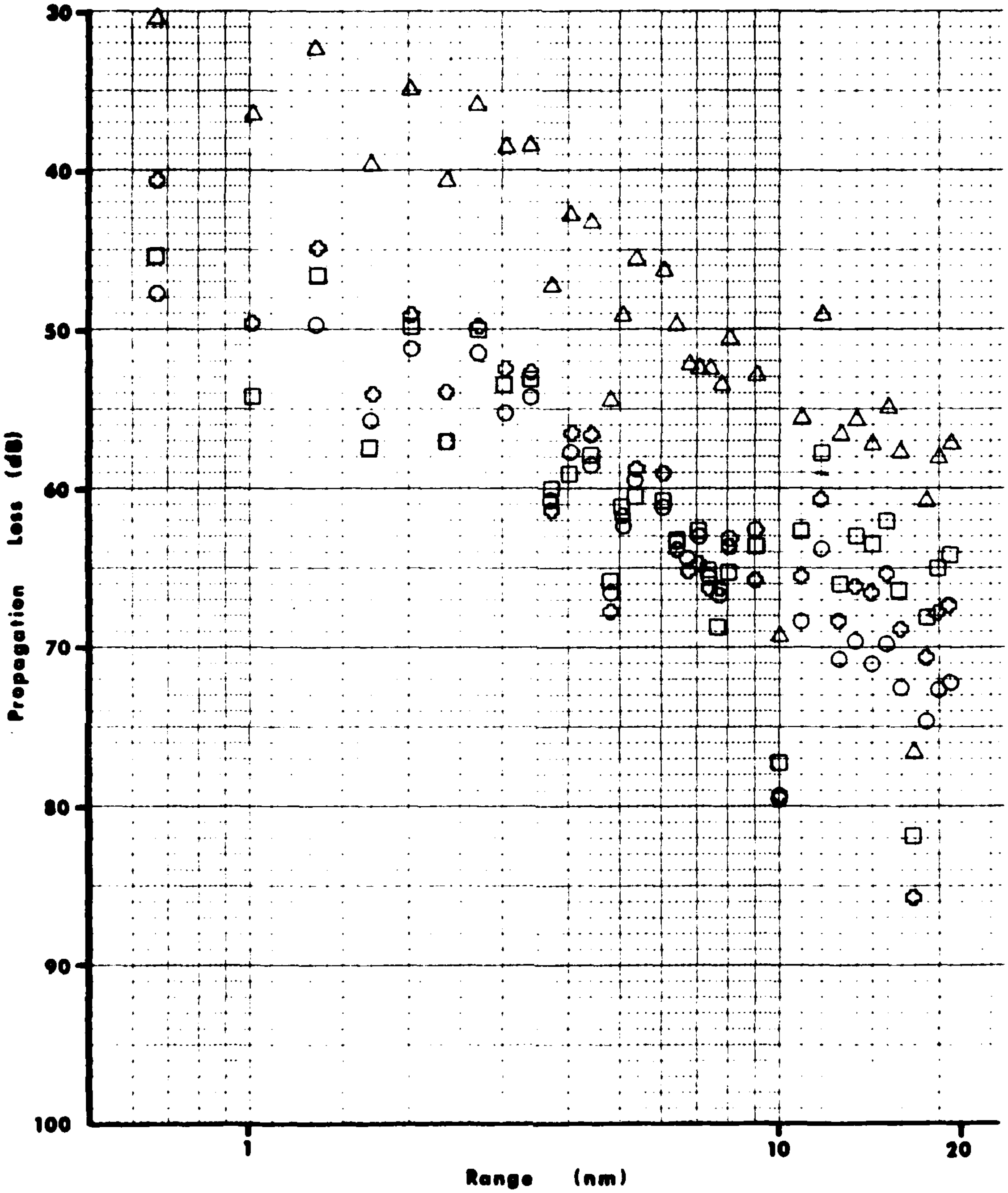

Figure B-9. Measured Propagation Loss for Run 1 at a Frequency of 50 Hz.

○ = Hydrophone. Triaxial Geophones: △ = Vertical, □ = Horizontal-2, ◇ = Horizontal-1.

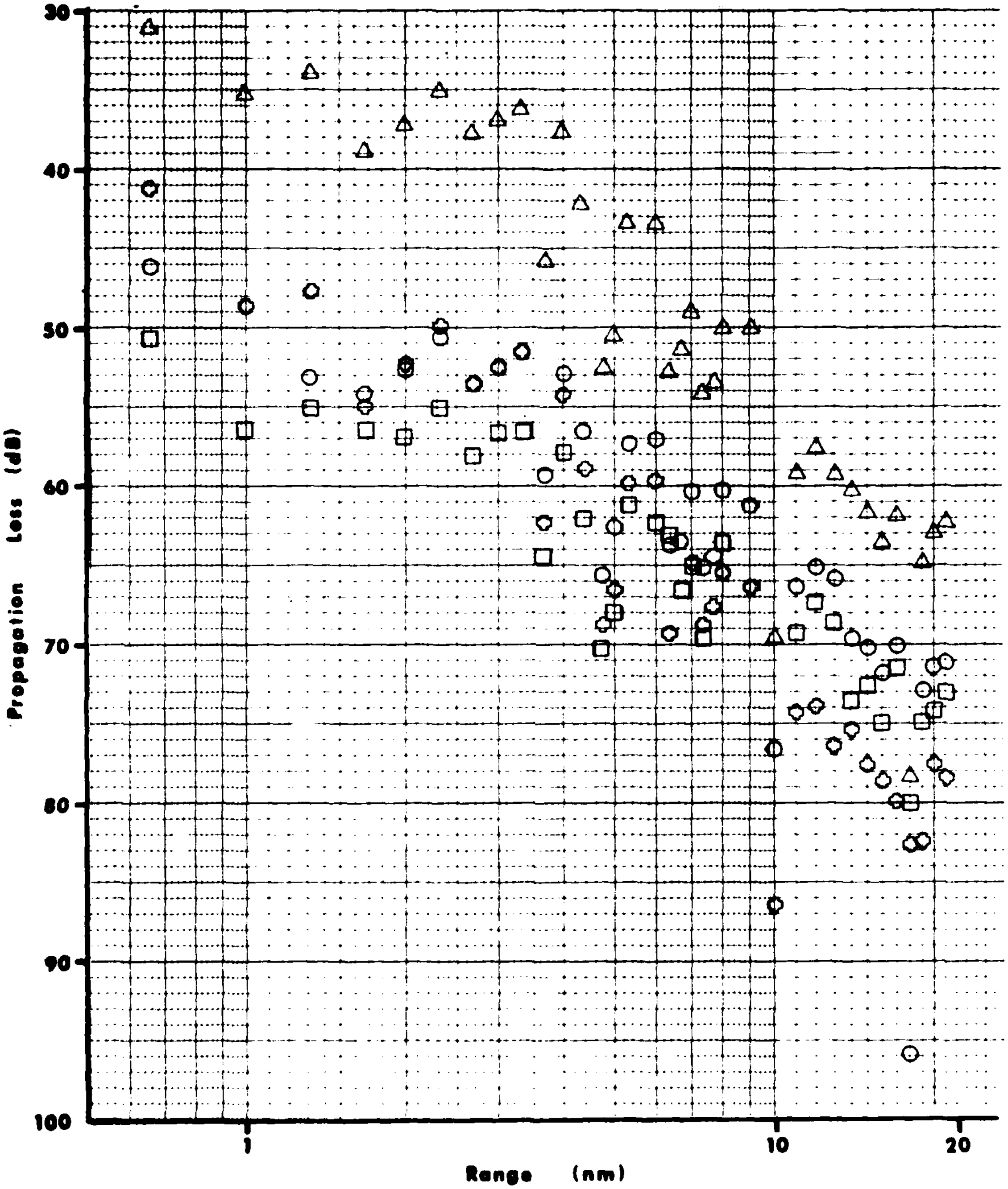

Figure B-10. Measured Propagation Loss for Run 1 at a Frequency of 63 Hz.

○ = Hydrophone. Triaxial Geophones: △ = Vertical, □ = Horizontal-2, ◇ = Horizontal-1.

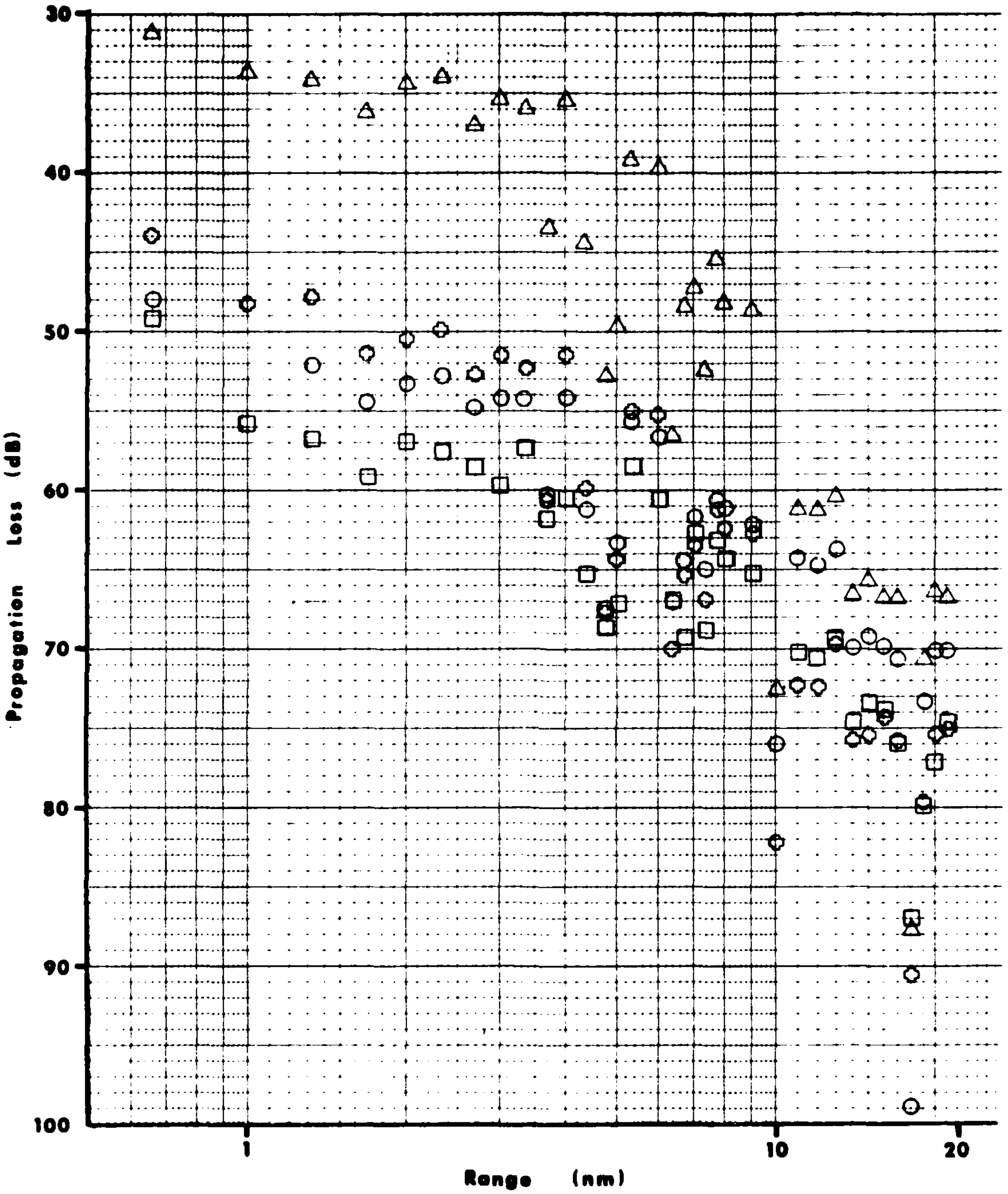

Figure B-11. Measured Propagation Loss for Run 1 at a Frequency of 80 Hz.

○ = Hydrophone. Triaxial Geophones: △ = Vertical, □ = Horizontal-2, ◇ = Horizontal-1.

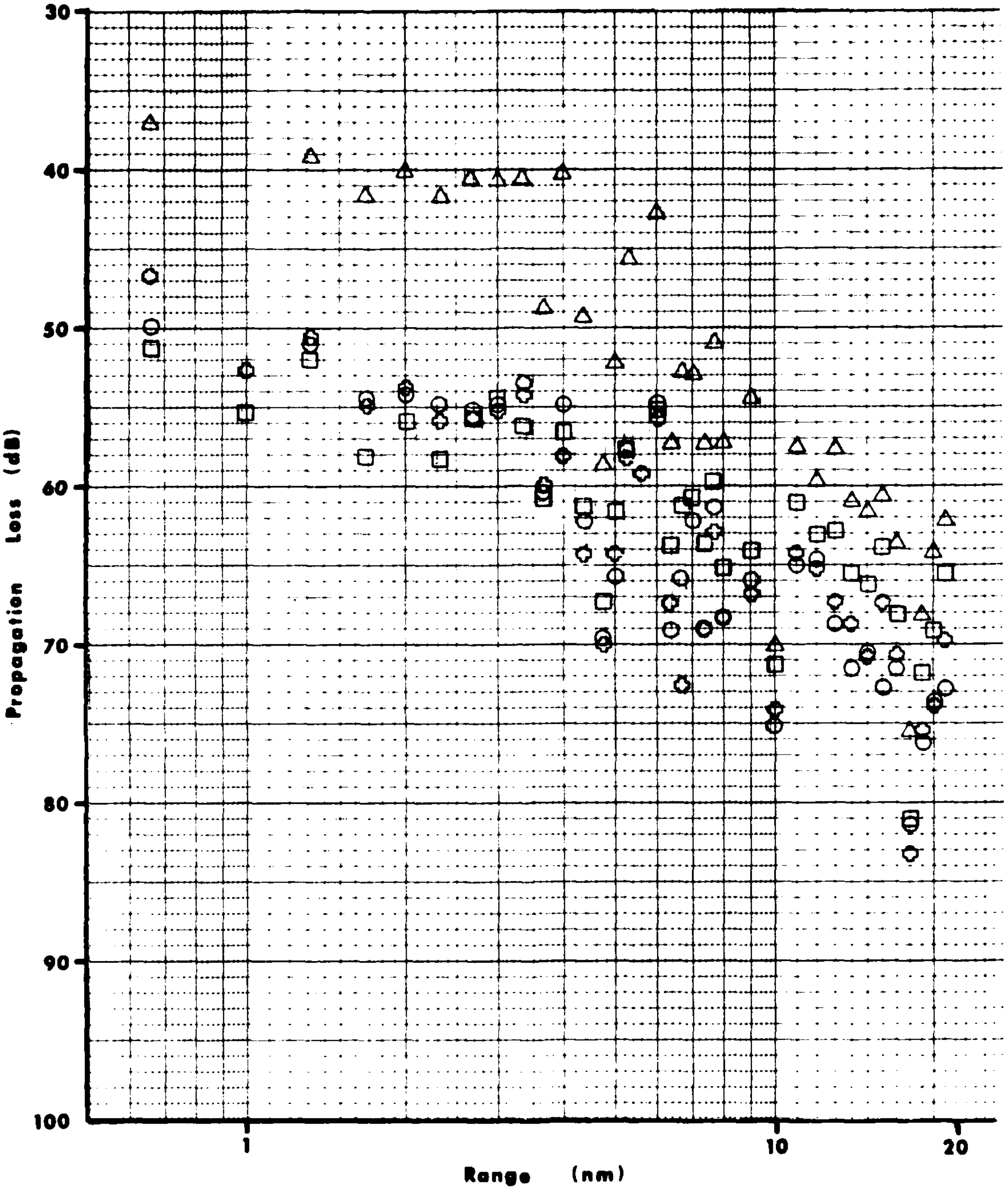

Figure B-12. Measured Propagation Loss for Run 1 at a Frequency of 100 Hz.

○ = Hydrophone. Triaxial Geophones: △ = Vertical, □ = Horizontal-2, ⬡ = Horizontal-1.

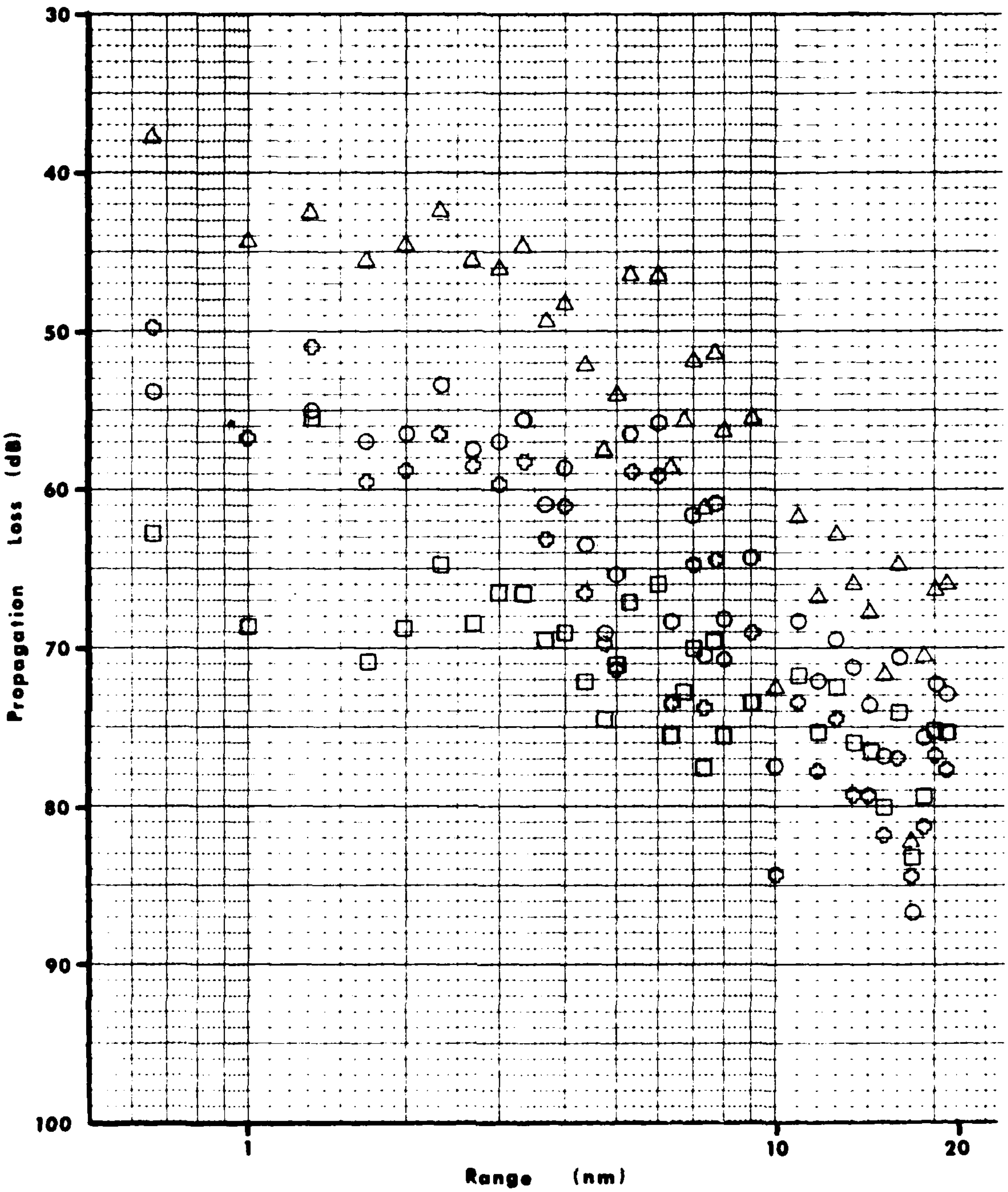

Figure B-13. Measured Propagation Loss for Run 1 at a Frequency of 125 Hz.

○ = Hydrophone. Triaxial Geophones: △ = Vertical, □ = Horizontal-2, ⌽ = Horizontal-1.

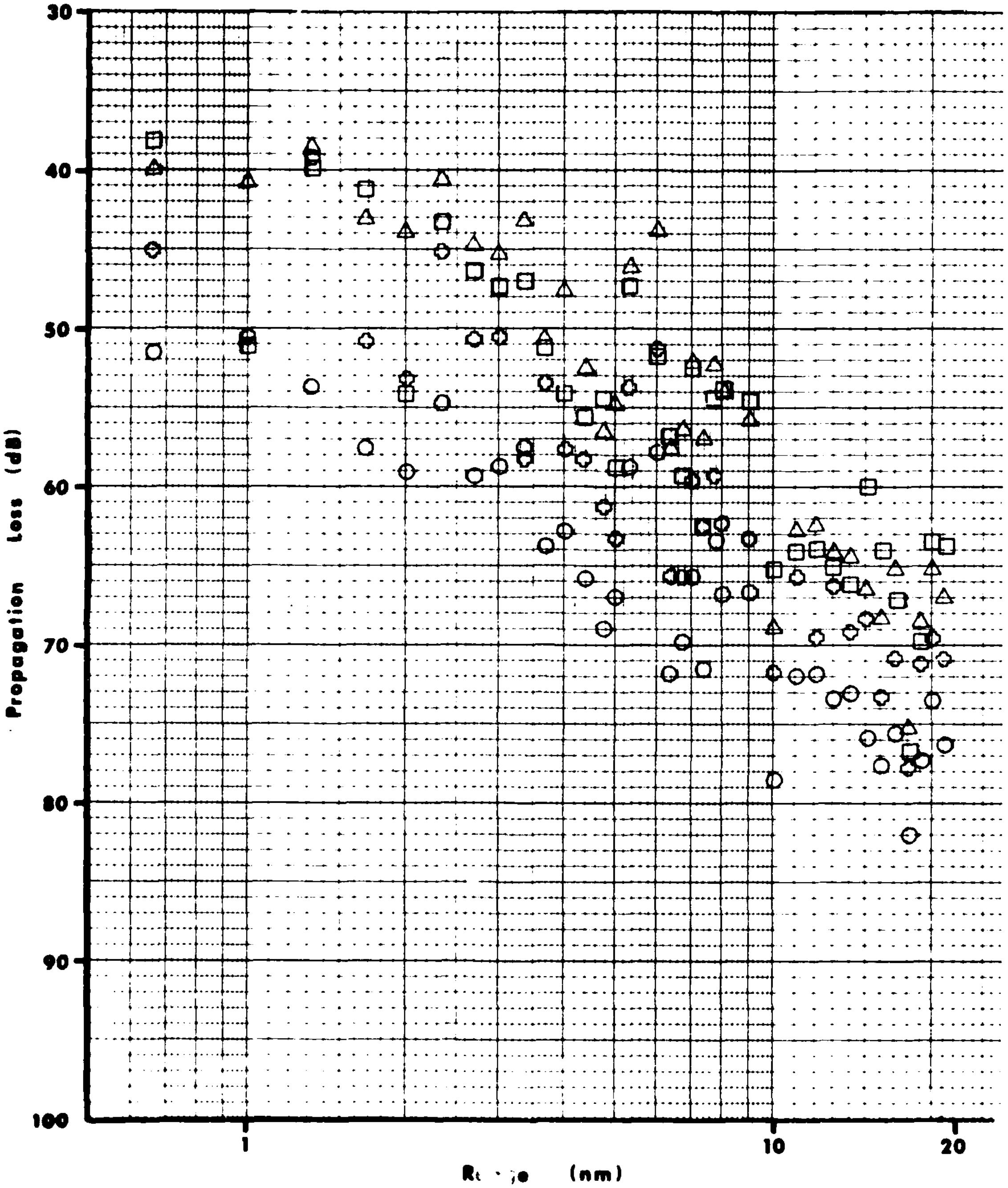

Figure B-14. Measured Propagation Loss for Run 1 at a Frequency of 160 Hz.

Hydrophone Triaxial Geophones: △ = Vertical, □ = Horizontal-2,
Horizontal-1

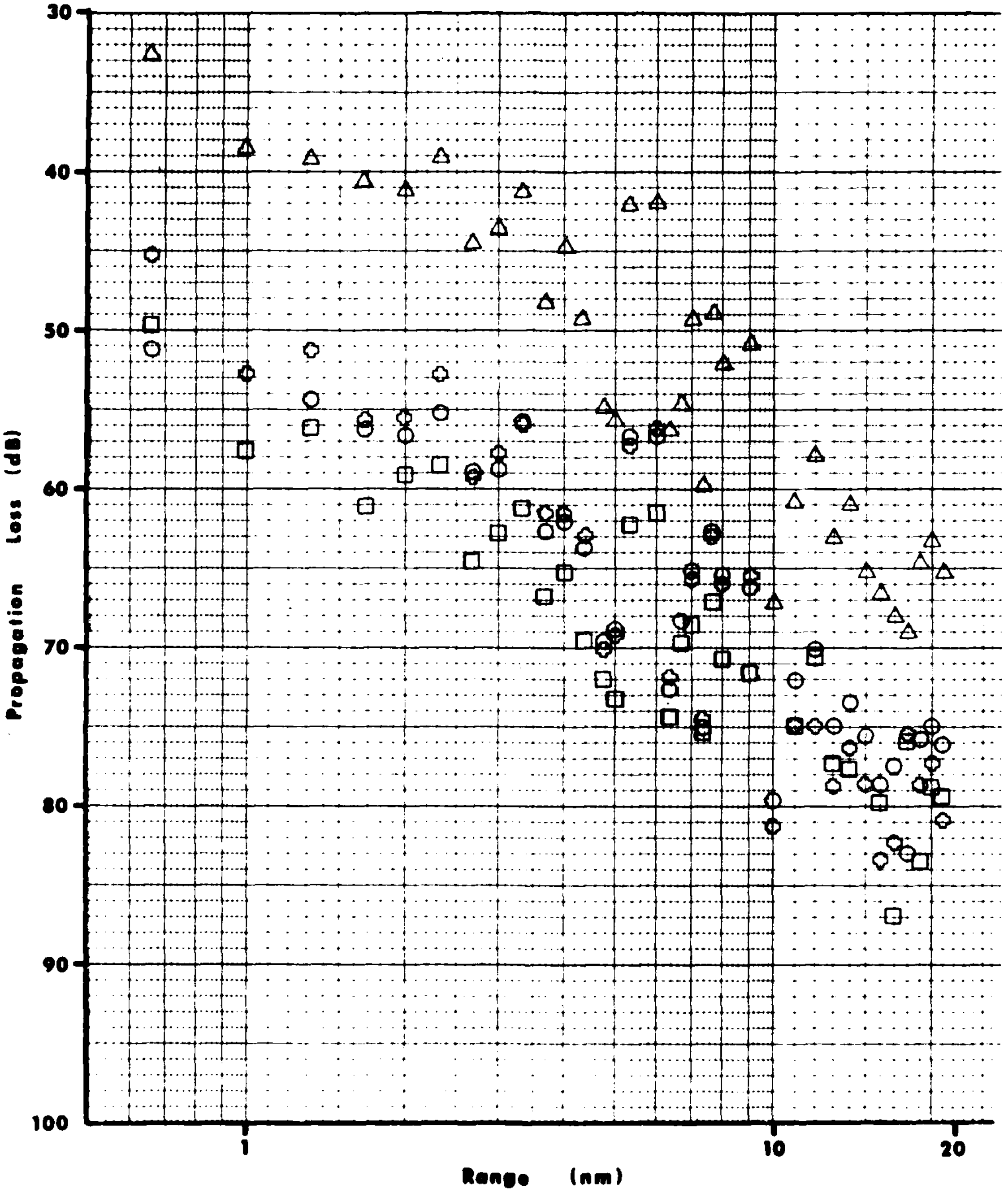

Figure B-15. Measured Propagation Loss for Run 1 at a Frequency of 200 Hz.

○ = Hydrophone. Triaxial Geophones: △ = Vertical, □ = Horizontal-2,
⬡ = Horizontal-1.

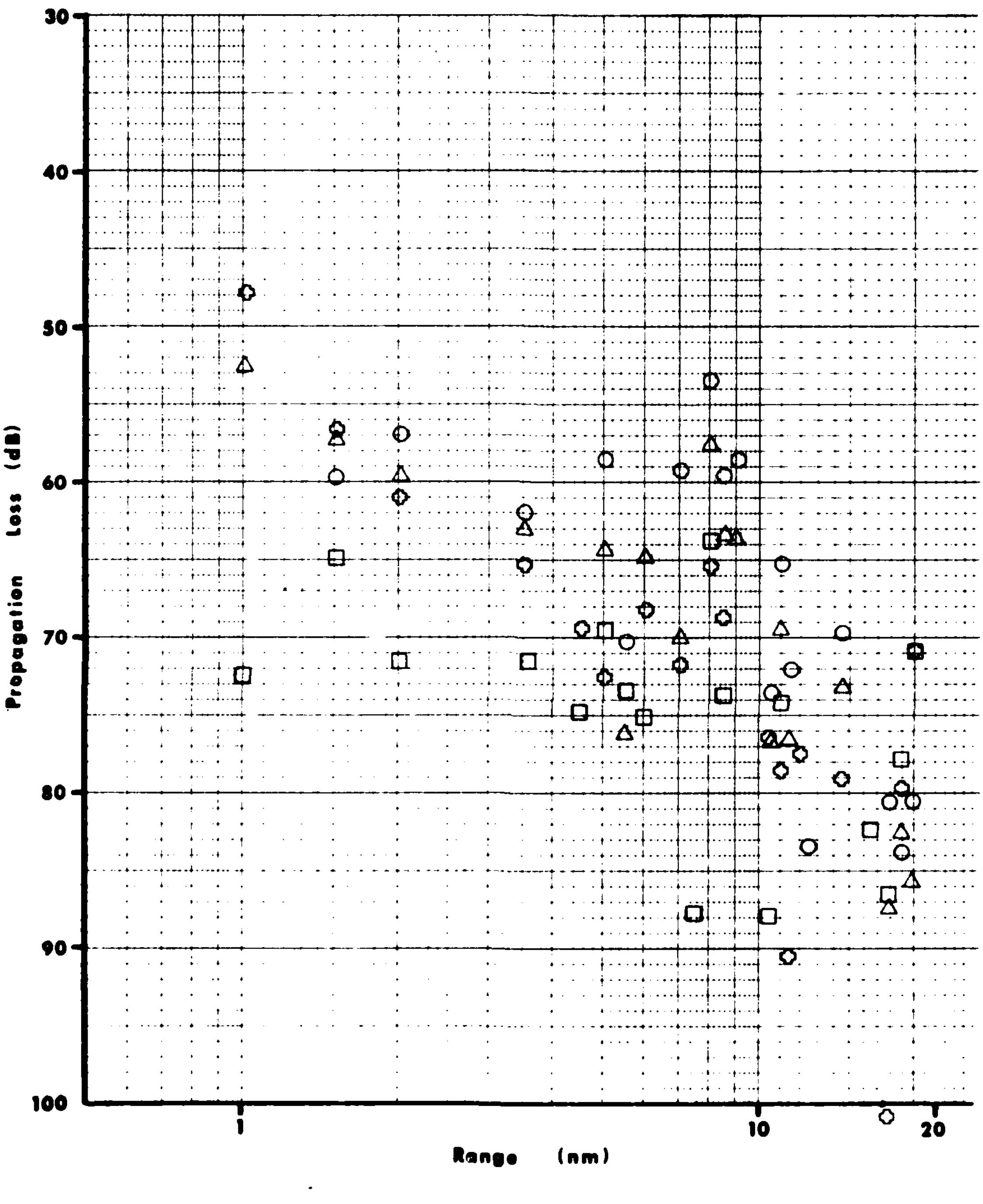

Figure B-16. Measured Propagation Loss for Run 2 at a Frequency of 8 Hz.

○ = Hydrophone. Triaxial Geophones: △ = Vertical, □ = Horizontal-2, ◇ = Horizontal-1.

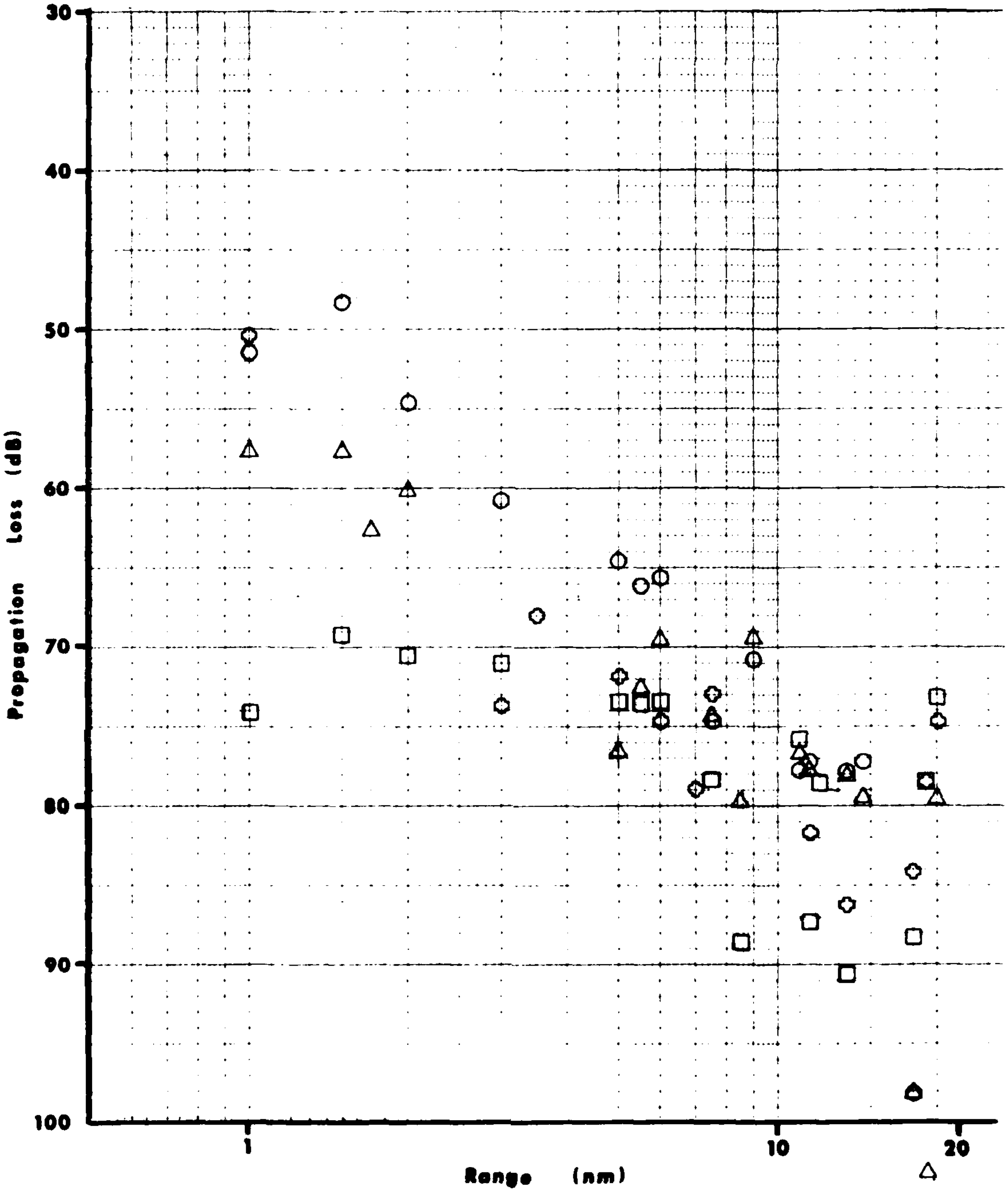

Figure B-17. Measured Propagation Loss for Run 2 at a Frequency of 10 Hz.

○ = Hydrophone. Triaxial Geophones: △ = Vertical, □ = Horizontal-2, ⬡ = Horizontal-1.

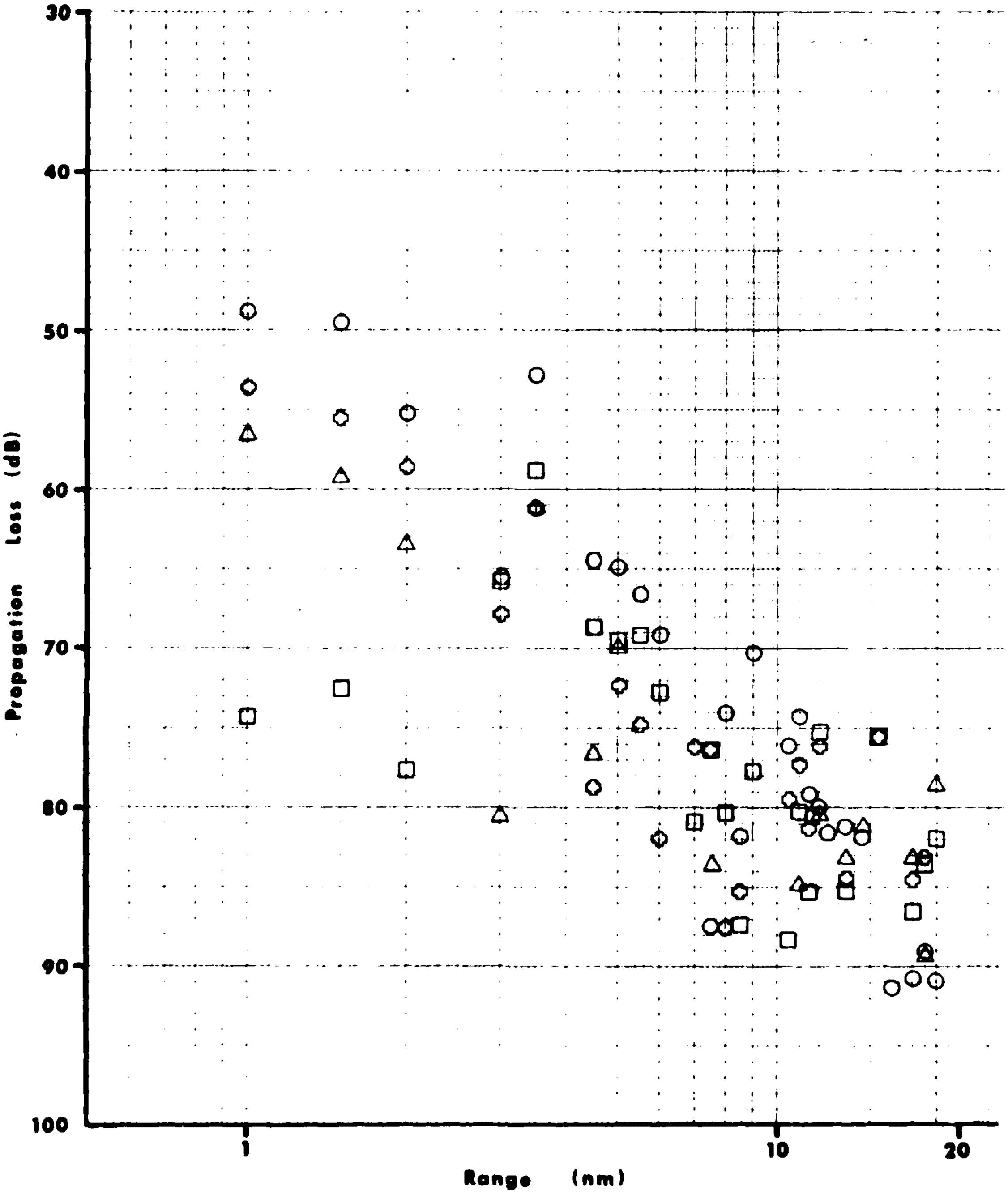

Figure B-18. Measured Propagation Loss for Run 2 at a Frequency of 12.5 Hz.

○ = Hydrophone. Triaxial Geophones: △ = Vertical, □ = Horizontal-2, ◇ = Horizontal-1.

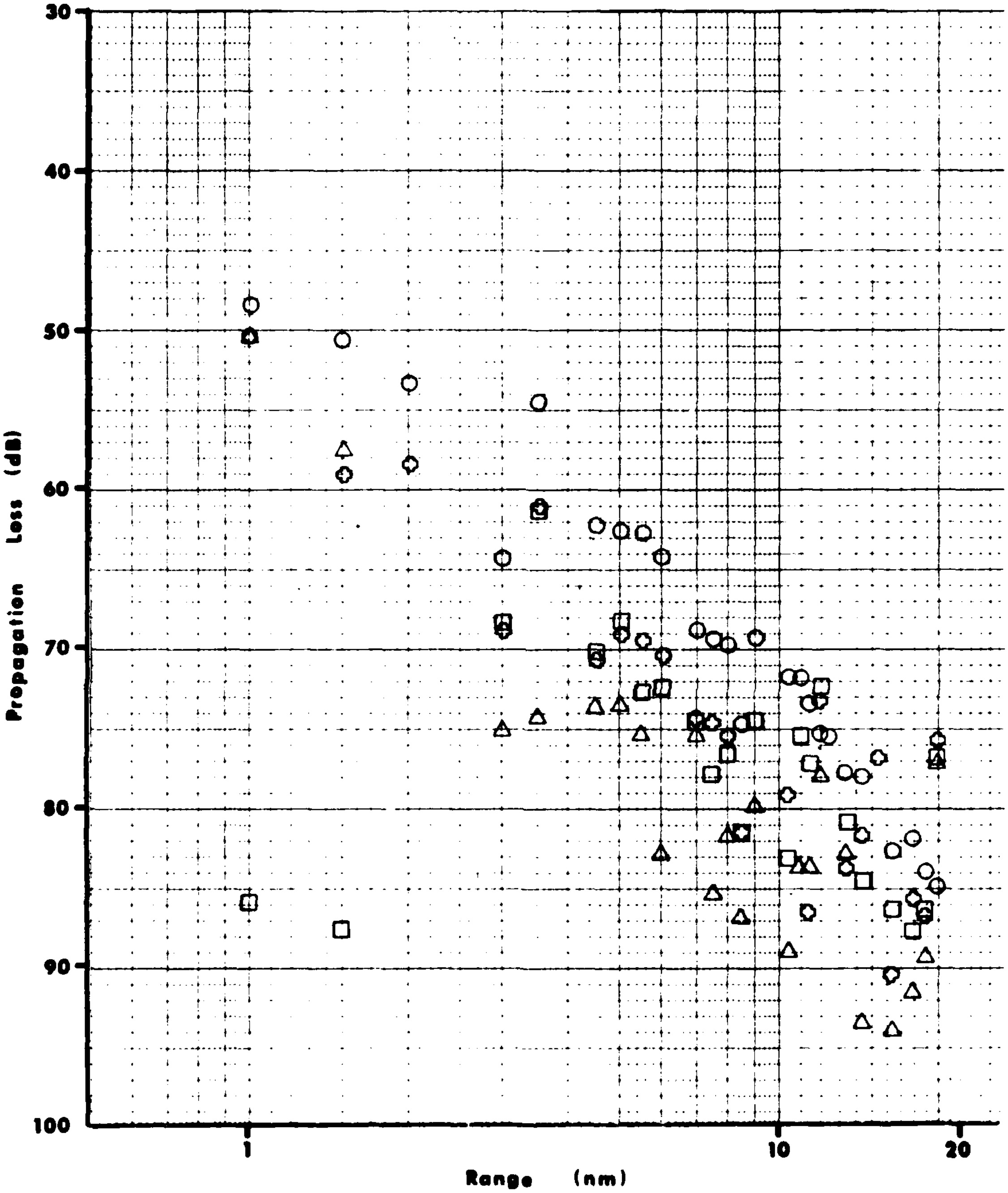

Figure B-19. Measured Propagation Loss for Run 2 at a Frequency of 16 Hz.

○ = Hydrophone. Triaxial Geophones: △ = Vertical, □ = Horizontal-2, ◇ = Horizontal-1.

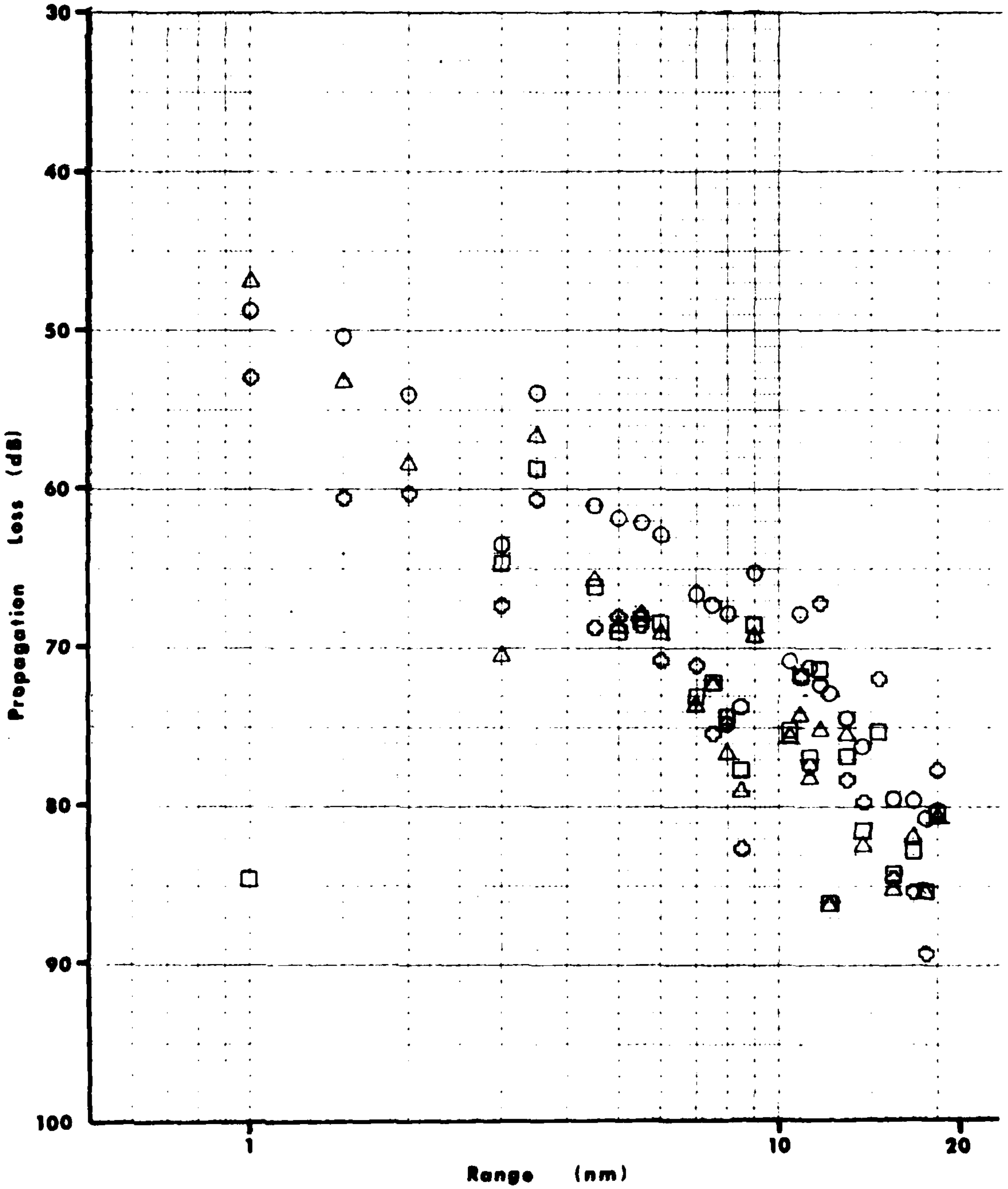

Figure B-20. Measured Propagation Loss for Run 2 at a Frequency of 20 Hz.

○ = Hydrophone. Triaxial Geophones: △ = Vertical, □ = Horizontal-2, ◇ = Horizontal-1.

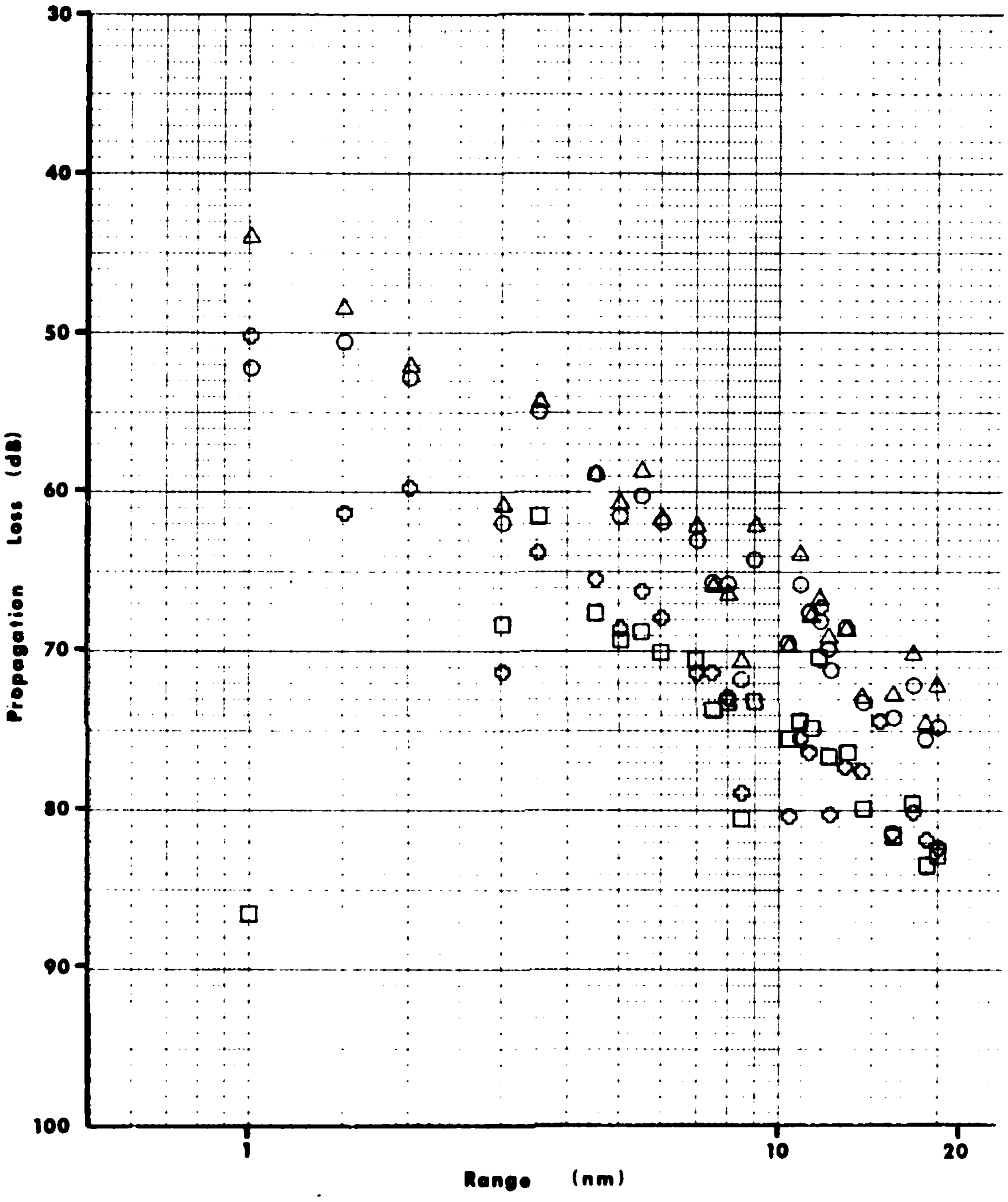

Figure B-21. Measured Propagation Loss for Run 2 at a Frequency of 25 Hz.

○ = Hydrophone. Triaxial Geophones: △ = Vertical, □ = Horizontal-2, ⬡ = Horizontal-1.

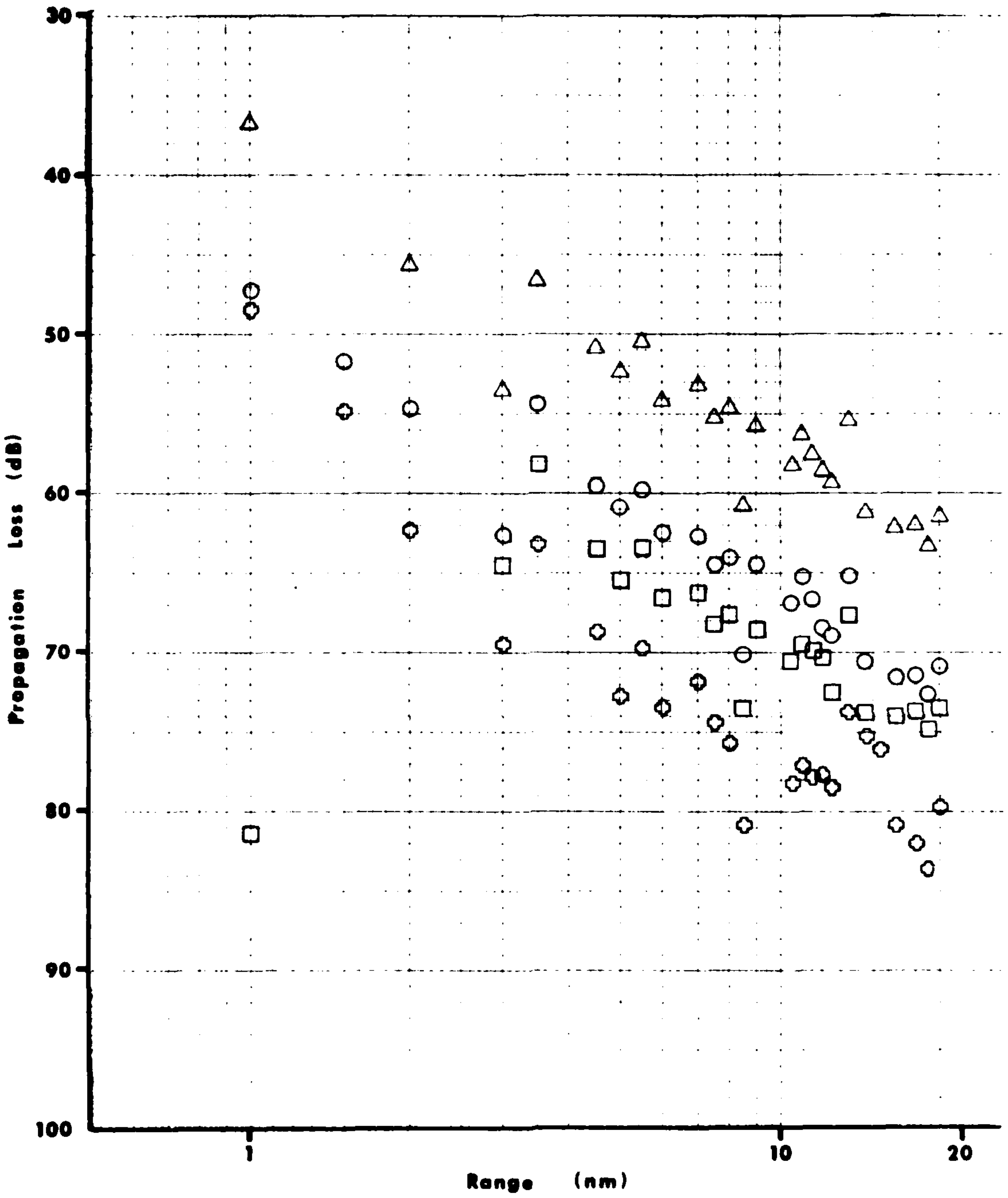

Figure B-22. Measured Propagation Loss for Run 2 at a Frequency of 31.5 Hz.

○ = Hydrophone. Triaxial Geophones: △ = Vertical, □ = Horizontal-2, ◇ = Horizontal-1.

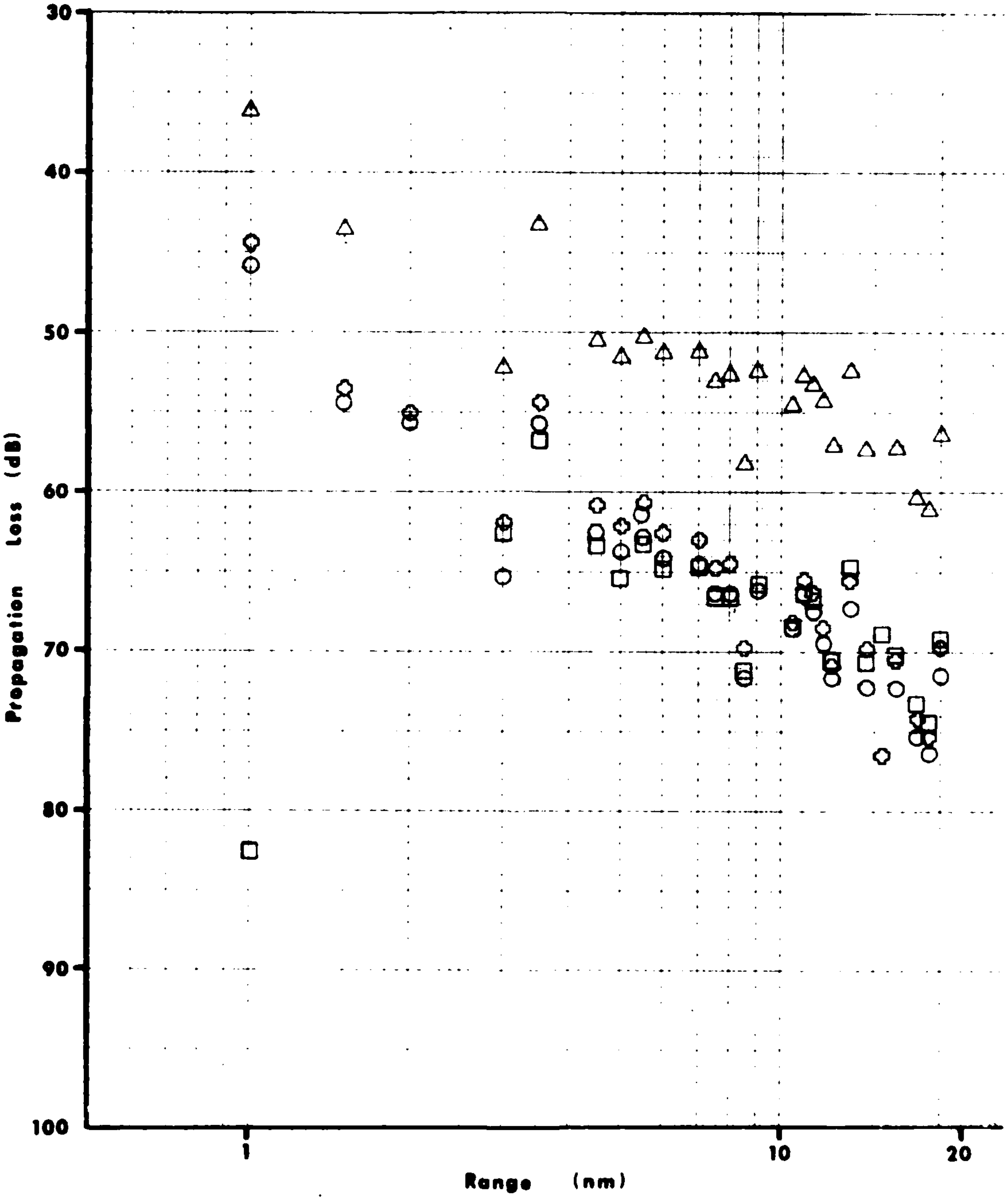

Figure B-23. Measured Propagation Loss for Run 2 at a Frequency of 40 Hz.

○ = Hydrophone. Triaxial Geophones: △ = Vertical, □ = Horizontal-2,
⬡ = Horizontal-1.

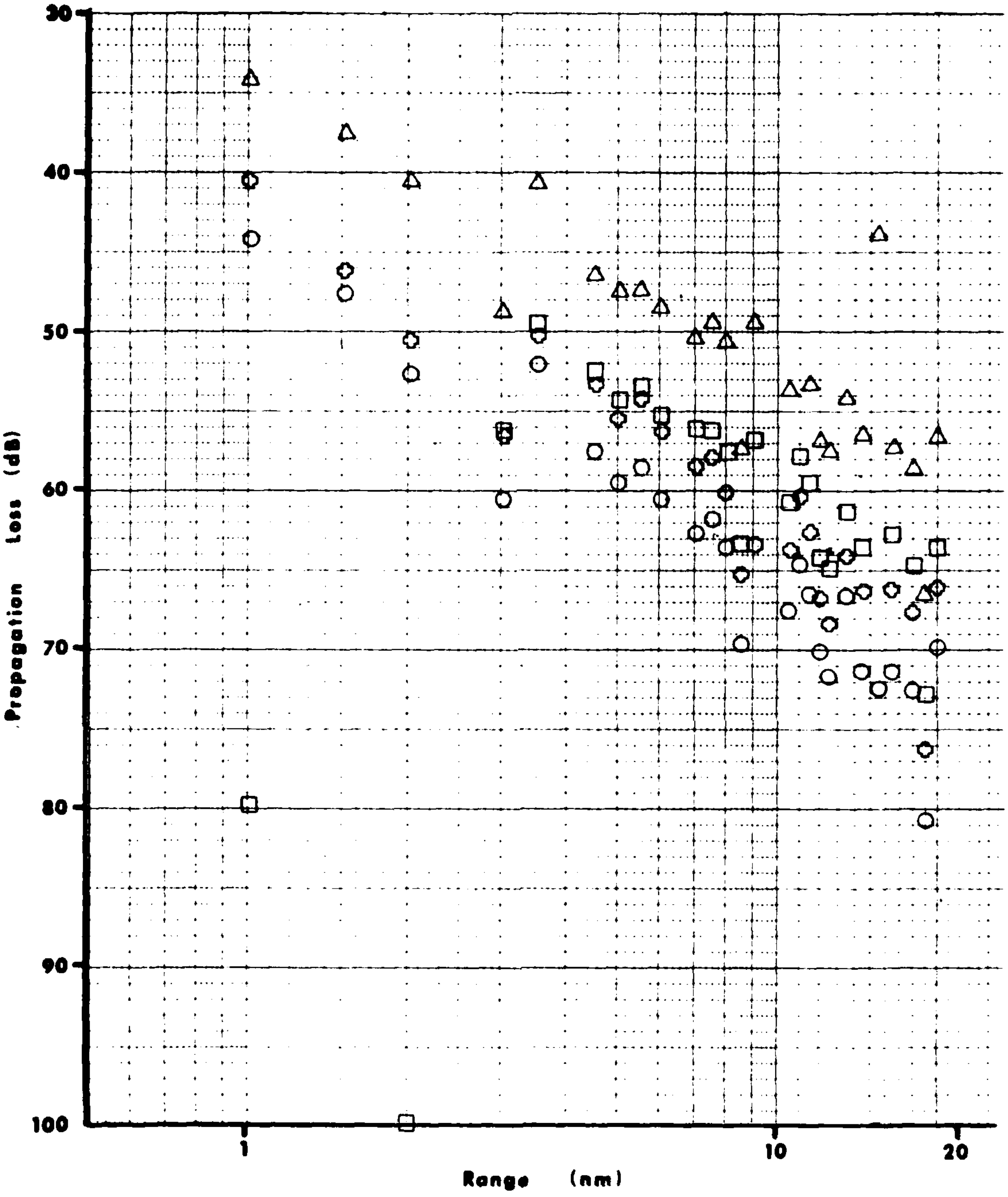

Figure B-24. Measured Propagation Loss for Run 2 at a Frequency of 50 Hz.

○ = Hydrophone. Triaxial Geophones: △ = Vertical, □ = Horizontal-2, ◇ = Horizontal-1.

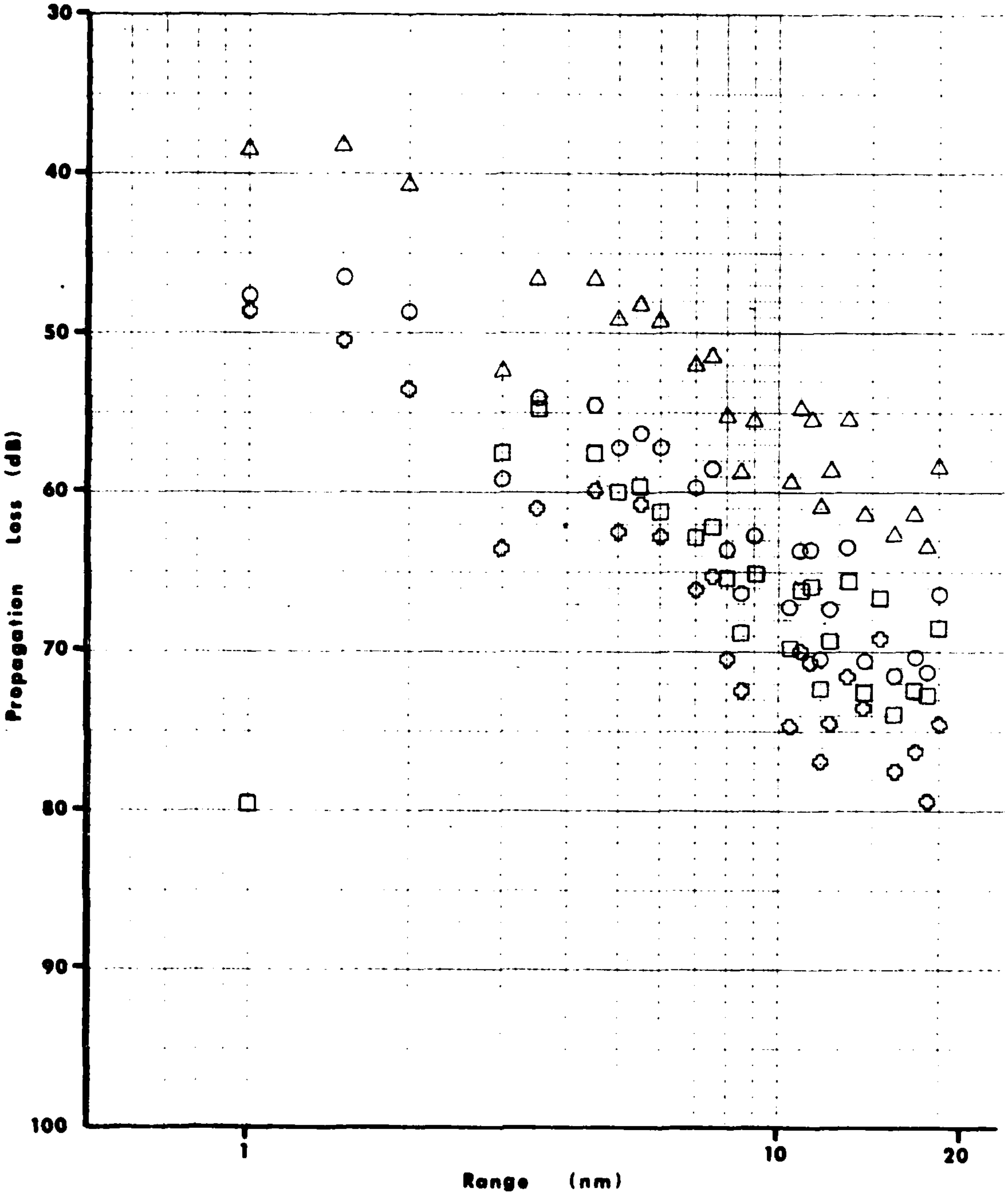

Figure B-25. Measured Propagation Loss for Run 2 at a Frequency of 63 Hz.

○ = Hydrophone. Triaxial Geophones: △ = Vertical, □ = Horizontal-2, ⌬ = Horizontal-1.

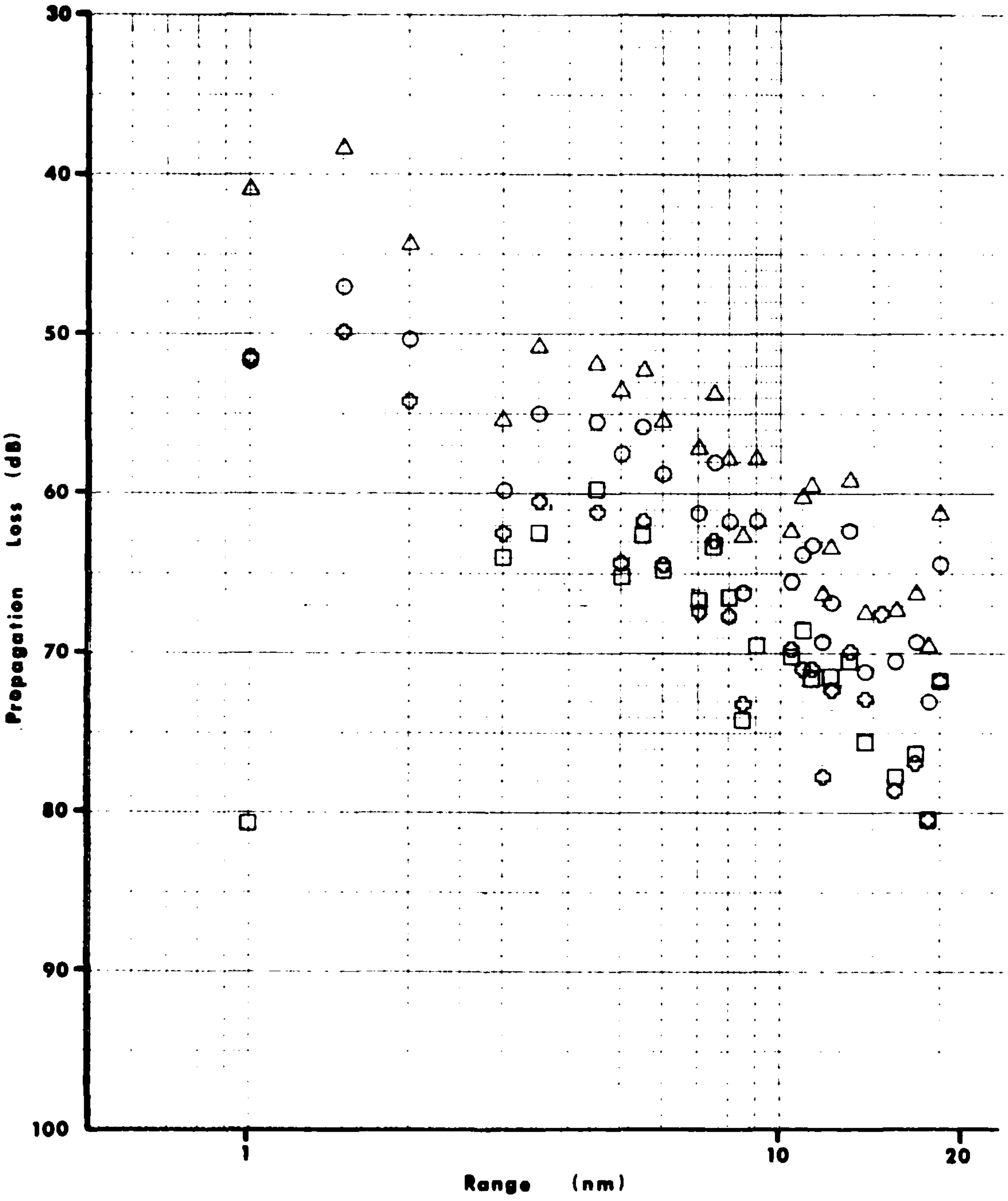

Figure B-26. Measured Propagation Loss for Run 2 at a Frequency of 80 Hz.

○ = Hydrophone. Triaxial Geophones: △ = Vertical, □ = Horizontal-2, ○ = Horizontal-1.

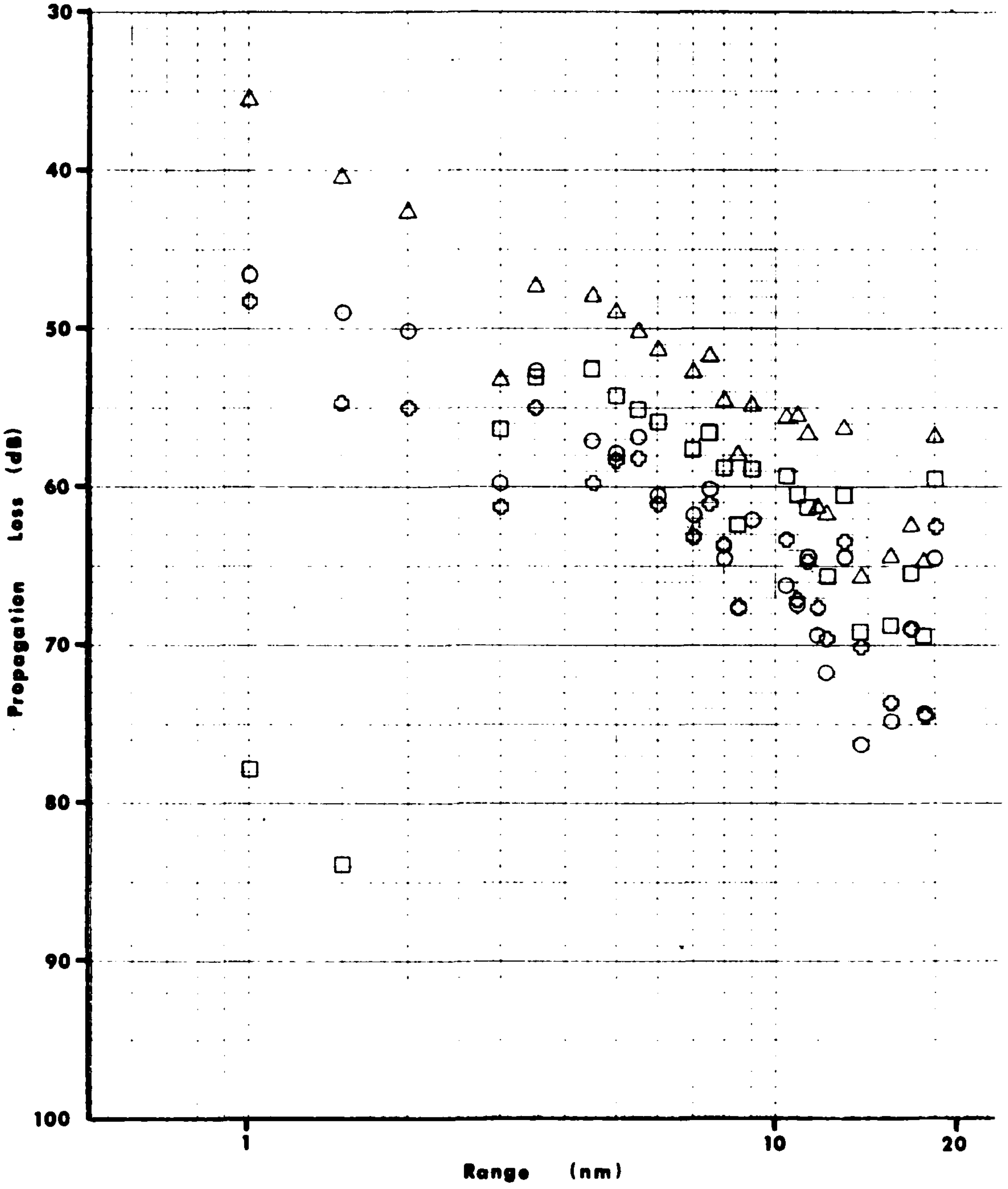

Figure B-27. Measured Propagation Loss for Run 2 at a Frequency of 100 Hz.

○ = Hydrophone. Triaxial Geophones: △ = Vertical, □ = Horizontal-2,
○ = Horizontal-1.

AD-A091 024 UNDERWATER SYSTEMS INC ROCKVILLE MD F/G 20/1
SOUND PROPAGATION SOUTH OF MARTHA'S VINEYARD.(U)
JUN 80 R J HECHT N00014-79-C-0466
UNCLASSIFIED NL

2 OF 2
AD A
091 024

END
DATE
FILMED
11-80
DTIC

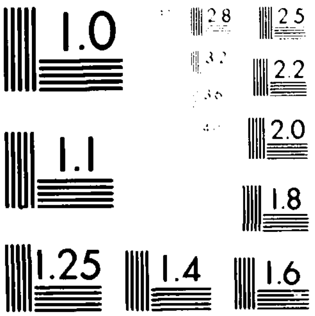

MICROCOPY RESOLUTION TEST CHART

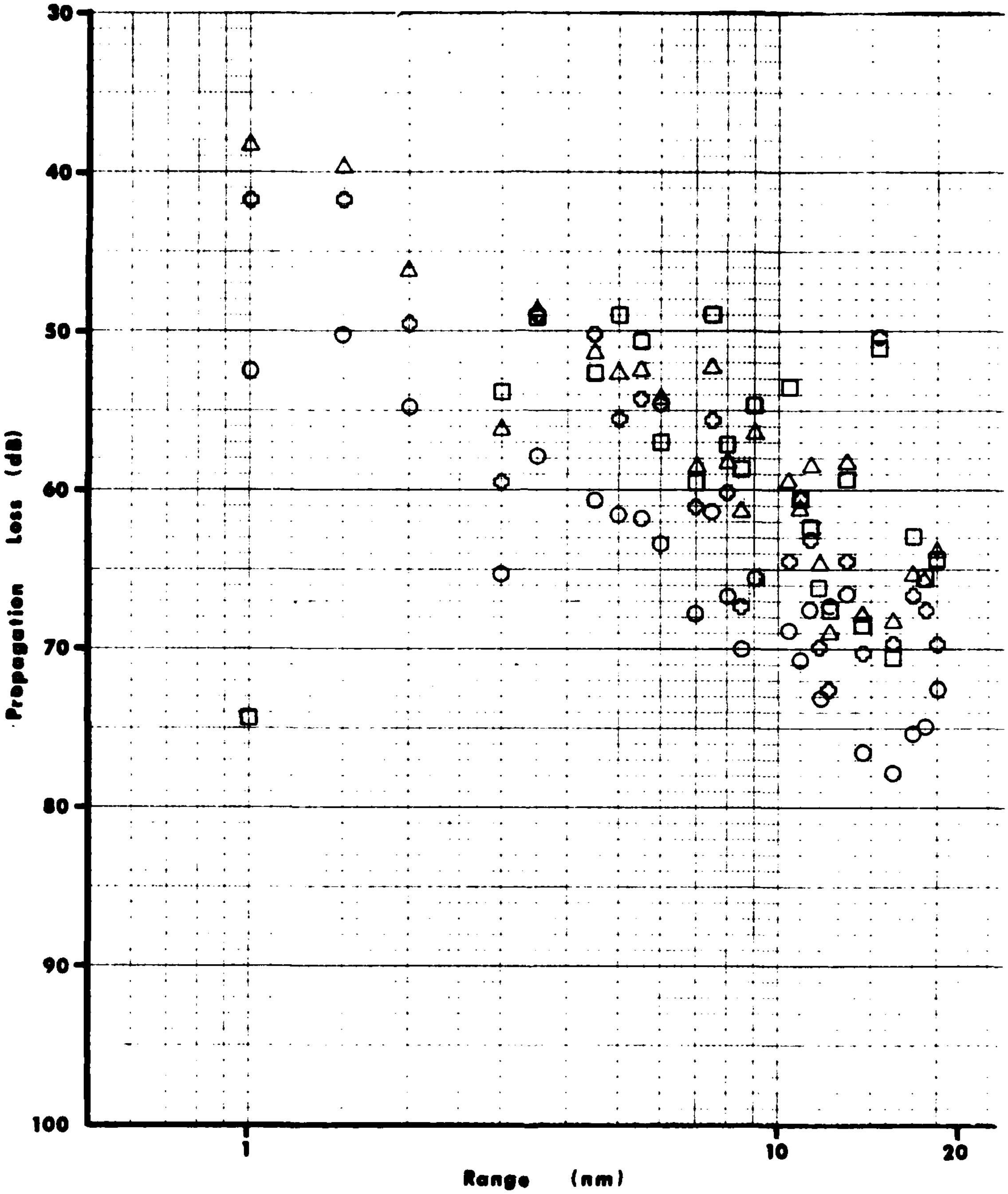

Figure B-28. Measured Propagation Loss for Run 2 at a Frequency of 125 Hz.

○ = Hydrophone. Triaxial Geophones: △ = Vertical, □ = Horizontal-2, ⬡ = Horizontal-1.

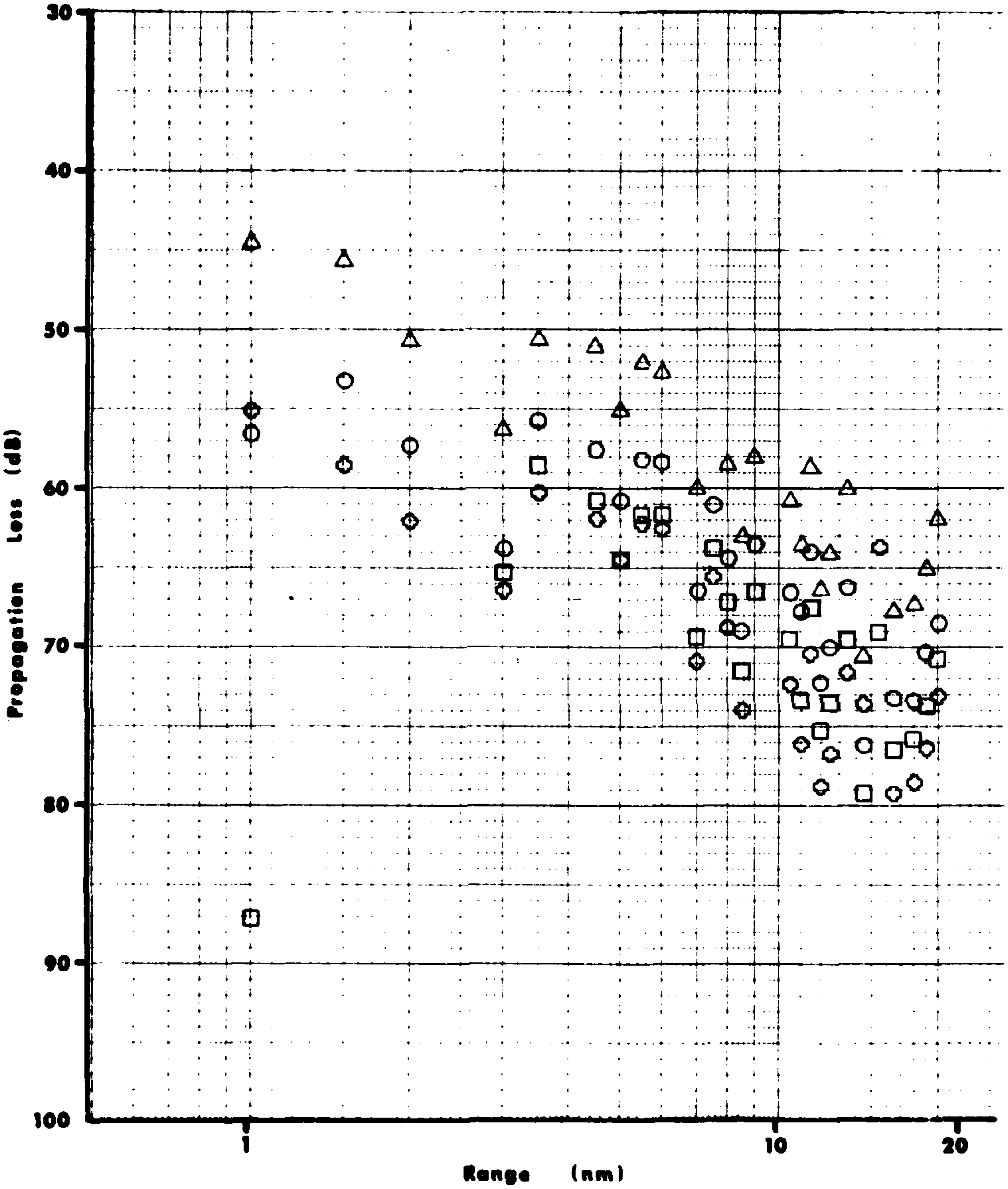

Figure B-29. Measured Propagation Loss for Run 2 at a Frequency of 160 Hz.

○ = Hydrophone. Triaxial Geophones: △ = Vertical, □ = Horizontal-2, ◇ = Horizontal-1.

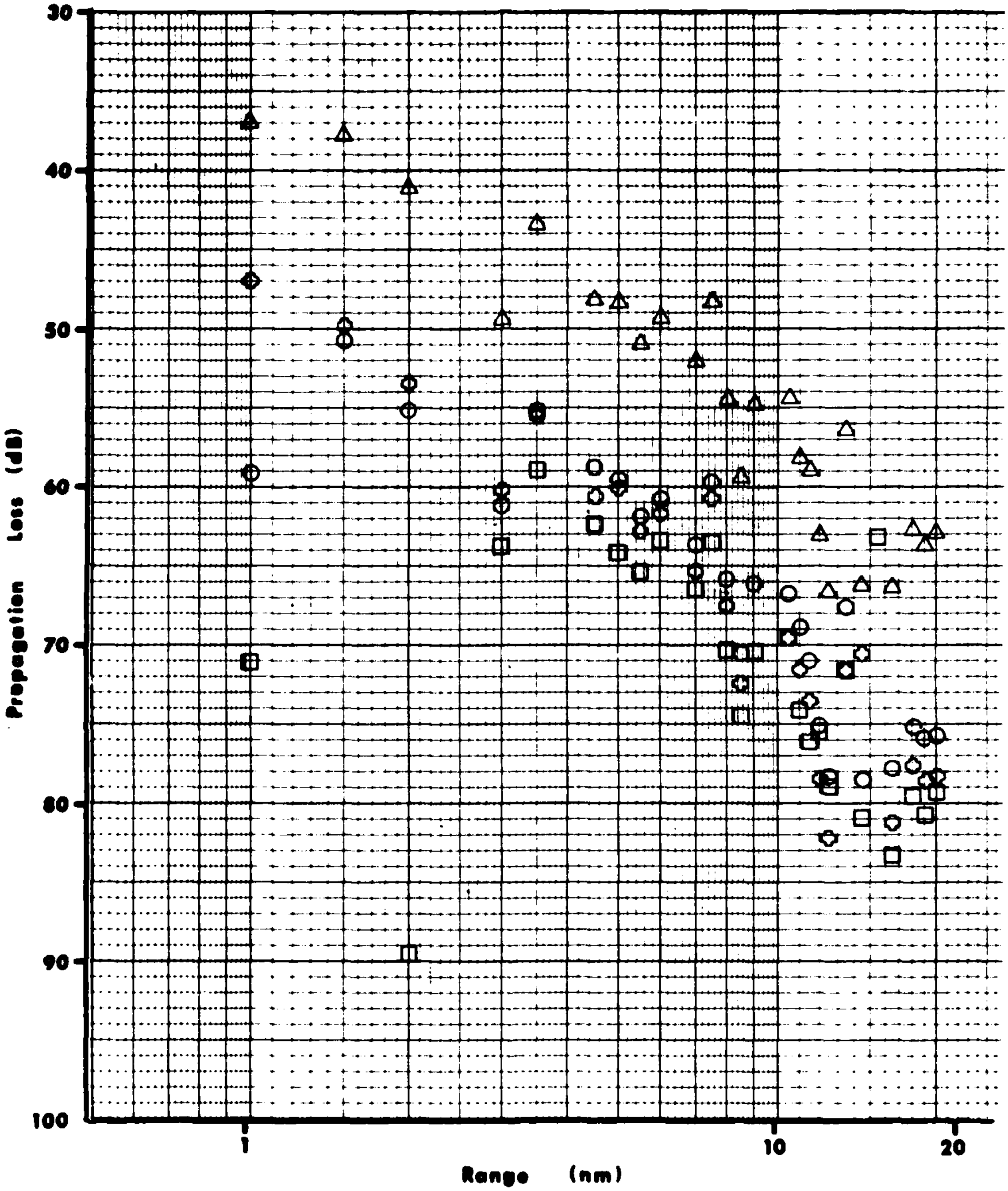

Figure B-30. Measured Propagation Loss for Run 2 at a Frequency of 200 Hz.

○ = Hydrophone. Triaxial Geophones: △ = Vertical, □ = Horizontal-2, ⬡ = Horizontal-1.

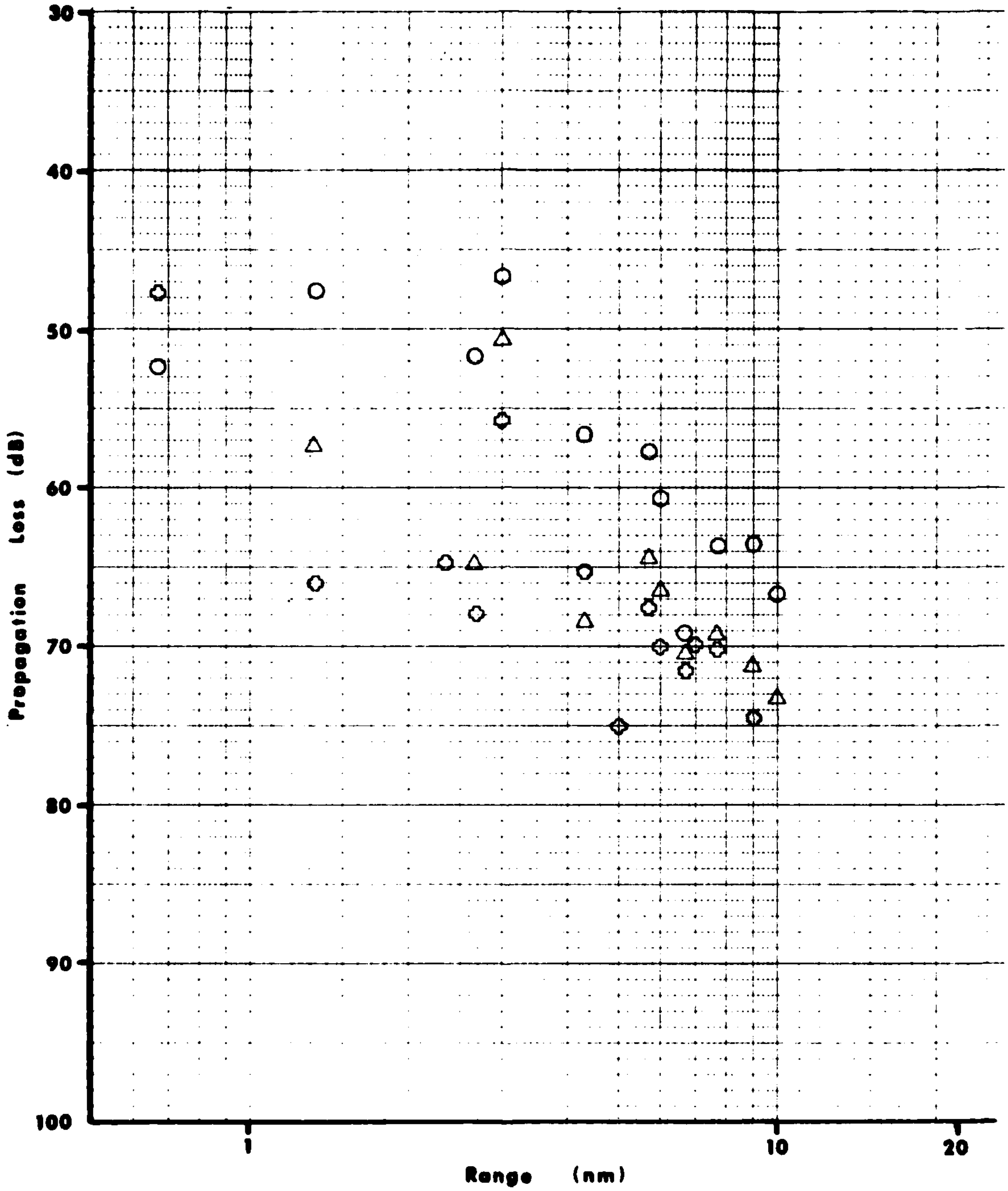

Figure B-31. Measured Propagation Loss for Run 3 at a Frequency of 8 Hz.

○ = Hydrophone. Triaxial Geophones: △ = Vertical, □ = Horizontal-2, ◇ = Horizontal-1.

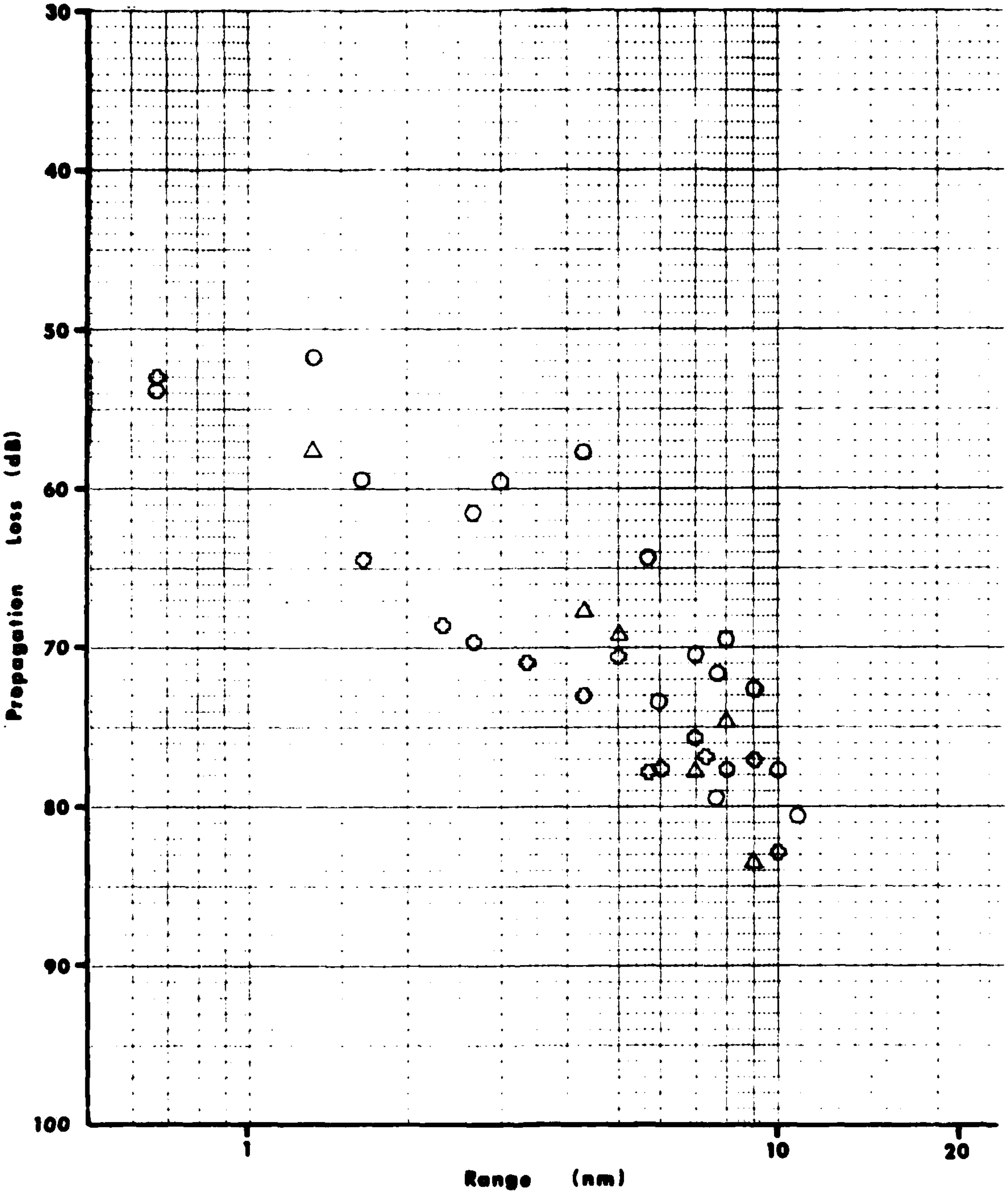

Figure B-32. Measured Propagation Loss for Run 3 at a Frequency of 10 Hz.

○ = Hydrophone. Triaxial Geophones: △ = Vertical, □ = Horizontal-2, ⬡ = Horizontal-1.

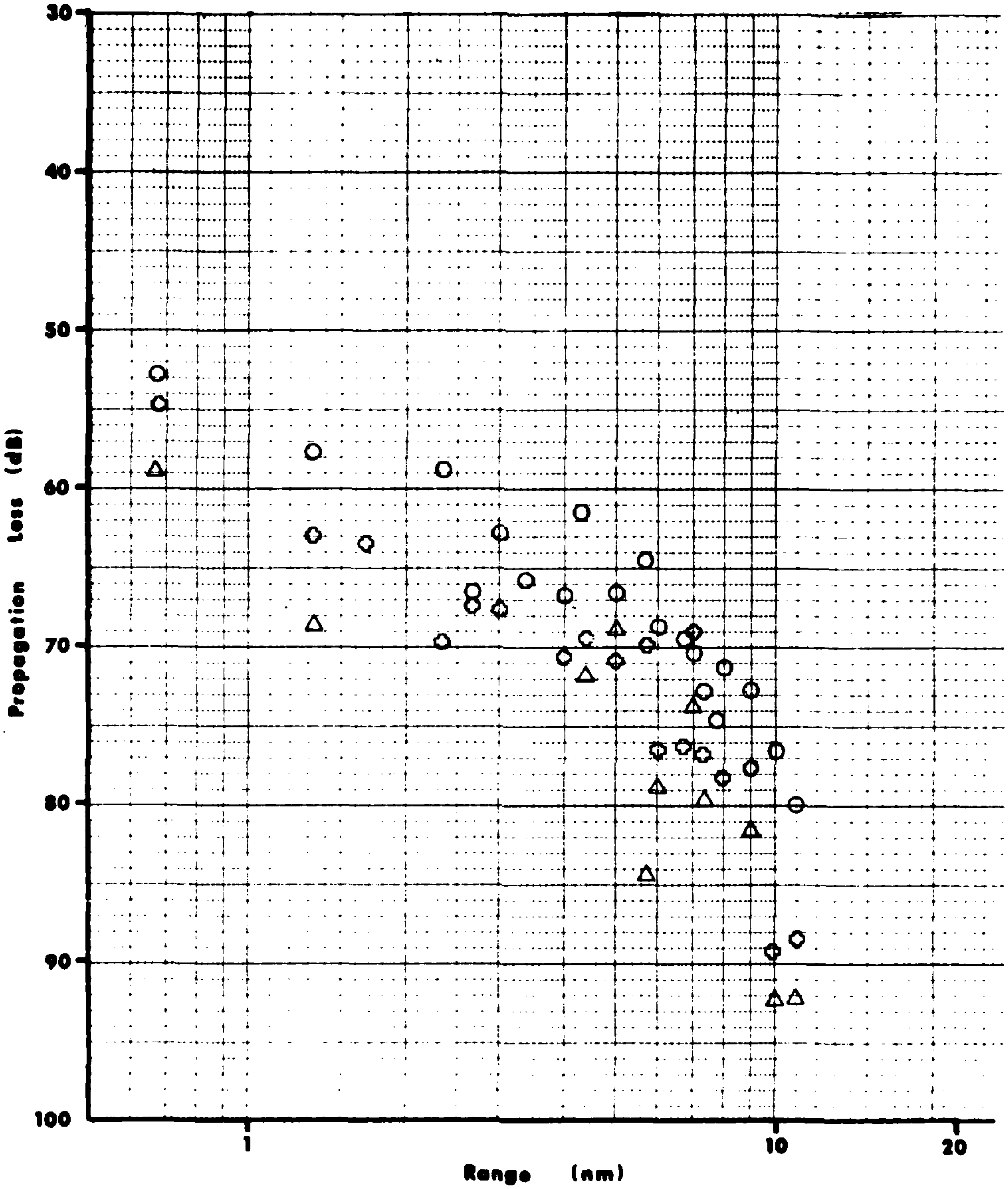

Figure B-33. Measured Propagation Loss for Run 3 at a Frequency of 12.6 Hz.

○ = Hydrophone. Triaxial Geophones: △ = Vertical, □ = Horizontal-2, ◇ = Horizontal-1.

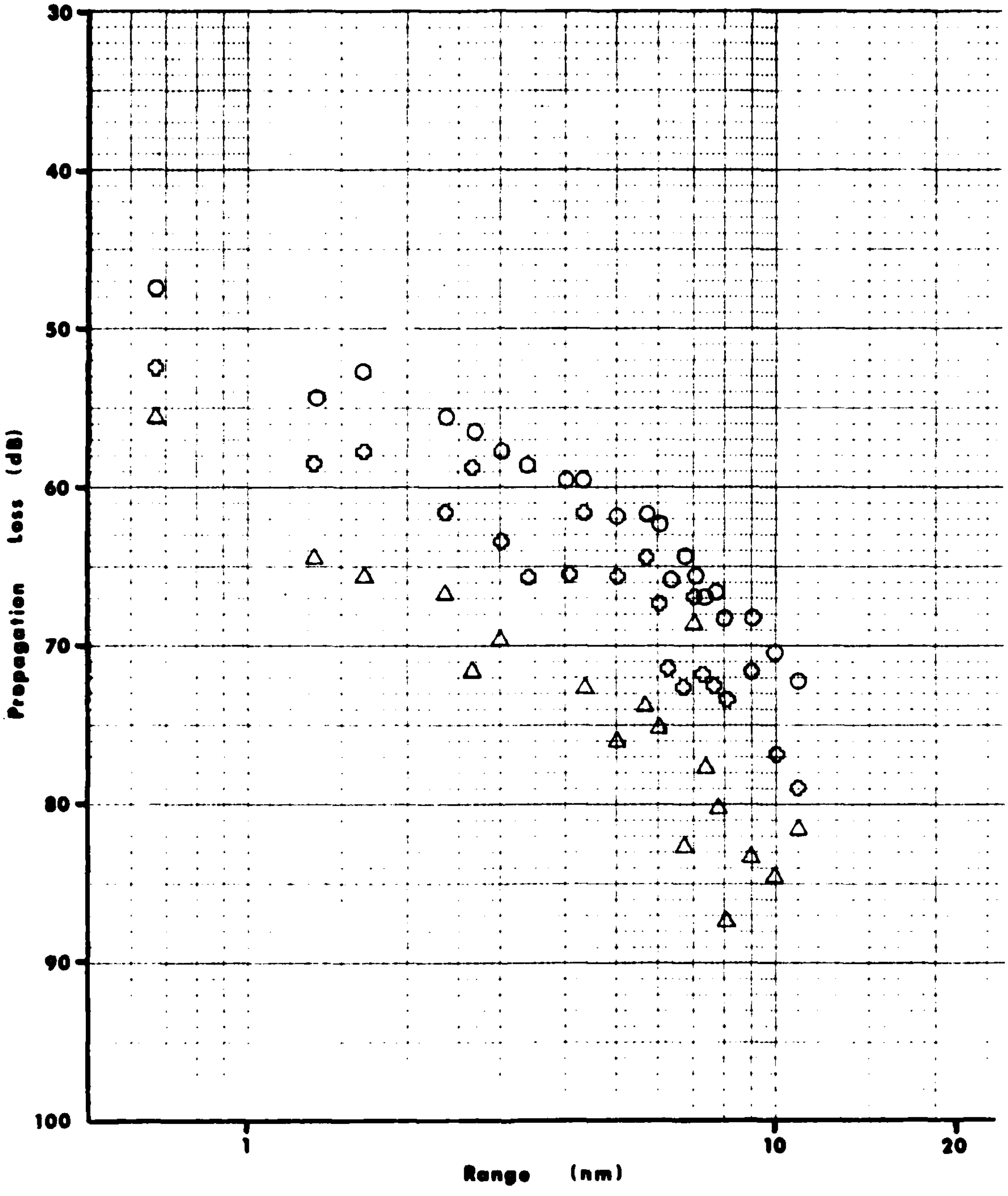

Figure B-34. Measured Propagation Loss for Run 3 at a Frequency of 16 Hz.

○ = Hydrophone. Triaxial Geophones: △ = Vertical, □ = Horizontal-2,
◇ = Horizontal-1.

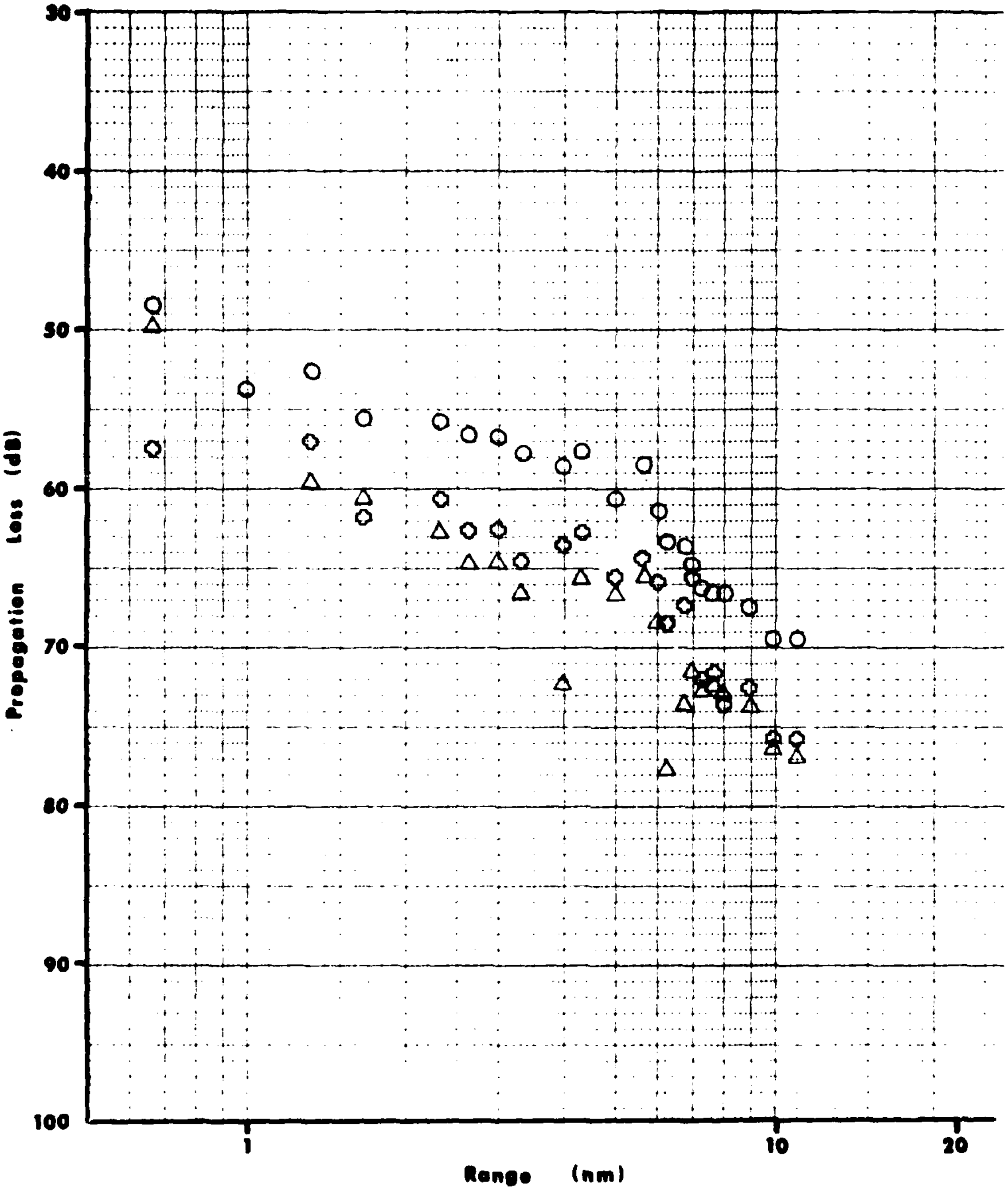

Figure B-35. Measured Propagation Loss for Run 3 at a Frequency of 20 Hz.

○ = Hydrophone. Triaxial Geophones: △ = Vertical, □ = Horizontal-2, ⬡ = Horizontal-1.

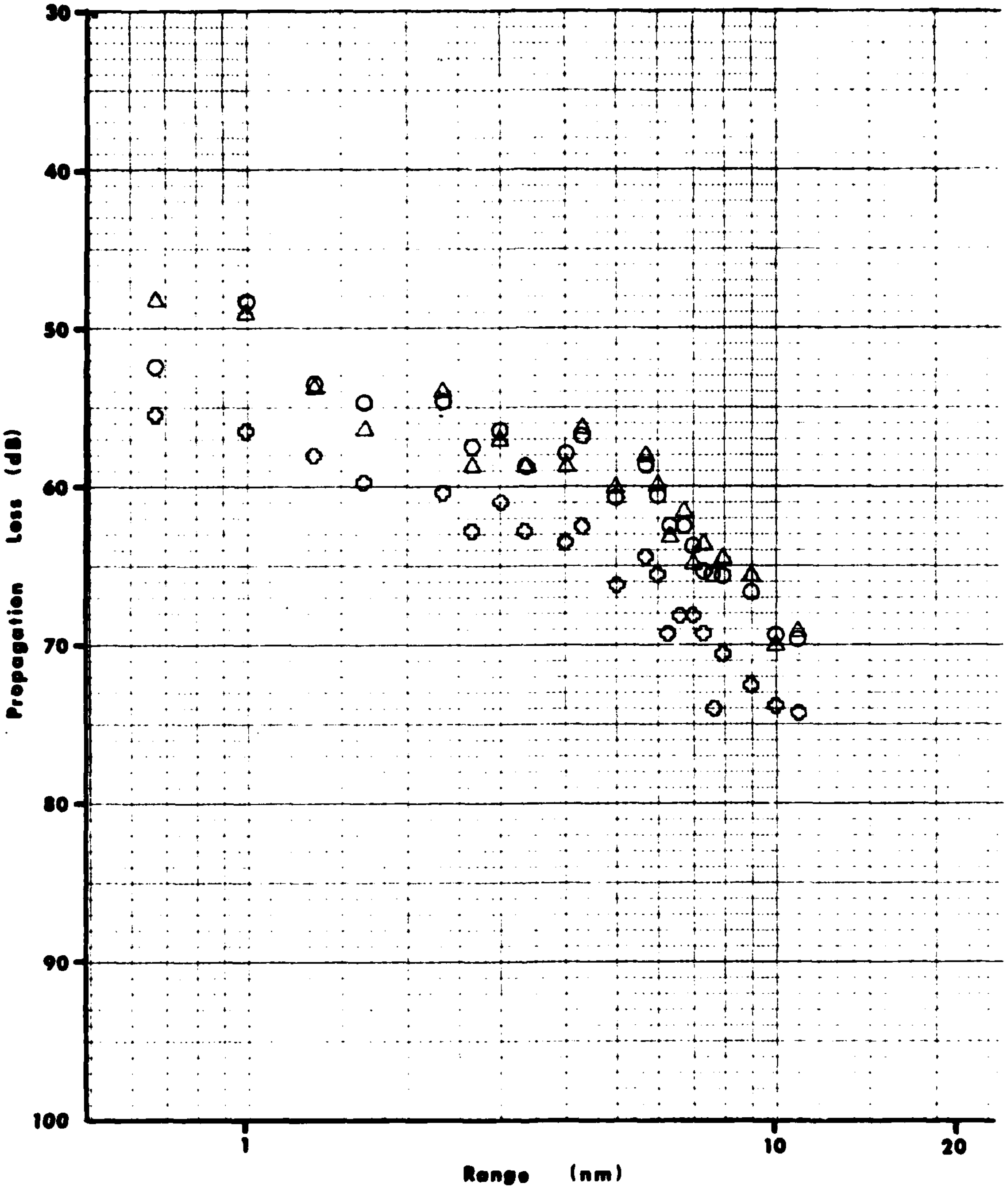

Figure B-36. Measured Propagation Loss for Run 3 at a Frequency of 25 Hz.

○ = Hydrophone. Triaxial Geophones: △ = Vertical, □ = Horizontal-2, ◇ = Horizontal-1.

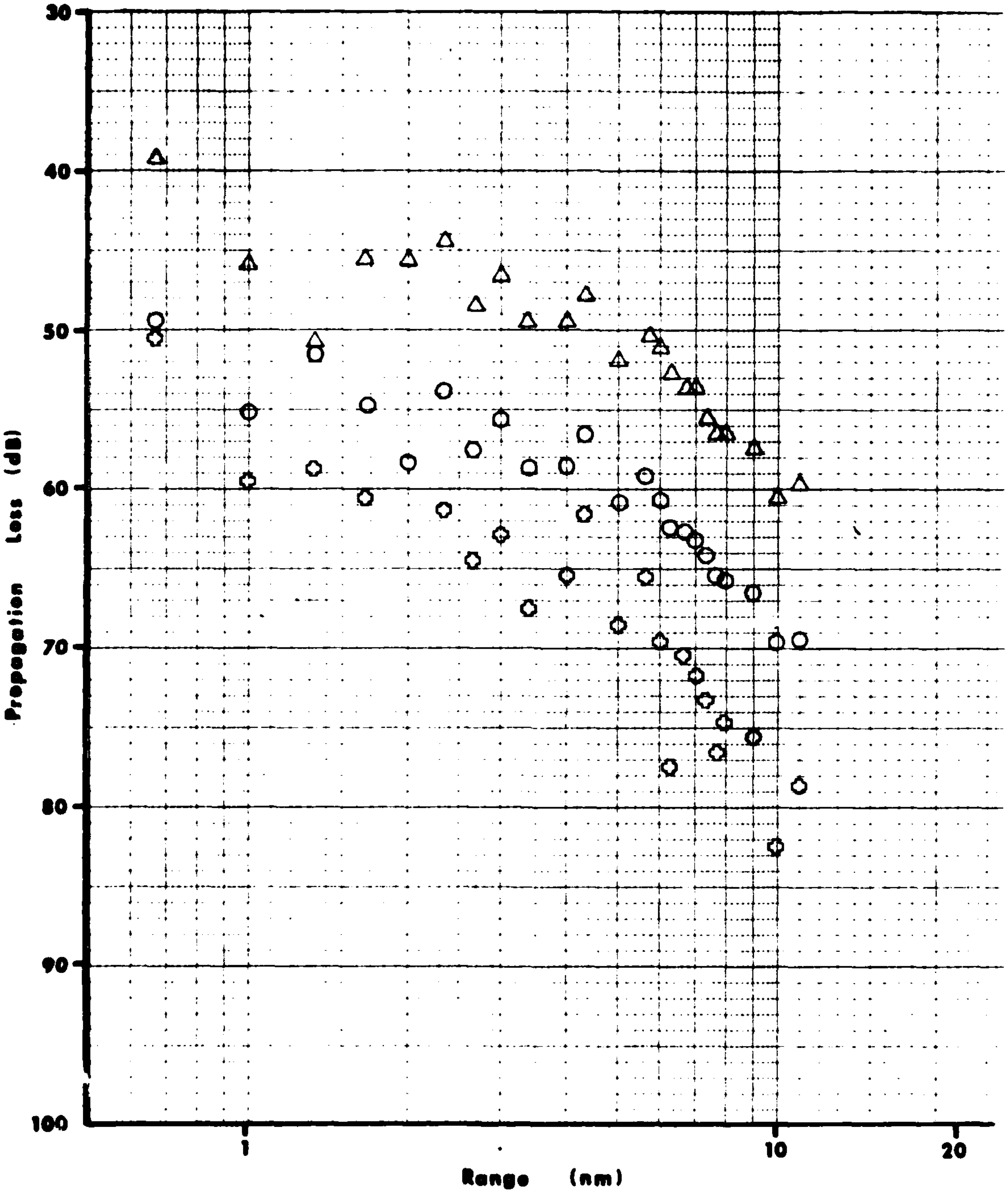

Figure B-37. Measured Propagation Loss for Run 3 at a Frequency of 31.5 Hz.

○ = Hydrophone. Triaxial Geophones: △ = Vertical, □ = Horizontal-2,
⬡ = Horizontal-1.

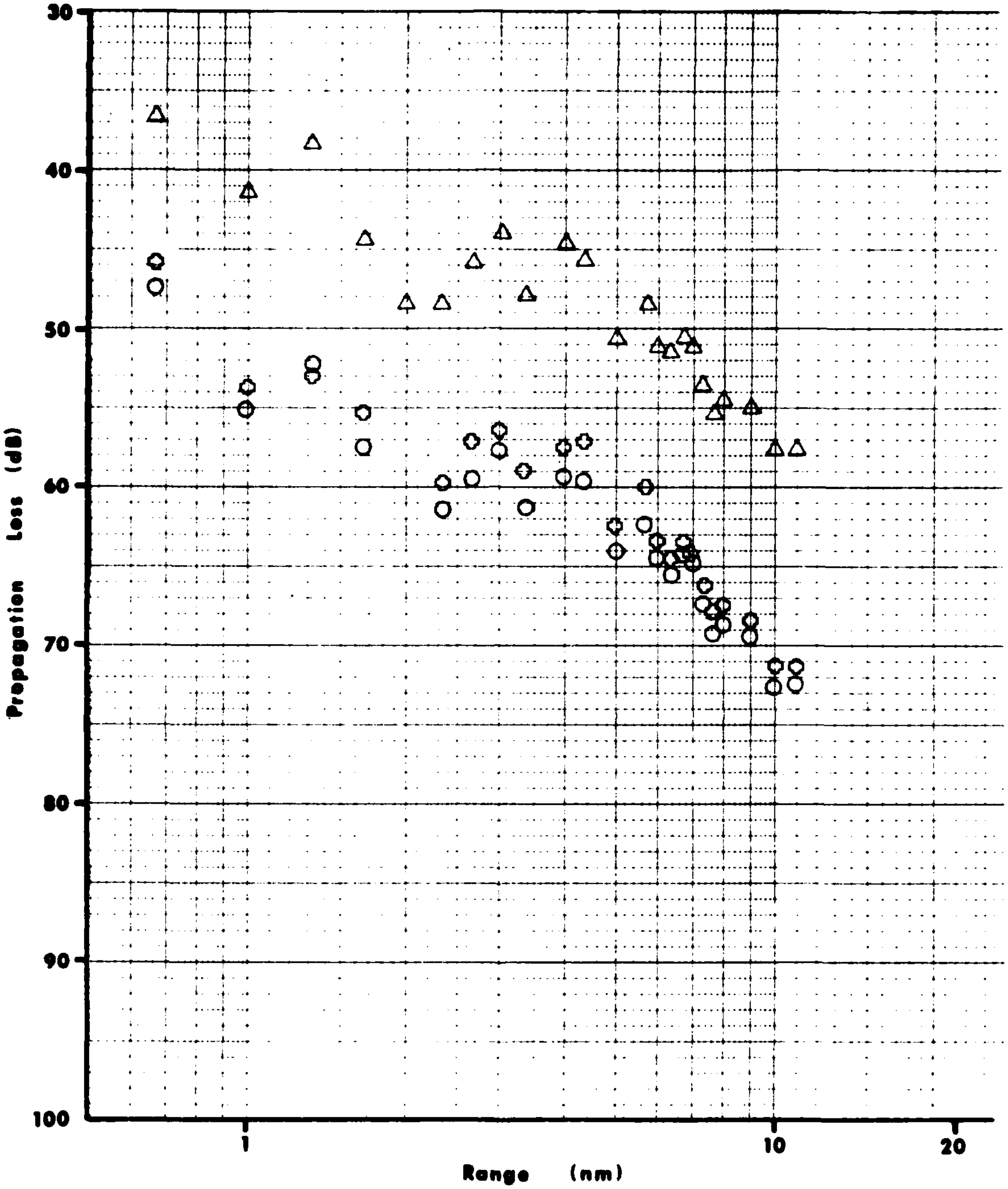

Figure B-38. Measured Propagation Loss for Run 3 at a Frequency of 40 Hz.

○ = Hydrophone. Triaxial Geophones: △ = Vertical, □ = Horizontal-2, ⬡ = Horizontal-1.

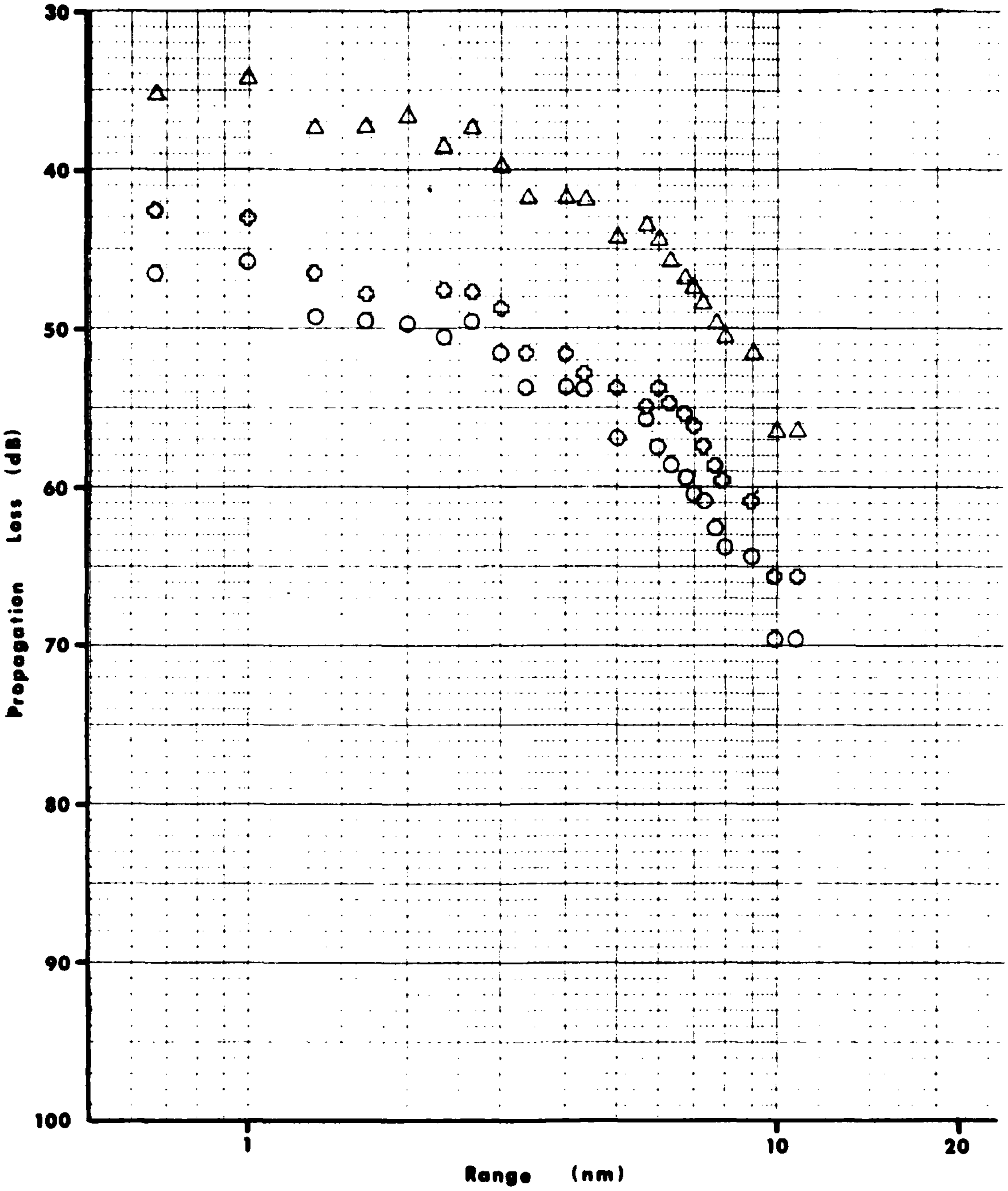

Figure B-39. Measured Propagation Loss for Run 3 at a Frequency of 50 Hz.

○ = Hydrophone. Triaxial Geophones: △ = Vertical, □ = Horizontal-2, ⌖ = Horizontal-1.

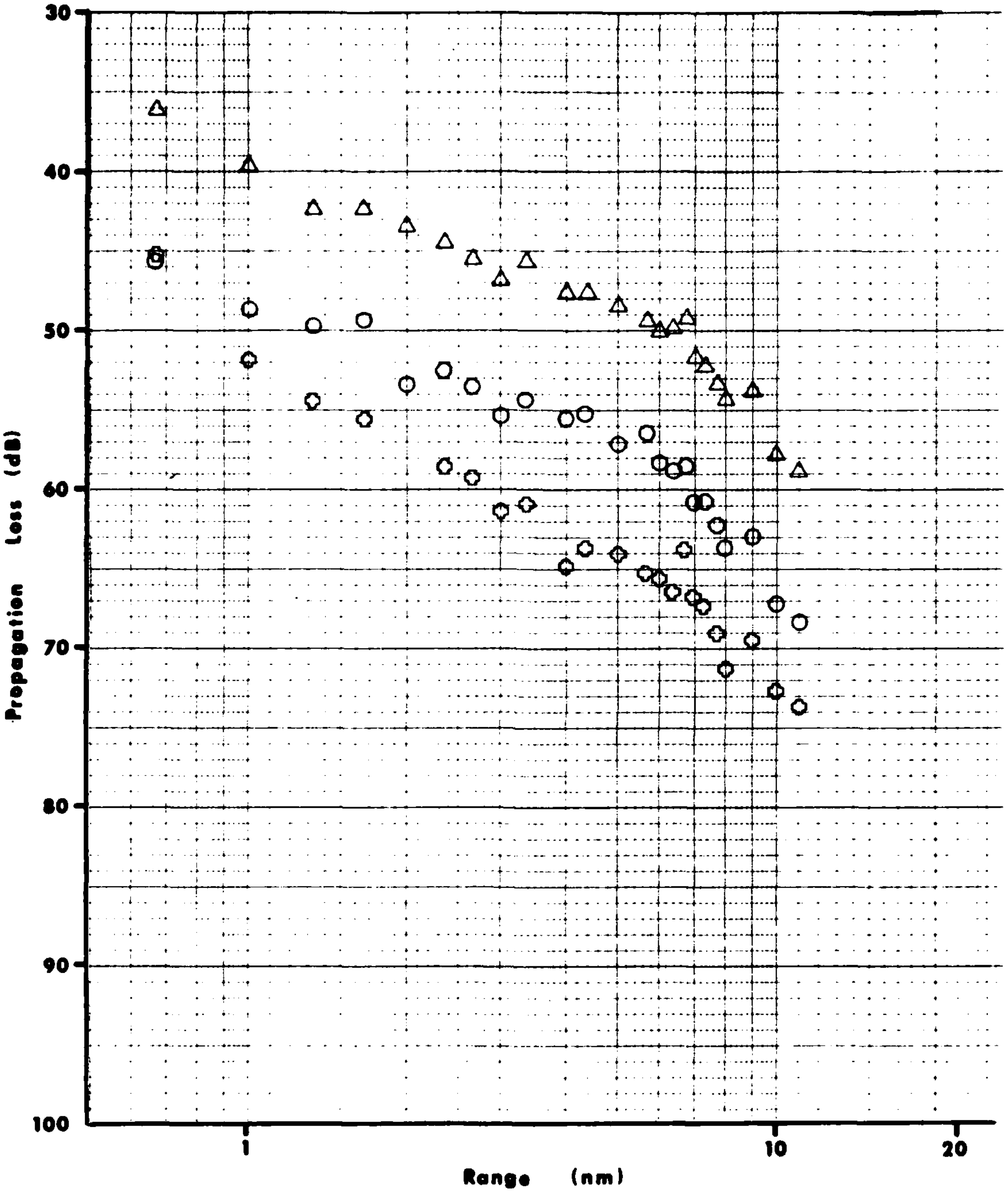

Figure B-40. Measured Propagation Loss for Run 3 at a Frequency of 63 Hz.

○ = Hydrophone. Triaxial Geophones: △ = Vertical, □ = Horizontal-2, ⬡ = Horizontal-1.

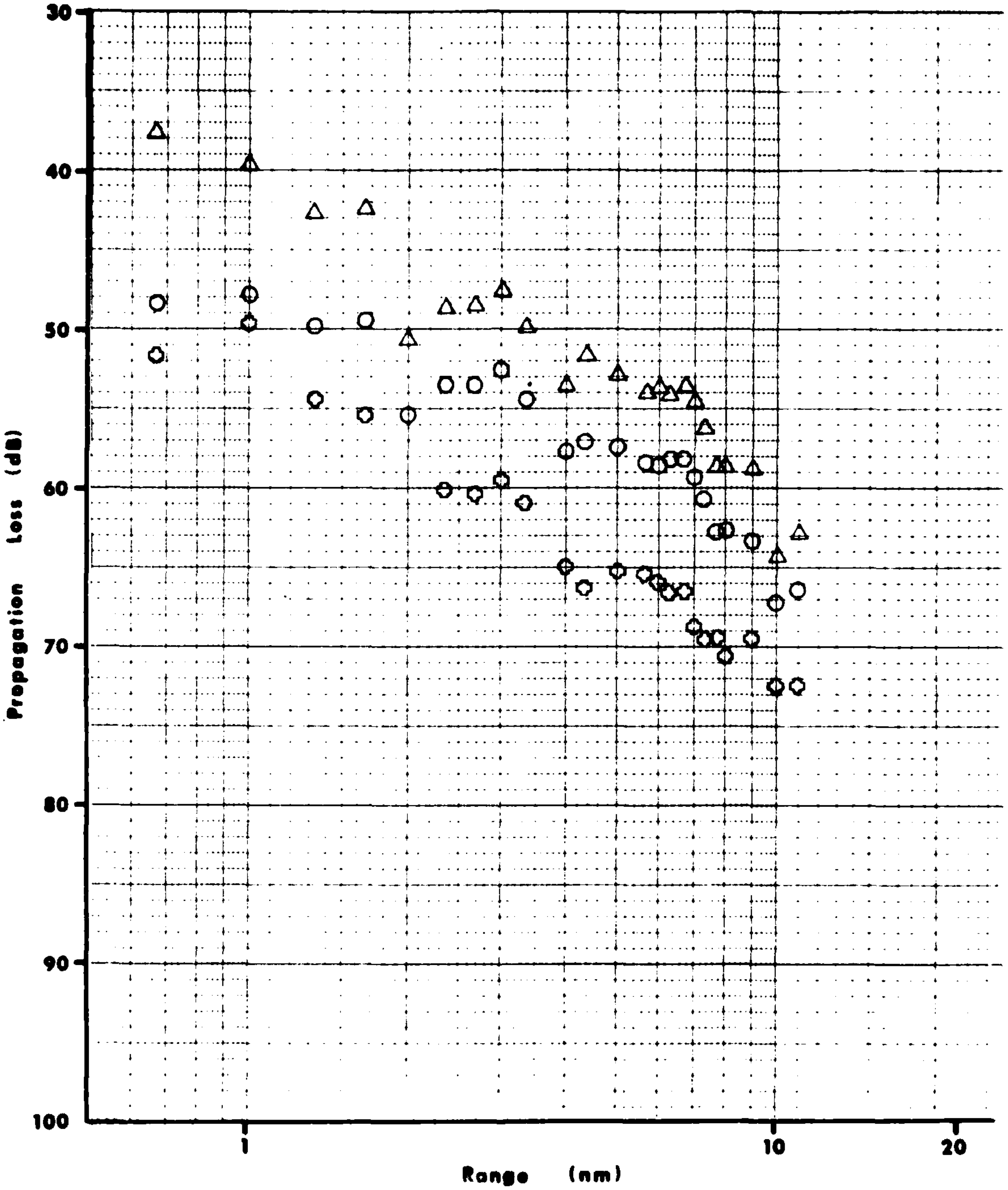

Figure B-41. Measured Propagation Loss for Run 3 at a Frequency of 80 Hz.

○ = Hydrophone. Triaxial Geophones: △ = Vertical, □ = Horizontal-2, ⬡ = Horizontal-1.

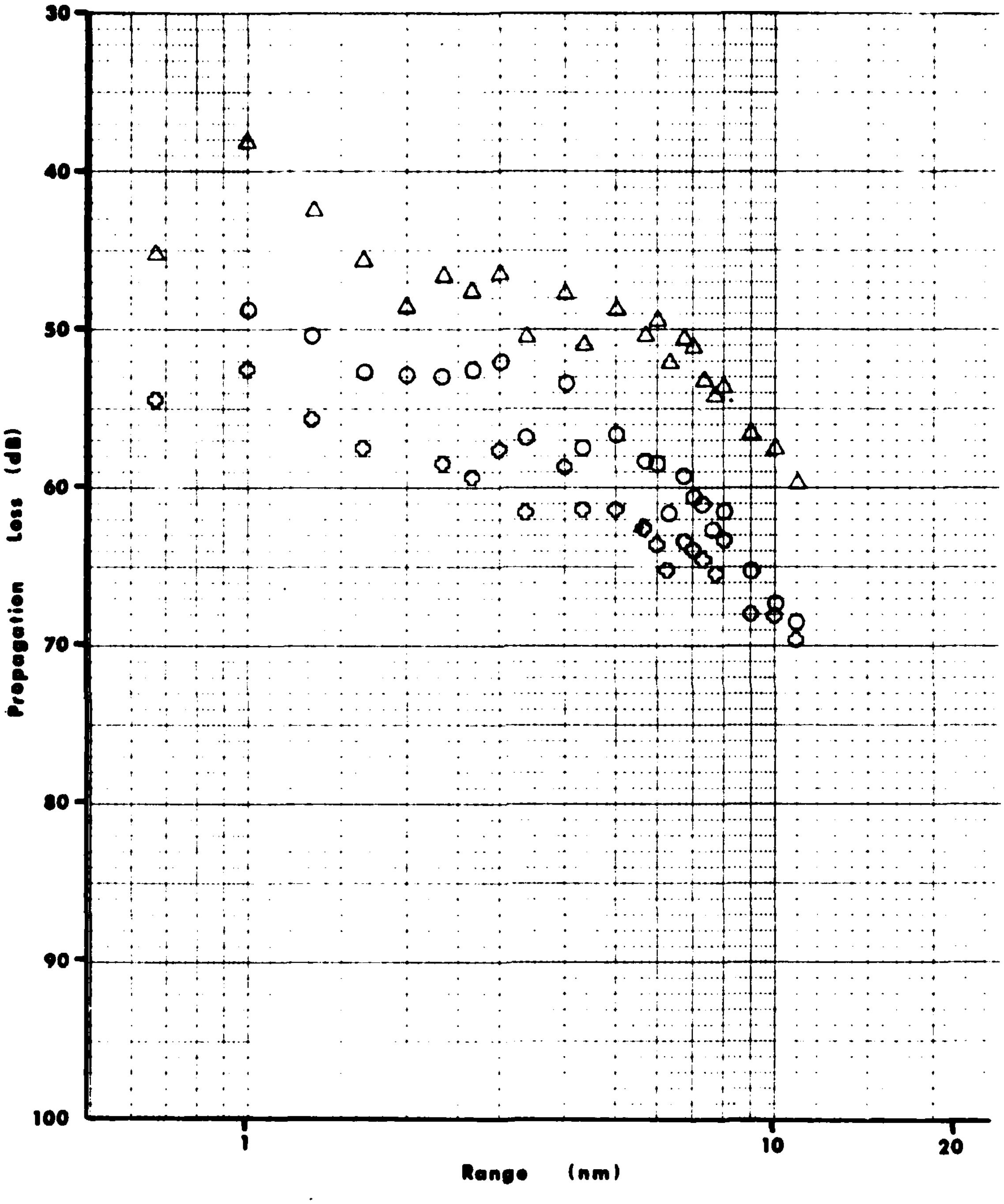

Figure B-42. Measured Propagation Loss for Run 3 at a Frequency of 100 Hz.

○ = Hydrophone. Triaxial Geophones: △ = Vertical, □ = Horizontal-2, ◇ = Horizontal-1.

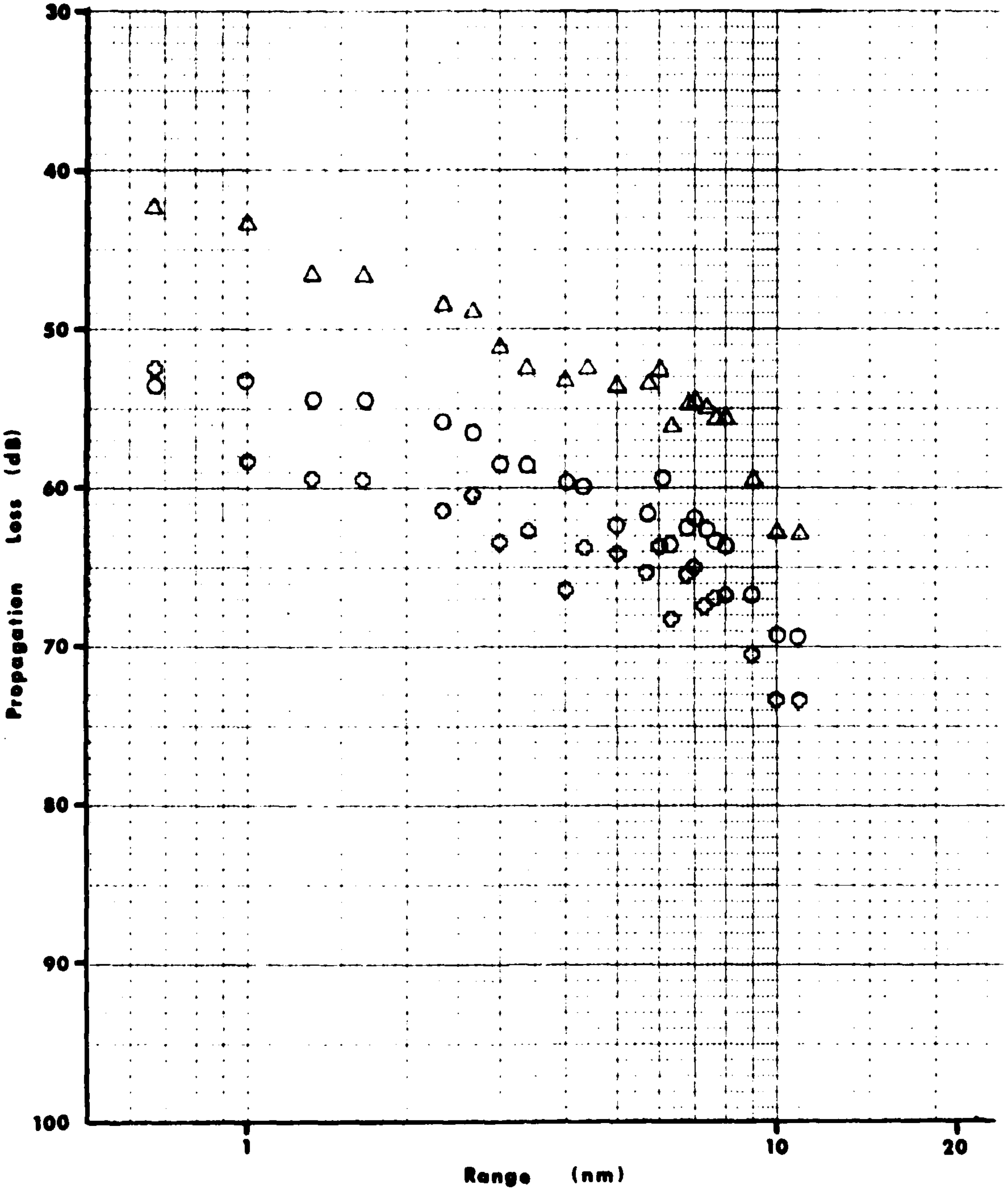

Figure B-43. Measured Propagation Loss for Run 3 at a Frequency of 125 Hz.

○ = Hydrophone. Triaxial Geophones: △ = Vertical, □ = Horizontal-2, ⬡ = Horizontal-1.

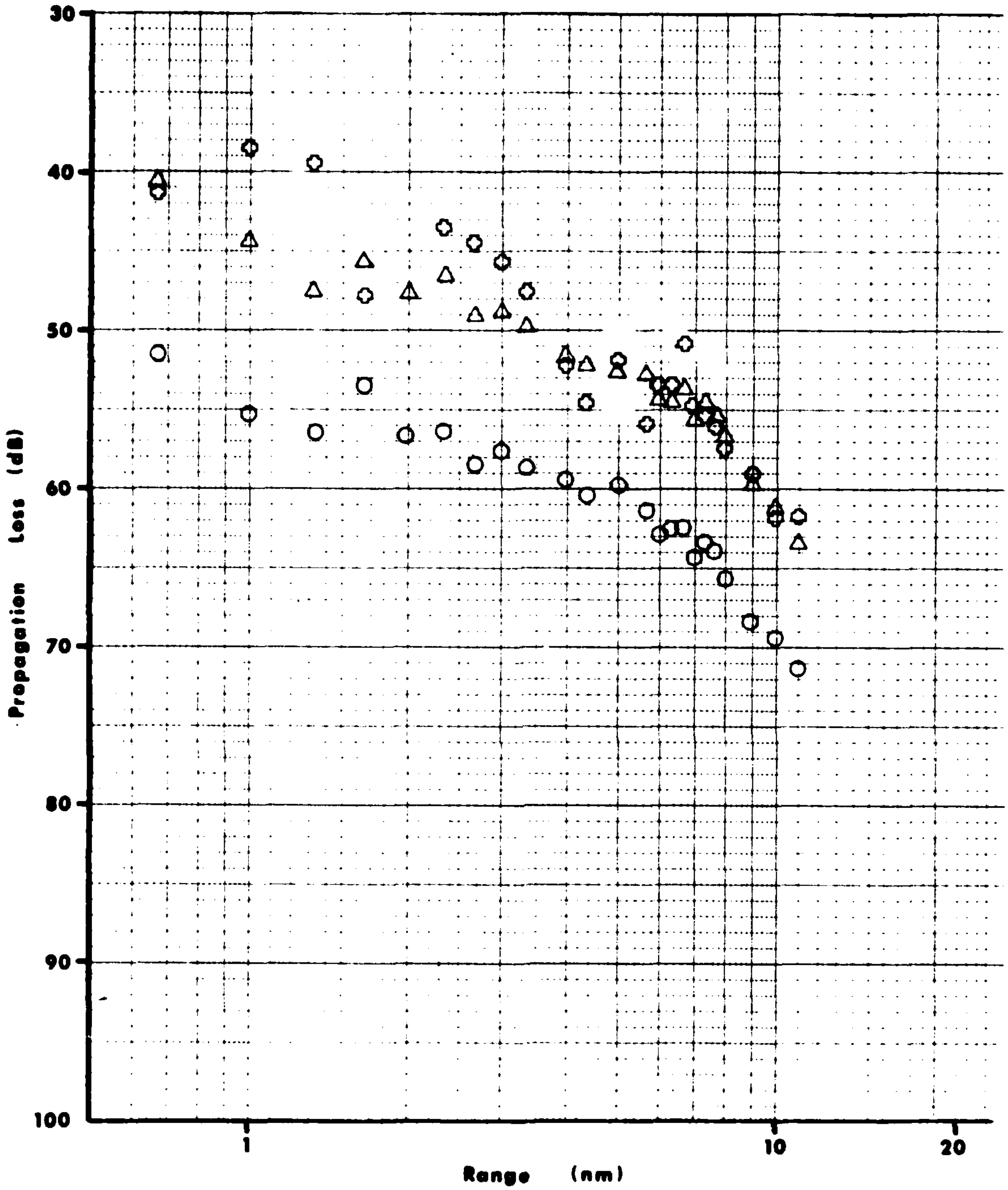

Figure B-44. Measured Propagation Loss for Run 3 at a Frequency of 160 Hz.

○ = Hydrophone. Triaxial Geophones: △ = Vertical, □ = Horizontal-2,
⬡ = Horizontal-1.

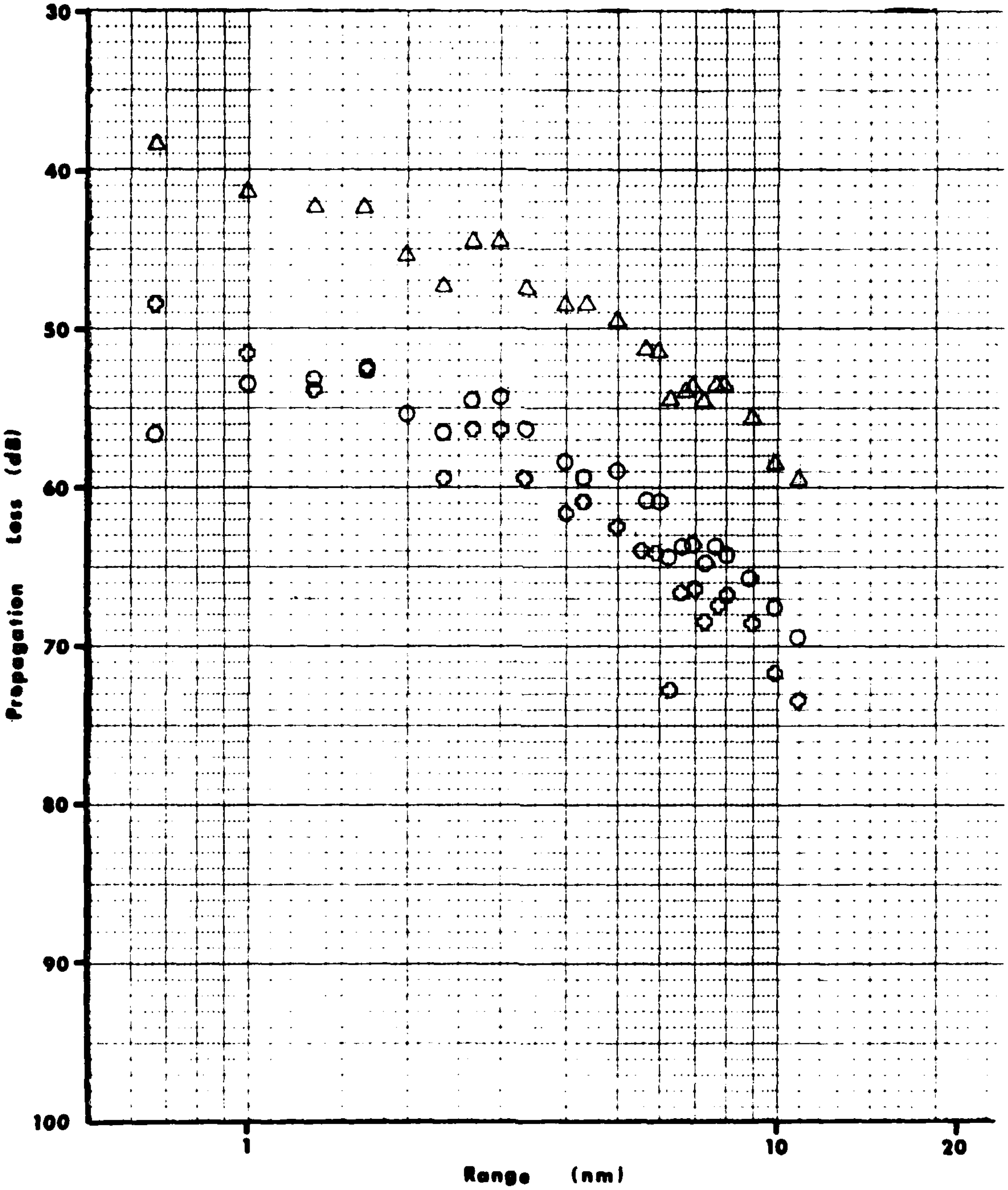

Figure B-45. Measured Propagation Loss for Run 3 at a Frequency of 200 Hz.

○ = Hydrophone. Triaxial Geophones: △ = Vertical, ☐ = Horizontal-2, ⬡ = Horizontal-1.

References

Appendix B

B1. Hecht, R. J., "Sound Propagation South of Martha's Vineyard," Underwater Systems, Inc., June 30, 1980.

B2. Underwater Systems, Inc., "SUS Source Level Handbook," draft report, December 1, 1979.

B3. Burgess, J. C., "Digital Spectrum Analysis of Periodic Signals," J. Acoust. Soc. Am., Vol. 58, No. 3, September 1975, p. 556.

B4. Bendat, J. S. and A. G. Piersol, Random Data: Analysis and Measurement Procedures, Wiley-Interscience, New York, 1971.

DISTRIBUTION LIST

Organization	No. Copies
OFFICE OF NAVAL RESEARCH	
ATTN: Code 464	2
Boston Branch Office Section D	1
NAVAL RESEARCH LABORATORY	
ATTN: Code 2627	6
Code 8120	1
NAVAL ELECTRONICS SYSTEMS COMMAND	
ATTN: Code 320	1
PME 124	1
NAVAL OCEAN RESEARCH AND DEVELOPMENT ACTIVITY	
ATTN: Code 360	1
NAVAL POSTGRADUATE SCHOOL	
ATTN: Dr. James Saunders	1
NAVAL COASTAL SYSTEMS CENTER	
ATTN: Code 792	1
NAVAL OCEAN SYSTEMS CENTER	
ATTN: Dr. Homer Bucher	1
UNIVERSITY OF TEXAS AT AUSTIN	
ATTN: Dr. Ken Hawker	1
UNIVERSITY OF TEXAS AT GALVESTON	
ATTN: Dr. Gary Latham	1
UNIVERSITY OF HAWAII	
ATTN: Dr. Gettrust	1
LAMONT-DOHERTY GEOLOGICAL OBSERVATORY OF COLUMBIA UNIVERSITY	
ATTN: Mr. R. E. Houtz	1
INSTITUTE OF ACOUSTICAL RESEARCH	
ATTN: Dr. M. Kronengold	1
SCIENCE APPLICATIONS, INC.	
ATTN: Dr. Eller	1
DEFENSE DOCUMENTATION CENTER	12